(E79-10082) AN INTEGRATED STUDY OF EARTH RESOURCES IN THE STATE OF CALIFORNIA USING REMOTE SENSING TECHNIQUES Annual Progress Report (California Univ.) 220 p HC A10/MF A01 CSCL 08F G3/43
N79-15361
Unclas 00082

SPACE SCIENCES LABORATORY

AN INTEGRATED STUDY OF EARTH RESOURCES IN THE STATE OF CALIFORNIA USING REMOTE SENSING TECHNIQUES

79-10082
CR-157975

A report of work done by scientists of 4 campuses of the University of California (Davis, Berkeley, Santa Barbara and Riverside) under NASA Grant NGL 05-003-404

Volume I of 2 volumes

Annual Progress Report
1 May 1978
Space Sciences Laboratory
Series 19, Issue 53

UNIVERSITY OF CALIFORNIA, BERKELEY

TABLE OF CONTENTS

Chapter 1

INTRODUCTION

Robert N. Colwell

As we near the conclusion of our work under this Integrated Study, the question that becomes increasingly relevant is this: To what extent are the potential users , especially in the State of California , actively accepting and using this modern remote sensing technology? One can find highly favorable but somewhat superficial answers to this question, including those documented with letters of praise written and signed by high officials in the very agencies that we seek most to serve. One has difficulty, however, trying to find answers which are both highly favorable and highly rigorous. To paraphrase the assertion made in Chapter 6 of this report by our Social Sciences Group, the transfer of a technology (remote sensing), can be considered completed only when that technology, being readily available in the marketplace, becomes generally accepted practice by the user agency. And, when the chief officer of that agency, upon routinely assessing all available technology that might be brought to bear on a specific problem, decrees that the technology in question is the one that shall be used. To date, there is virtually no instance of truly modern remote sensing technology which has been fully transferred to the managers of California's natural resources.

Amplifying on this statement, and the problems which technology transfer implies, our report states, in Chapter 6, that remote sensing technology will not transfer itself. Instead, there is commonly a 5-stage "adoptive process" by which this new technology is perceived, internalized and used: (1) awareness (2) interest (3) evaluation (4) trial, and (5) adoption. Since this process may take years, there frequently are problems in maintaining the necessary momentum, especially when there usually are disruptions in personnel and support along the way that can undermine both credibility and morale. Even after remote sensing technology has been adopted, it still may take years before this new technology will begin to bear fruit.

In addition, the following pitfalls are likely to be encountered: (1) Oversell results in the raising of user expectations to levels beyond what current capabilities can deliver; (2) Overkill results when the user is urged to use elaborate techniques of computer-assisted analysis even when the desired information could have been derived quite adequately through the use of simple, inexpensive, and more readily understood manual interpretation techniques; (3) Undertraining results when a novice who has just completed an "appreciation" course in remote sensing, is required to plunge directly into the demanding tasks that are involved in making operational use of modern remote sensing technology; (4) Under involvement results when the user agency, plagued by a lack of qualified and/or motivated personnel, turns over the bulk of the work to consultants or others who lack familiarity with the user agency's resource problems and information needs and perhaps even with the resource as well; (5) Spurious Evaluation results when the user agency, forced by those in higher authority or by others into a "rush to judgment," produces premature, incomplete, incestually-validated and usually overly-optimistic appraisals; and (6) Misapplication results, in part, from the sheer glamour of the shiny new tool known as "remote sensing" and is perhaps best metaphorized by the saying, "give a small boy a hammer and he soon discovers that everything needs pounding."

In light of the foregoing, let us now return to the question, "to what extent are the potential users in the State of California actively accepting and using this modern remote sensing technology?" From the preceding discussion, state and local resource managers require more than a few years to adapt to their specific needs a technology as complex as remote sensing. Therefore, our overall conclusion is that here in the State of California, solid progress is being made and at a rate as rapid as might have been anticipated or rightfully expected. Furthermore, we believe that we can attribute much of this progress to the very substantial effort that we have made, even from the inception of this "Integrated Study" nearly nine years ago, to involve the potential users (i.e. the resource managers) throughout the entire process of technology development and transfer. In relation to the ultimate technology transfer objective of our study, the importance of having involved the ultimate users can scarcely be overemphasized. Nor can this involvement be overemphasized as we seek to provide a truly meaningful answer to the question that comprises the central theme of this introductory chapter: to what extent are California's potential users actually using, or at least progressing toward, the use of this remote sensing technology? Highly specific answers to that multifaceted question will be found in Chapters 3 through 5 of this report. We trust that those generally favorable answers when viewed in the light of the chapter-by-chapter "backup information" in support of them will not be regarded as the overly optimistic products of spurious evaluations made in the ivory-towered or ivy-clad vacuums of our own academia. In this regard, let us emphasize that a two-fold major reason why we have had the services of a Social Sciences Group throughout this study is to help point the way toward the achievement of true technology acceptance and to help us differentiate true acceptance from fancied acceptance of the type that might result from equal parts of wishful thinking and unwarranted optimism by our team of remote sensing scientists. Typical of the warnings that we have been given in this matter, is the following excerpt from Chapter 6 of the present progress report:

"Most potential users of remote sensing technology are simply unmoved by paper-and-pencil evaluation games. They recognize that externally-prepared benefit-cost ratios exclude many of the considerations most important to them. They see impacts on their own decision processes, job security, and organizational behavior being overlooked and obscured behind voluminous but vacuous evaluative reports. The result for the technology developers is ofen an evaluative "boomerang effect" in which users perform their own subjective assessments and conclude, for various reasons, that fruits from the technology are not worth their price."

Each evaluation relative to technology acceptance that has appeared in our Progress Reports since the start of this "Integrated Study" has been made in the light of this admonition.

Finally, we believe that the heavy concentration of our present efforts on the preparation of "Procedural Manuals" is essential to the maintaining of momentum toward our longer term goal. That goal is to bring about the complete acceptance and intelligent day-to-day utilization of modern remote sensing technology by resource managers in California, as well as in other parts of the world. As exemplified by the material appearing in Chapters 3, 4, and 5 of this, and the two preceding progress reports, procedural manuals relate specific ways in which remote sensing techniques can be used advantageously in the inventory and management of California's natural resources. Furthermore, in each instance the manuals seek to describe those means by highly specific, step-by-step procedures. In the development of each of these Procedural Manuals, care has been exercised by our investigators to ensure that they were responsive to the intended user's needs. This included care in writing the step-by-step procedures, not only in a manner that could be understood, but also in a manner that could not be misunderstood.

As we near the final iteration on most of these Procedural Manuals, we continue to solicit reactions to them both from California's resource managers and from all other readers of this Progress Report.

Chapter 2

WATER SUPPLY STUDIES BY THE DAVIS CAMPUS GROUP

Co-Investigator: Ralph Algazi

Contributor: Minsoo Suk

Chapter 2

WATER SUPPLY STUDIES BY THE DAVIS CAMPUS GROUP

Co-Investigator: Ralph Algazi

Contributor: Minsoo Suk

(Explanatory Note by R. N. Colwell, Principal Investigator of the Integrated Study that is being performed under this grant):

Attention is invited to Special Study No. 3 in the Dec. '77 Progress Report entitled "Satellite Land Use Acquisition and Applications to Hydrologic Planning." That report was prepared by the long-time Co-Investigator from the Davis Campus for this NASA-funded, integrated study, Dr. Ralph Algazi and by his associate Dr. Minsoo Suk. Furthermore, the material contained in that Special Study is highly compatible with the emphasis that has been given during the past several years by all of our study participants relative to the remote sensing of California's water resources. Nevertheless, the material does not appear in that Progress Report as a complete chapter, even though the contributions from Algazi et al. have been so treated in the past. This change merely reflects the orderly transition that has been occurring during the past year (with NASA approval) as the Algazi team has been bringing to a close its studies as funded under this particular NASA grant, and transferring its remote sensing-related activities to follow-on programs under separate funding.

The change just described is regarded by all concerned parties, both within NASA and within the University of California, as a healthy transition. This is especially so because the newly directed efforts of the Algazi team are brought about by their having been designated as participants in an Applications Systems Verification Test relative to uses that can be made of remote sensing in the estimation of water supply. Thus their re-directed efforts represent a logical step toward bringing about the acceptance by user agencies of certain kinds of remote sensing technology that have been developed, at least in part, by the Algazi group during their several years of participation in this grant.

It is for the reasons indicated above that (1) for the first time there is not a full chapter in this Progress Report detailing grant-funded activities of the Algazi group, and (2) there is nevertheless a substantial contribution from that group appearing in Chapter 7 of our semi-annual progress report of 31 December, 1977.

8

Chapter 3

WATER SUPPLY STUDIES BY
THE BERKELEY CAMPUS GROUP

Co-Investigator: Siamak Khorram

Contributors: H. Gregory Smith, Edwin F. Katibah,
Randall W. Thomas, James M. Sharp, and
Agnis Kaugers

Remote Sensing Research Program
Berkeley Campus
University of California

May 31, 1978

Table of Contents

10

Table of Contents (Continued)

//

INTRODUCTION

The focus of the work that has been performed during the present reporting period, by the Remote Sensing Research Program personnel at the Berkeley Campus, has been on completion of the remote sensing-aided procedural manuals on water supply forecasts. This work is described in terms of stepwise procedures which might best be followed by managers of water resources who are interested in using remote sensing techniques as an aid for water resources inventory, development, and management.

The procedural manuals which follow this section are entitled:

1. Remote Sensing as a Aid in Determining the Areal Extent of Snow

2. Remote Sensing as an Aid in Determining the Water Content of Snow

3. Remote Sensing as an Aid in Watershed-Wide Estimation of Solar and Net Radiation

4. Remote Sensing as an Aid in Watershed-Wide Estimation of Water Loss to the Atmosphere

5. Outline for Remote Sensing as an Aid in the Inventory and Management of the Multiple Resource Complex for a Given Wildland Area

The manual on snow areal extent estimation is based on manual analysis of Landsat imagery supported by aerial photography and may be easily used by any resource manager.

The manual on snow water content estimation is based on snow areal extent data and a physical model for conversion of snow-cover data to water content of snow. These conversion models may be refined by further research.

The manuals on solar and net radiation estimation and water loss to the atmonphere estimation are both based on a data bank composed of Landsat digital data, NOAA-4 satellite thermal data, terrain variations, and climatic data obtained from ground meteorological stations.

12

Since both of these manuals consider variations in climate and terrain conditions, they may be applied to watersheds with different geographical locations. However, it should be mentioned that not all the climatic effects have been taken under consideration.

These procedures for solar and net radiation estimation require sophisticated computer facilities and special software packages for Landsat and NOAA-4 satellite data processing. Therefore, their applications are limited to the availability of hardware facilities with required software programs.

The mathematical models used for solar and net radiation are based on energy-balanced equations and the results are in agreement with the data collected on the test site. This remote sensing-aided procedure for daily estimation of radiation components is recommended for application under most climatic and geographic conditions. The level I mathematical model for water loss (evapotranspiration) estimation, which is fully described and applied to the study area, is based on a semi-empirical model. More refined models (level II and III) need to be applied to the study area for more accurate performance. It should be mentioned that it is very difficult to make, and, to the best of our knowledge, presently there is no operational method available for evapotranspiration estimation from wildland areas. This is the first time that remotely-sensed spatial data have been applied to watershed-wide evapotranspiration estimation and the results have been adequately accurate to be used in water yield prediction models.

Presently, with the cooperation of the U.S. Forest Service at Plumas National Forest, the Plumas County Planning Department, and the California Department of Water Resources, we are continuing the use of remote sensing for inventory and management of the multiple resource complex within the Upper Middle Fork of the Feather River Watershed.

13

Procedural Manual

REMOTE SENSING AS AN AID IN WATERSHED-WIDE ESTIMATION OF SOLAR AND NET RADIATION

Principal Investigator: Robert N. Colwell

Principal Scientist
and Project Manager: Siamak Khorram

Project Scientists: H. Gregory Smith and
Edwin F. Katibah

NASA Grant NGL-05-003-404

Remote Sensing Research Program
University of California, Berkeley
May, 1978

PROCEDURAL MANUAL FOR
REMOTE SENSING AS AN AID IN WATERSHED-WIDE ESTIMATION
OF SOLAR AND NET RADIATION

INTRODUCTION

Of the tremendous quantity of radiant energy emitted by the sun, only a very small portion is intercepted by the earth and its atmosphere. This small portion is the ultimate source of almost all of the earth's energy. This amount of incident radiation is known as the solar constant which is defined (U.S. Army Corp of Engineers, 1956) as: "the intensity of solar radiation received on a unit area of a plane normal to the incident radiation at the outer limit of the earth's atmosphere with the earth at its mean distance from the sun". The value of the solar constant is generally taken to be 1.94 Langleys per minute which is based on the 1913 Smithsonian standard scale. There has been evidence that this value is too low; a value of 2.00 ly/min. has been offered (Miller, 1955).

The portion of the solar radiation which actually reaches the earth's surface depends upon the transparency of the atmosphere. In the absence of clouds these amounts are quite constant. The atmospheric transmission coefficient varies from about 80 percent at the time of the winter solstice to about 85 percent at the time of the summer solstice (U.S. Army Corp of Engineers, 1956). Atmospheric transmission coefficients are based on the total insolation received at the earth's surface and include both the direct and diffused radiation.

By far the largest variations (in the amount of solar radiation transmitted by the atmosphere) are caused by clouds. The transmitted radiation varies with type, height, density, and amount of clouds. The quantitative consideration will be discussed later. Since clouds are such a powerful controlling factor in radiative heat exchange, other minor factors such as humidity of the air are often ignored.

Similar to the clouds effects, the ground cover conditions such as a forest canopy exert a powerful controlling influence on net all-wave radiation exchange in hydrologic processes. However, the forest canopy has a different effect than that of clouds, particularly with respect to shortwave radiation. While both the clouds and trees restrict the transmission of radiation, clouds are highly reflective, while the forest canopy absorbs much of the radiation. Consequently, the forest canopy tends to be warmed and in turn gives up a portion of its absorbed energy for evapotranspiration.

15

Objective

The objective of this procedural manual is to describe a remote sensing-aided methodology developed by personnel of the Remote Sensing Research Program for accurate and location-specific estimation of radiation components. These components include net shortwave (solar) radiation, net longwave radiation, and net radiation on the earth's surface. The results of this study are designed to be readily incorporated into evapotranspiration and other hydrologic models for water yield forecasts (Khorram, et al., 1976). Since the inputs to the radiation estimation models entail both climatic and physiographic conditions of the watershed, the effect of climatic variability has been implicitly accounted for.

Definitions

Total incoming radiation (D and I) is defined as the direct (D) and diffused or indirect (I) shortwave radiation reaching the ground through the atmosphere. Some of this incident radiation is reflected back to the atmosphere (R), which is called reflected radiation and the rest is absorbed by objects on the earth's surface. Part of the absorbed radiation is dissipated to the atmosphere from the ground (G) as longwave radiation. In turn, a portion of this dissipated longwave radiation is absorbed by the clouds and atmospheric particles and part of it is returned to the ground (A). This returned longwave radiation from the atmosphere to the ground (A) is called atmospheric radiation. The difference between upgoing (G) and atmospheric (A) longwave radiation may be defined as the net longwave radiation. Net radiation (Q_n), as it is shown in the following equation is the sum of the net shortwave radiation (D+I-R) and net longwave radiation (-G+A).

$$Q_n = (D+I-R) + (A-G) \qquad (1)$$

PROCEDURE

Prior to radiation estimation, the study area must be defined and the watershed boundary delineated. All of the information must be in common register, in this case Landsat-based; therefore, the Landsat data should be geometrically corrected and the watershed boundary transferred to a Landsat data format. The techniques for geometric correction and for watershed boundary determination are described in Appendix I.

The procedure for estimating net radiation is composed of a series of mathematical models and techniques for providing the required input information to the models. The items of input

The resulting equation is:

$$Q_{nL} = (-0.24 + 0.158 \times 10^{-10} T_k^4)\ (0.2 - 0.8\ \frac{n}{N})\ \text{in cal. Cm}^{-2} \cdot \text{min}^{-1} \quad (7)$$

Step 3. Net Shortwave Radiation Computation

The value of Q_s is estimated by Linacre (1967) by means of the modified Angstrom equation.

$$Q_s = Q_A\ (c + d\ \frac{n}{N}) \quad (8)$$

where Q_A is the value of Q_s above the atmosphere, c and d are empirical constants related to the atmospheric turbidity, and n and N are as previously defined. n is measured and values of N depend on the latitude and time of year, and are available in standard meteorological tables. The values of n may be gained through remote sensing techniques using NOAA satellite data; however, n is normally measured in the field. Table 1 shows the values for c and d. Linacre's equation is not exact because it does not allow for the varying importance of cloudiness at different times of the day.

The values of Q_A for a day or less (considering slope and aspect) are estimated by the following equation (Frank and Lee, 1966):

$$Q_A = \frac{I_o}{e^2}\ (t_2 - t_1)\ \sin\theta' \cdot \sin\delta + \frac{12}{\pi} \cdot \cos\theta' \cdot \cos\delta.$$

$$(\sin wt_2' - \sin wt_1') \text{ where} \quad (9)$$

I_o = solar constant

e = radius vector, ratio of the earth-sun distance at a particular time to its mean

t_1 = number of hours before solar noon (negative)

t_2 = number of hours after solar noon (positive) information are physiographic data, climatic data, and some standard meteorological constants.

Step 1. Allwave Radiation Model

The net radiation flux $Q_n = (1-\alpha)\ Q_s - Q_{nL}$ (2)

where α is albedo, Q_s is the total flux of shortwave radiation from the sun and the sky, and Q_{nL} is the net upward flux of longwave radiation.

Step 2. Net Longwave Radiation Computation

The net longwave radiation is computed as follows:

$$Q^*_{nL} = Q_{Ld} - Q_{Lu} \quad (3)$$

$$Q_{Ld} = 0.971 \times 10^{-10} T_k^4 - 0.245 \text{ (cal. cm.}^{-2}\text{min}^{-1}) \quad (4)$$

$$Q_{Lu} = 0.813 \times 10^{-10} T_k^4 \text{ (cal. Cm}^{-2} \cdot \text{min}^{-1}) \quad (5)$$

where Q^*_{nL} is the net flux of longwave radiation in cloudless conditions, Q_{Ld} is the downward flux of longwave radiation from the formula of Swinback, 1963, (T_k) is the ambient temperature in degrees of Kelvin and Q_{Lu} is the upward flux of longwave radiation from a surface with unit emissivity (Linacre, 1968).

Then

$$Q_{nL} = Q^*_{nL} \left[b + (1-b) \frac{n}{N} \right] \quad (6)$$

where there are n hours of actual sunshine in a daylength of N hours. The term b has been taken to be either 0.10 (Penman, 1948), 0.20 (Kramer, 1957), 0.24 (Impens, 1963), or 0.30 (Fitzpatrick and Stern, 1965); a value of 0.20 may be adopted as a compromise (Linacre, 1968).

δ = solar declination

w = angular velocity of the earth's rotation (15 degrees per hour)

$\frac{12}{\pi} = \frac{1}{w}$ in radians

$\theta = \arcsin(\sin k \cdot \cos h \cdot \cos \theta + \cos k \cdot \sin \theta)$ in which θ = terrestrial latitude

k = slope inclination in degrees

h = slope azimuth (aspect) in degrees from the north

$$wt' = wt + \alpha \tag{10}$$

where

$$\alpha = \arctan \left(\frac{\sin h \cdot \sin k}{\cos h \cdot \cos \theta - \cos h \cdot \sin k \cdot \sin \theta}\right) \tag{11}$$

Step 4. Albedo Calculation

The reflection or albedo is the ratio of reflected to incident radiation, usually expressed as a percentage. The values of albedo for the total range of solar radiation, and in some cases for the visible electromagnetic range only, are shown in Table 2. The figures given in that table illustrate what can be observed directly from an airplane. The sea appears darkest, relative to white strips of surf and sand dunes. Woods show up darker than fields, and snow-covered areas are light. One can see here how this affects the whole heat economy of the earth's surface and therefore all hydrologic processes. Albedo is influenced not only by the nature of a surface, but also by its moisture content at any time, i.e. wet surfaces appear darker than dry surfaces.

The procedure for making albedo calculations is based on a vegetation/terrain analysis of the watershed. Once the ground cover is determined, an albedo index is assigned for each type of vegetation or ground cover (based on the published values of albedo appearing in Table 1) and the albedo map of the watershed is prepared. A stepwise procedure for vegetation/terrain analysis is described in Appendix II, following this procedural manual.

Step 5. Net Radiation Determination

Combining the equations for net shortwave and net long-wave radiation, the net radiation on the earth's surface can be estimated by the following equation:

$$Q_n = (1-\alpha)\ Q_s\ (-0.245 + 0.158 \times 10^{-10} T_k^4)\ (0.2 + 0.8\ \frac{n}{N}) \qquad (12)$$

The values of the various radiation components estimated by this method are site-specific and consider the effects of slope, aspect, latitude, cloud cover and elevation.

Step 6. Preparation of Topographic Inputs to the Radiation Models

The topographic characteristics of the watershed are some of the major factors affecting the amount of solar radiation. These characteristics include elevation, slope and aspect.

The elevation, slope, and aspect maps are constructed from the elevation contour data on U.S. Geological Survey topographic maps, 15' series. The procedure involves the orientation of each Landsat picture element (pixel) in the watershed. Each pixel is defined in terms of its x, y, and z coordinate dimensions. The x and y coordinates locate the center of the pixel while the z coordinate defines the average elevation. Each pixel can be "tilted" and/or rotated. The tilt and rotation functions are considered to be the slope and aspect of the pixel, respectively.

The detailed procedures for coordinate determination and topographic analysis are described in Appendix III.

Step 7. Preparation of Climatic Input Variables to Radiation Models

The collection and integration of climatic information are basic to the use of simulation models that are used in the estimation of solar and longwave radiation, and evapotranspiration for a watershed. The manner in which the information is collected, along with the type(s) of data used are dependent on the specific models used and the desired nature of the final output. Among all of the climatic factors, temperature plays a very essential role in radiation models.

Lack of adequate ground meteorological stations, in general, creates a problem in satisfying climatic data input requirements for radiation models. Therefore, we have chosen two alternative solutions: (1) computer-assisted interpolation of existing climatic data over the watershed; and (2) the use of the National Oceanic and Atmospheric Administration (NOAA-4) satellite Very High Resolution Radiometer (VHRR) data for the generation of temperature maps for the area.

Collection and interpolation of ground meteorological stations data are composed of the following steps:

a. Identification and selection of ground meteorological stations

b. Registration of the data

c. Recording and coding of the data

d. Data interpolation for climatic parameter of interest

e. Preparation of the data in a format to be used in simulation models

f. Generation of final products

The detailed description and the techniques for the above-mentioned steps are given in Appendix IV of this manual.

Data processing techniques for the NOAA-4 satellite thermal (VHRR) data as well as a brief description of the VHRR scanner and data acquisition system and required system capabilities for NOAA-4 data processing are given in Appendix IV of this manual. NOAA-4 satellite data processing entails the following steps:

a. Data acquisition

b. Location of the study area on the raw thermal data

c. Geometric correction of the data

d. Data enhancement and noise elimination

e. Transformation of voltage values to temperature values

f. Transformation of temperature data to the desired coordinate system

g. Preparation of final temperature map of the area of interest

21

Step 8. Preparation of Final Products

After all the inputs (both constants and variables) to the radiation models have been prepared, each of the radiation components may be estimated. These output products consist of shortwave radiation (net solar radiation) by using equation (8), net longwave radiation by using equation (7), and net radiation on the earth surface by using equation (12). The output products are the areal distribution of parameters of interest for a given site and date and percentage distribution of data over the study area.

Table 1. Published Values of the Factors c and d in Equation (9).

Source (1)	Location (2)	Latitude (3)	c (4)	d (5)	c+d (6)
Black et al (1954)	Stockholm, Fairbanks	59,65°N	0.22	0.52	0.74
Monteith (1966)	Lerwick	60°N	0.23	0.56	0.79
Penman (1948)	Rothamsted, U.K.	52°N	0.18	0.55	0.73
Baier and Robertson (1963)	Canada	52°N	0.25	0.62	0.87
Black et al. (1954)	Kew, U.K.	51°N	0.19	0.57	0.76
Van Wijk (1963)	Gembloux	51°N	0.15	0.54	0.69
" " "	Versailles	49°N	0.23	0.50	0.73
Tanner and Peltcn (1960)	Wisconsin	43°N	0.18	0.55	0.73
de Villeie (1965)	El Aouina	37°N	0.28	0/43	0.71
de Vries (1958)	Deniliquin	36°S	0.27	0.54	0.81
Damagnez (1963)	Tunisia	35°N	0.16	0.59	0.75
Prescott, (1940)	Canberra	35°S	0.25	0.54	0.79
Black et al (1954)	Dry Creek	35°S	0.30	0.50	0.80
Page (1961)	Capetwon	34°S	0.20	0.59	0.79
Glover (1958)	Durban	30°S	0.25	0.50	0.76
Yada (1959)	Delhi	29°N	0.31	0.46	0.77
Glover (1958)	Pretoria	26°S	0.25	0.50	0.75
" "	Windhoek	23°S	0.26	0.52	0.78
Page (1961)	Tananarive	19°S	0.30	0.48	0.78
Smith (1964)	Jamaica	18°N	0.31	0.49	0.80

Table 1, continued

Source (1)	Location (2)	Latitude (3)	c (4)	d (5)	c+d (6)
Fitzpatrick (1967)	Kimberly	16°S	0.33	0.43	0.76
Cackett (1964)	Central Africa	15°S	0.32	0.47	0.79
Page (1961)	Dakar	15°N	0.10	0.70	0.80
Yada (1959)	Madras	13°N	0.31	0.49	0.80
Davies (1965)	Kano	12°N	0.26	0.54	0.80
Smith (1964)	Trinidad	11°N	0.27	0.49	0.76
Stanhill (1963)	Benin City[a]	7°N	0.26	0.38	0.64
Davis (1965)	Accra	6°N	0.30	0.37	0.67
Black et al (1954)	Batavia etc.	6°S	0.29	0.29	0.58
Page (1961)	Leopoldville	4°S	0.21	0.52	0.73
" "	Singapore	1°N	0.21	0.48	0.69
Glover (1958)	Kabete, Kenya	1°S	0.24	0.59	0.83
Page (1961)	Stanleyville	1°N	0.28	0.40	0.68
Rijks (1964)	Kampaia	0°	0.24	0.46	0.70
Mean Values			0.245	0.507	0.752
Hounam (1963)	Australia	12-43°S	0.26	0.50	
Davies (1965)	West Africa	5-15°N	0.19	0.60	
Black et al (1954)	general	-	0.23	0.48	
Page (1961)	tropics	-	0.23	0.52	
Turc (1961)	general	-	0.18	0.62	

[a] Davies (1965) gave 0.28 and 0.33 for c and d respectively

SOURCE: Linacre, 1968

TABLE 2

Stand	Albedo Percent	Source
Fresh snow cover	75-95	Geiger
Dense cloud cover	60-95	"
Old snow cover	40-70	"
Clean firn snow	50-65	"
Ice, sparse snow cover	69	Smithsonian table
Clean glacier ice	20-50	"
Light sand dunes, surf	30-46	Geiger
Sandy soil	15-40	"
Meadow and fields	12-30	"
Meadow, low grass	15-25[a]	Smithsonian table
Field, plowed, dry	20-25[a]	"
Densely built-up area	15-25	Geiger
Woods	5-20	"
Dark cultivated soil	7-10	"
Douglas-fir	13-14	Avery
Pine	14	Brooks
Conifers	10-15	Budyko
Deciduous forest, fall	15[a]	Krinov
Deciduous forest, summer	10[a]	"
Coniferous forest, summer	8[a]	"
Coniferous forest, winter	3[a]	"
Meadow dry grass	10[a]	"
Field Crops, ripe	15[a]	"
Spruce	8-9	Baumgartner
Earth roads	3[a]	Krinov
Black top roads	8[a]	Sewing Handbook
" " "	9[a]	Krinov

25

Table 2, continued

Stand	Albedo Percent	Source
Concrete road	35[a]	Krinov
Buildings	9[a]	"
Mountain tops, bare	24[a]	"
Clay soil dry	15[a]	Sewing Handbook
Clay soil wet	7.5[a]	"
Clouds, stratus overcast, 0-500 feet thick	5-63	"
Clouds, stratus overcast, 500-1,000 feet thick	31-75	"
Clouds, stratus overcast, 1,000-2,000 feet thick	59-84	"
Clouds, dense, opaque	55-78	"
Clouds, dense, nearly opaque	44	"
Clouds, thin	36-40	"
Clouds, stratus, 600-1,600 feet thick	78	"
Clouds, stratocumulus overcast	56-81	"
Clouds, altostratus, occasional breaks	17-36	"
Clouds, altostratus, overcast	39-59	"
Clouds, cirrostratus and altostratus overcast	49-64	"
Clouds, cirrostratus overcast	44-50	"

Whole earth: From measurements on the bright and dark portions of the moon, Danjon[b] has calculated the albedo of the earth in the visible portion of the spectrum at 39 percent. Fritz[c] has extended the calculation to include infrared and ultraviolet radiation, obtaining a total albedo of the earth of 35 percent. Baur and Philipps[d] have calculated the total albedo to be 41.5 percent

[a]visual albedo

[b]Danjon, A., Ann. l'Obs. Strasbourg 3, No. 3, 1936, P. 139

[c]Fritz, S., Bull. Amer. Meteorol. Soc., Vol. 29, 1948, p. 303; Vol. 31, 1950, p. 251; Journ. Meteorol., Vol. 5, 1949, p.277

[d]Baur, F., and Philipps, H., Gerl. Beitr. Geophys., Vol. 42, p.160

APPENDIX I

GEOMETRIC CORRECTION AND WATERSHED BOUNDARY DETERMINATION

The Landsat digital data, as it is received from the EROS Data Center, contains a certain amount of spatial distortion when compared to commonly used planimetric map projections. Consequently, it is necessary to spatially transform either the Landsat data to the map projections or vice-versa. For this project the transformation of the planimetric map data to the Landsat spatial format was done for ease of handling.

Following is a procedure for geometric correction which uses watershed boundary determination as an appropriate example of the application of this technique.

The determination of the exact watershed boundary on the Landsat digital data is necessary to:

a. Provide an accurate and meaningful summation of computer generated data for the watershed;

b. Minimize computer-related expenses by analyzing only the area of the watershed on the Landsat data; and

c. Provide a useful visual presentation format for the graphic display of computer generated data for the watershed.

Procedure

1. Watershed boundary delineation

   a. Acquire U.S. Geological (USGS) topographic maps in either 1:24,000 (7.5' series), 1:62,500 (15' series), or 1:250,000 scale formats. (Note: The map scale selected should be compatible with the digitizing facilities available. In the case of this example 1:250,000 scale maps were used due to the large size of the watershed.)

   b. Delineate the watershed boundary in pencil on the map(s) using the elevation contours to find the ridges and other topographic indication of watershed extent such as the drainage network (usually shown in blue). Figure 1 shows a small portion of the Middle Fork of the Feather River Watershed boundary with the corresponding elevation contour lines.

c. Emphasize the final watershed boundary location on the topographic map(s) by inking them in using a fine drafting pen.

2. Control point selection

a. Acquire a 9x9 inch (or larger) simulated color infrared Landsat image, identical to the Landsat digital data to which the watershed boundary will be fitted.

b. Using the USGS topographic maps (on which the watershed boundary has been located) identify a network of points, both inside and outside of the watershed boundaries, which can be seen and accurately located on both the topographic maps and the Landsat simulated color infrared image. Bends in rivers, and lakes and reservoirs will probably provide the majority of useful control points for most areas. In selecting control points on lakes and reservoirs, use the dam or outflow site for point location to minimize the effects of horizontal point placement error due to the raising or lowering of the bodies of water.

c. Once a complete set of control points has been selected and plotted on the USGS topographic map(s), each point should be labeled for future reference. Figure 2 shows the final control point and watershed boundary location for a test watershed, the Middle Fork of the Feather River in the Sierra Nevada Mountains of California.

d. The next step involves the location of the control points on the Landsat digital data. The easiest way to accomplish this task requires displaying the Landsat data on an interactive display system utilizing a color display and keyboard. The general area in which the control is located is first found by overlaying a Landsat quadrant grid (Figure 3) over a Landsat 9x9 inch image (either in print or transparency form). By using these coordinates to determine the general control point location, an image is raised on the interactive display system in which the control point is located. Using a cursor built into the system or by using a grid displayed along with the image on the television screen the operator can find the pixel nearest to the control point and record its absolute x and y coordinates.

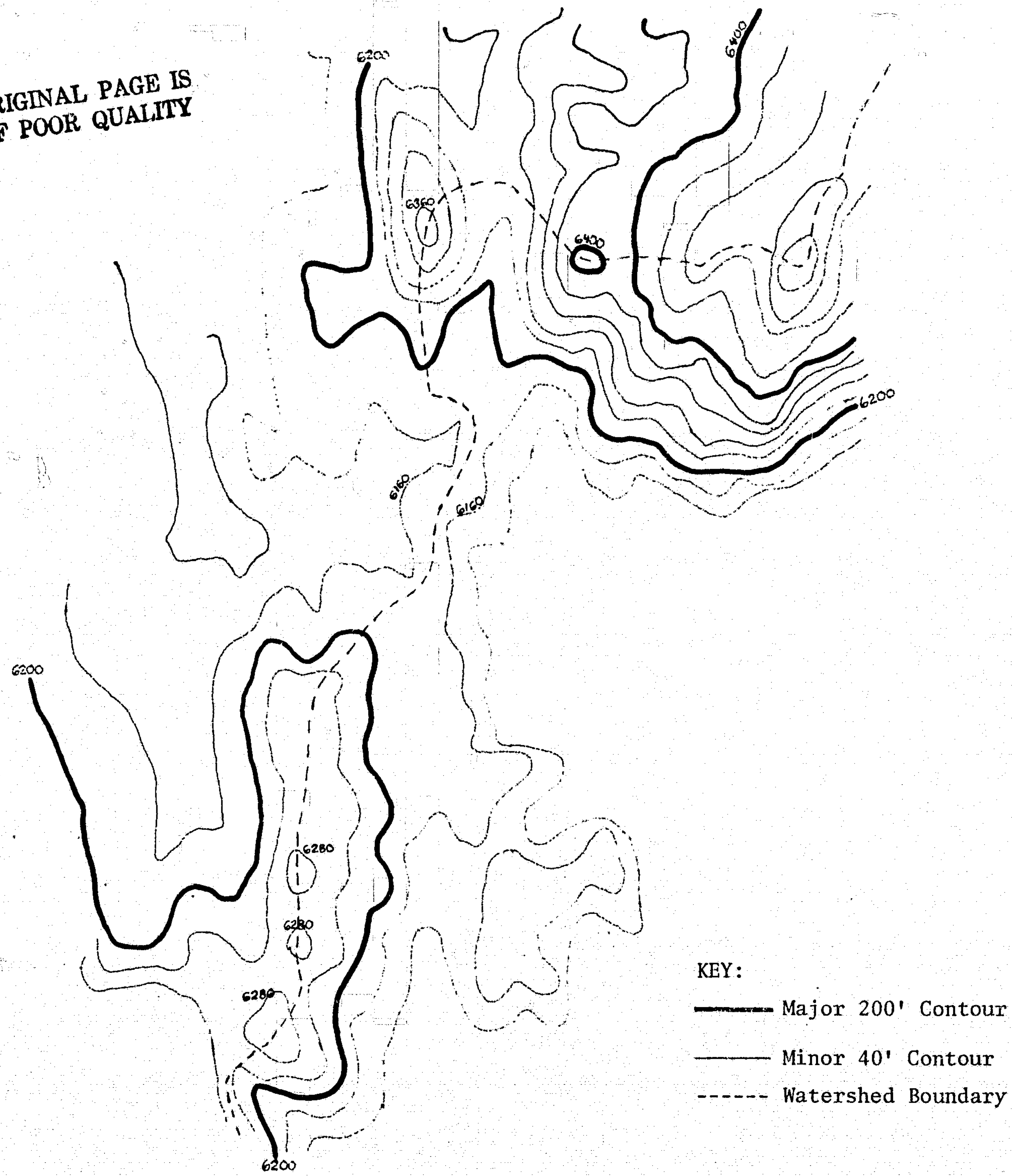

Figure 1. This diagram represents an enlarged portion of the USGS Chilcoot, California, 1:62,000 (15') scale topographic map. The delineated watershed boundary, located on the ridge, is outlined by the dashed line.

3. Digitizing the control points and watershed boundary

   a. The USGS topographic map(s) with the watershed boundary and control points delineated on it should now be digitized. The process of digitizing calculates an x and y coordinate value for each control point and for each point on the line defining the watershed boundary. Since the coordinates of each control point and the line defining the watershed boundary are done on the same map base, the actual geometric location of the watershed boundary in relation to the control points can be calculated and the watershed boundary can be located on Landsat digital data.

   b. To complete the digitizing process, a computer compatible tape (CCT) of the digitized control points and watershed boundary is generated. A suggested format would have the tape organized so that the first file would contain the control point's x and y coordinate values, while the second (and last) file would contain the x and y coordinates of points on the watershed boundary.

   c. Finally, a list of control points should be prepared showing Landsat control coordinates (in pixels) versus digitized control point coordinates. Table 1 gives an illustration of such a listing.

4. Transformation of the digitized watershed boundary into Landsat coordinates

   a. The first step in the process of defining the mathematical relationships between the control points in digitizing and Landsat coordinates is to eliminate those control points which have been miscalculated in either their digitizing coordinates or Landsat coordinates or both. To do this, a linear (first order) regression is used in the form of:

$$\text{XLandsat} = a + b_1 \text{ Xscanner} + b_2 \text{ Yscanner}$$

$$\text{where: } b_2 \text{ Yscanner} \longrightarrow 0$$

$$\text{YLandsat} = a + b_1 \text{ Xscanner} + b_2 \text{ Yscanner}$$

$$\text{where: } b_1 \text{ Xscanner} \longrightarrow 0$$

   The entire set of control points is processed through the first order regression. The control points exhibiting the largest residuals are removed from the data set. The remaining control points are again run through the regression

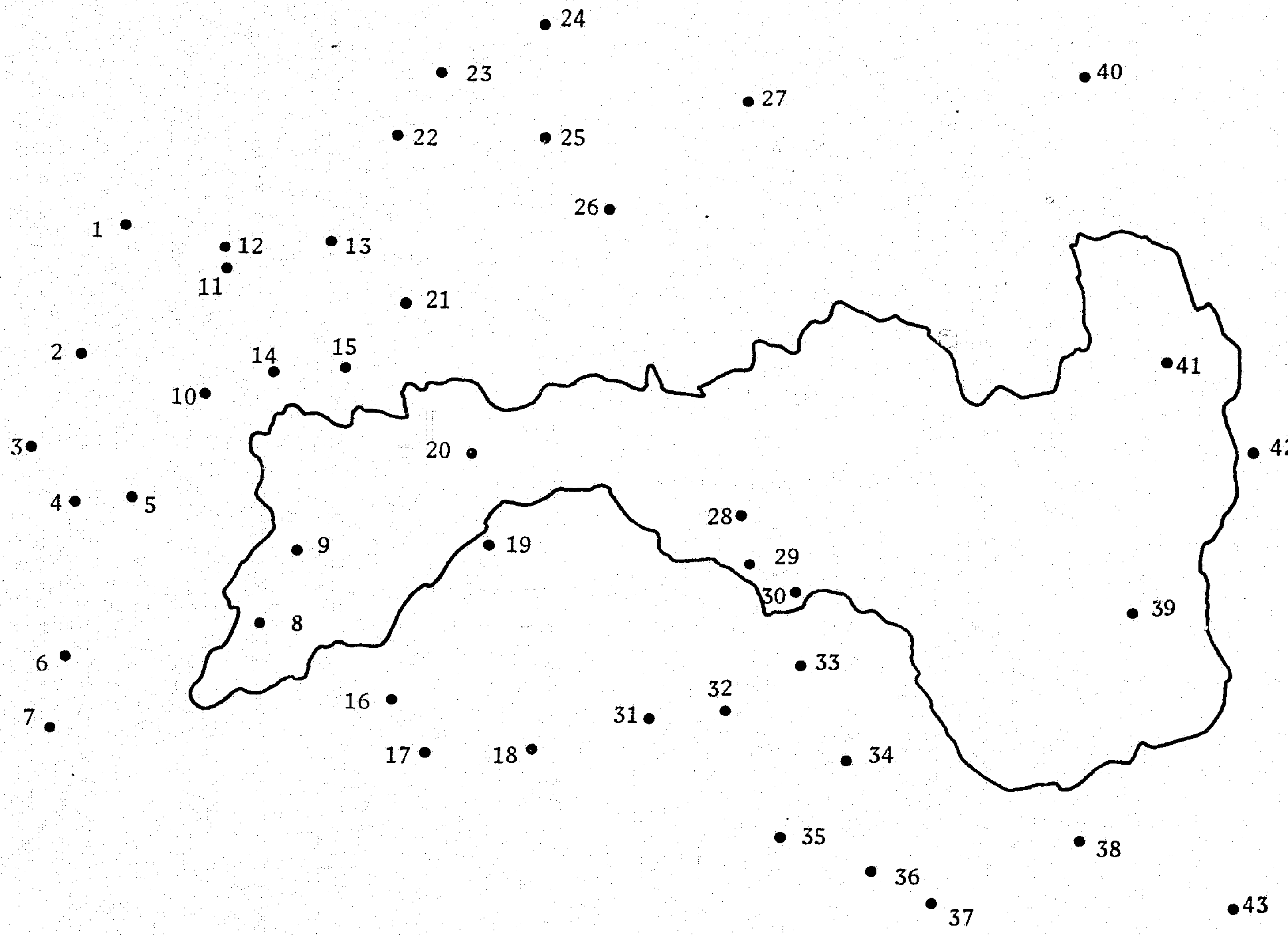

Figure 2. Boundary limits and location of control points within the watershed covering the Middle Fork of the Feather River.

31

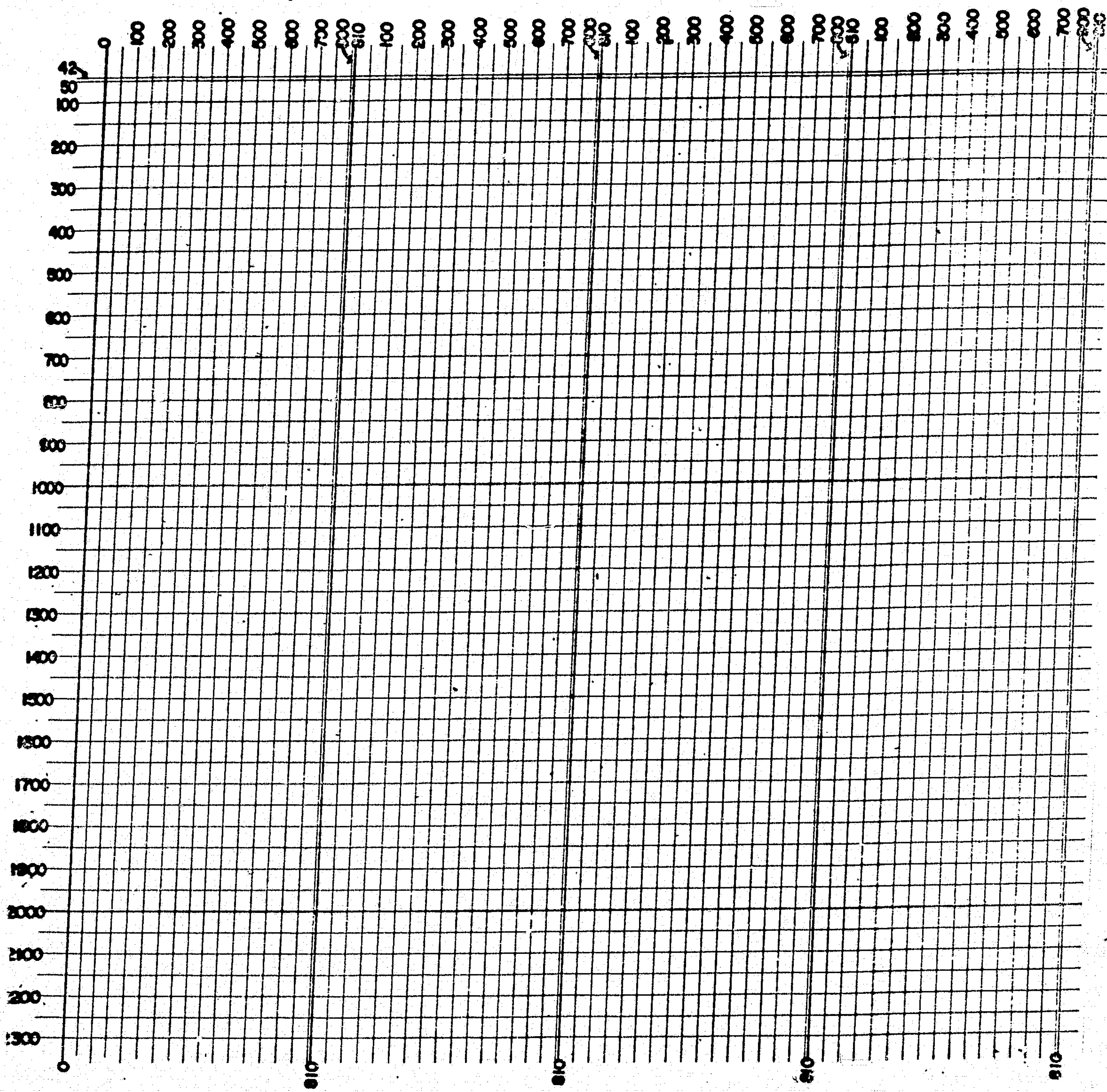

Figure 3. Landsat quadrant grid.

		Digitized Control Coordinates		Landsat Control Coordinates	
Number	Control Point Name	x	y	x	y
1	Philbrook Reservoir	0318	1027	0867	1585
2	Stirling City Res.	0096	1522	0857	1761
3	Magalia Reservoir	0001	1822	0817	1898
4	Concow Dam	0005	2108	0925	1956
5	Bardees Bar	0228	2120	1019	1935
6	Cannon Reservoir	0004	2846	0990	2163
7	Oroville North	0003	3146	1009	2256
8	Evans Bay	0582	2693	1316	2164
9	Sky High Bend	0857	2398	1336	1951

Table 1

Listing of geometric control points with digitized coordinates and Landsat coordinates.

equation and the entire process continued until no control point has a residual exceeding a preset amount ($\pm$ 2.000, for example). Note that since we are fitting points to the Landsat format, all residuals are expressed in terms of Landsat picture elements (pixels). Care should be taken during the process of eliminating those control points that have large residuals, so that an "adequate" number of points will be left in all areas of the watershed. In severe cases, new control points may have to be chosen if large areas of the watershed boundary are left unrepresented.

b. Once the final set of control points has been selected (Step 1), the points are processed once more by a quadratic (second order) regression equation in the form of:

$$XLandsat = a + b_1\ Xscanner + b_2\ X^2scanner + b_3\ Yscanner + b_4\ Y^2scanner$$

$$\text{where: } b_3\ Yscanner + b_4\ Y^2scanner \dashrightarrow 0$$

$$YLandsat = a + b_1\ Xscanner + b_2\ X^2scanner + b_3\ Yscanner + b_4\ Y^2scanner$$

$$\text{where: } b_1\ Xscanner + b_2\ X^2scanner \dashrightarrow 0$$

The coefficient values generated by the second order regression are now used to transform the watershed boundary (previously defined in terms of digitizing coordinates) into a Landsat compatible form.

5. The masking of Landsat digital data with the watershed boundary

a. One of the more important uses of defining the watershed boundary is to "mask" the Landsat digital data. In order to do this the computer compatible tape generated in Step 3.b. of this section is used in conjunction with the second order regression coefficients generated in Step 4.b. previously to produce a new computer compatible tape in which the digitizing coordinate values for the watershed boundary and control points have been converted into Landsat coordinate values.

b. This new computer compatible tape of the watershed boundary and control points now allows Landsat data in any form (raw, recalibrated, classified, etc.) to be masked using the watershed boundary.

Note: The basic procedure described in the fourteen steps above represents the geometric correction and subsequent application of a specific type of ancillary data (planimetric watershed boundary) to Landsat digital data. The same basic procedure applies to all other ancillary data that is to be "fitted" to Landsat satellite data, modified as necessary.

APPENDIX II

REMOTE SENSING-AIDED PROCEDURE FOR VEGETATION/TERRAIN ANALYSIS

INTRODUCTION

Knowledge of the spatial distribution of vegetation/terrain features within a watershed is necessary for determining evapotranspiration ratios and generating of albedo indices for radiation models. Albedo is used directly as an input to the shortwave radiation model, which ultimately is used in the watershed-wide calculation of evapotranspiration.

The procedure used to develop the vegetation/terrain distribution for a given watershed is based upon the computer-aided classification of Landsat digital data. Basically this classification involves the selection of training statistics based on the unsupervised classification of specific test sites located throughout the watershed and surrounding area. Those training statistics, representing spectral information about specific vegetation/terrain classes, are then used to derive a supervised, watershed-wide classification to yield the final vegetation/terrain distribution.

Procedure

1. Gathering of remote sensing and ancillary data

   a. Determine a specific Landsat scene which satisfies certain minimum criteria such as:

      1) High sun angle so that shadows on the landscape are held to a minimum.

      2) Cloud free imagery in the area to be classified.

      3) Freedom from bad data on the Landsat data such as bad scan lines, etc.

      4) Snow-free imagery, to as large an extent as possible

      These criteria imply, then, a late spring through early fall date of Landsat imagery. In attempting to select a date within this period of time, actual spectral response of major vegetation types should be considered. If, for instance, annual grassland is a major vegetation component within a watershed, then it may be appropriate

35

to choose a date in which the vegetation is most highly contrasted with the surrounding vegetation complex. This date, then, may be in early summer to early fall when the grasslands have lost their near-infrared spectral response due to drying.

b. Once a date of Landsat imagery has been selected and acquired (in both a hardcopy and digital tape form), a set of high altitude aerial photographs should be acquired that covers the area to be analyzed. The date of this imagery should depict the vegetation complex in the same physiologic state as the Landsat scene selected. It does not necessarily need to be taken in the same year as the Landsat scene.

c. Watershed boundary descriptions such as those used in the Geometric Correction and Watershed Boundary Determination section should be obtained. These will aid in helping to select the appropriate spectral training sites.

2. Selection of spectral training sites

a. Using the Landsat imagery, the aerial photography, and the watershed boundary maps, training sites should be selected throughout the watershed and surrounding areas. These sites should encompass the spectral variation that is likely to occur throughout the watershed. This task requires the extensive knowledge of an analyst thoroughly familiar with the watershed.

b. The selected training areas should be located on the Landsat digital data and the aerial photography. The location of these sites on the Landsat digital data is most easily accomplished through an interactive television display of the Landsat data. The x and y coordinates of the training site block corners can be found easily by displaying the Landsat image and determining the training site location from its general position on either the aerial photography or watershed boundary maps. The exact position of the training site should be defined by the Landsat image of the training site. This area can now be plotted with greater flexibility on the aerial photography. This is due to the display restrictions usually associated with the Landsat digital data. Figure 1 shows the spatial distribution of Landsat training sites throughout a sample watershed, the Middle Fork of the Feather River. Figures 2 and 3 illustrate the appearance of a specific training site (Block No. 1) on high altitude aerial photography and Landsat imagery respectively.

3. Unsupervised classification of the training sites.

   a. Once the position of the training sites on the Landsat digital data has been determined, a computer compatible tape is made with each training site occupying one file on the tape.

   b. The next step is to use an unsupervised classification algorithm to "cluster" the Landsat pixels at each training site into like groups. A commonly used computer program for this purpose is the Iterative Self-Organizing Data Analysis Technique(A) or ISODATA, which was originally developed by Hall and Ball (1965 and 1967). A variation on this program, called ISOCLAS, was developed by Kan and Holley (1972) specifically for multispectral scanner data such as Landsat. This program, ISOCLAS, is probably the most commonly used program in use for unsupervised classification. Thorough familiarity with this, or any other program used for unsupervised classification is suggested before attempting this phase of the watershed-wide vegetation/terrain classification.

   c. The end product of an unsupervised image classification program such as ISOCLAS is a list of image "classes" defined by their spectral mean, standard deviation, and co-variance. Table 1 shows these parameters for a single training site which will be used for the remainder of the examples. These classes will now become the basis for the final supervised classification for the entire watershed.

   d. In order to attempt to assign specific vegetation/terrain classes to each cluster, a technique called 7/5 ratioing is used to help "spectrally" organize the data. Table 2 depects the 7/5 ratio information for the training site cluster data shown in Table 1.

   e. To help better organize the data for display purposes, unique colors are given to each cluster starting with the lavenders and the reds for the high 7/5 ratio clusters, down through the browns and oranges, the yellows, the greens, and finally the blues for the lowest 7/5 ratio clusters. A visual output, such as could be seen on a television monitor is shown in Figure 4.

   f. Using the aerial photography of the specific training site being classified (Figure 1) and the 7/5 ratio, the analyst can begin to group and separate the various clusters into meaningful vegetation/terrain classes. Table 3 shows the result of this process. Note the arrangement of the resultant class/cluster groupings.

37

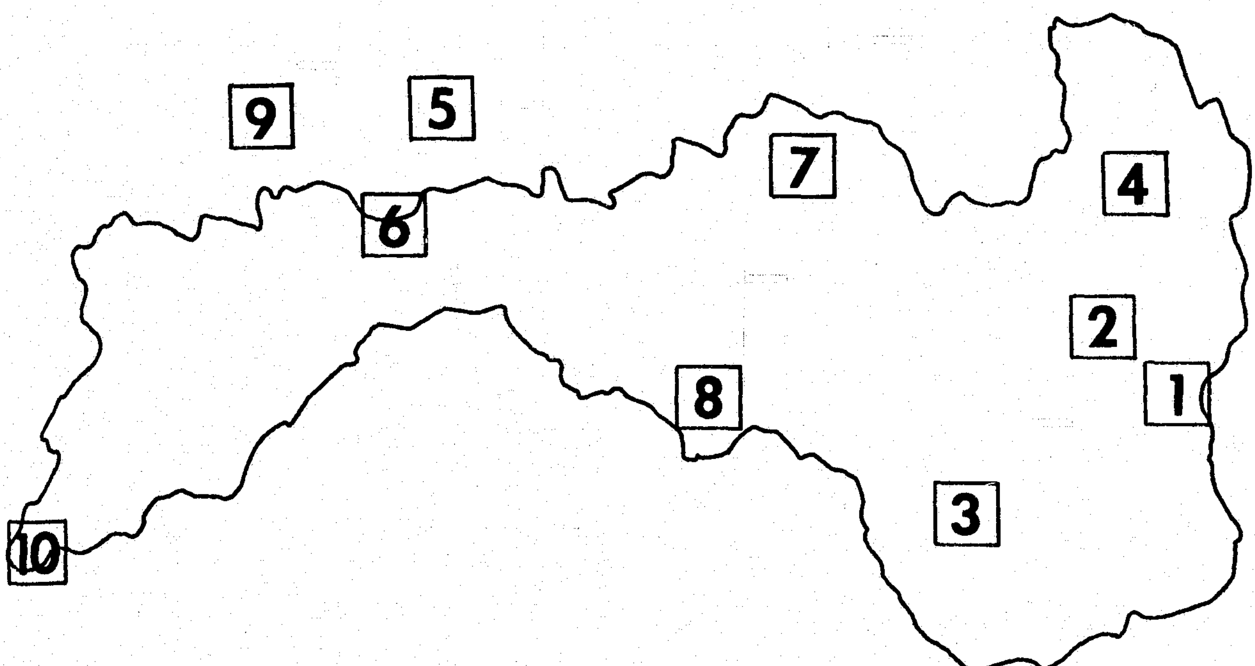

Figure 1. Distribution of Landsat test sites throughout the Middle Fork of the Feather River Watershed and surrounding area.

Area 1	Sierra Valley Mountains
Area 2	Sierra Valley Area 1
Area 3	Sierra Valley Area 2
Area 4	Frenchman Reservoir Area
Area 5	Quincy/American Valley
Area 6	Serpentine Area
Area 7	Davis Lake Area
Area 8	Gold Lake Area
Area 9	Silver Lake Area
Area 10	Middle Fork /Lake Oroville

Figure 2. Small scale aerial photograph of ISOCLAS block 1 taken from a U-2 aircraft on September 9, 1975.

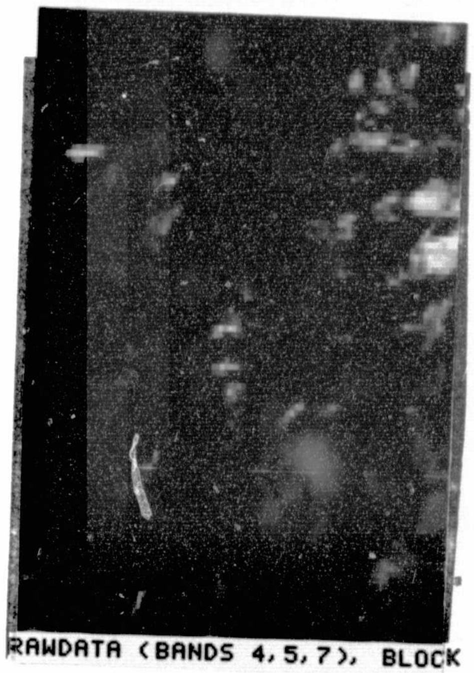

Figure 3. Landsat "raw" image of ISOCLAS block 1. Simulated color infrared rendition using MSS bands 4, 5, and 7.

4o

Cluster	MSS Band 4		MSS Band 5		MSS Band 6		MSS Band 7	
	Mean	STD	Mean	STD	Mean	STD	Mean	STD
1	21.27	1.20	28.81	2.26	33.79	2.19	17.34	1.44
2	30.37	1.25	31.68	1.75	35.95	1.62	18.19	1.13
3	24.27	2.16	23.90	1.63	29.89	1.81	15.99	1.57
4	23.73	1.35	35.57	2.08	38.70	2.64	19.62	2.49
5	18.97	2.05	15.66	2.17	31.83	2.05	19.21	1.47
6	28.34	1.05	27.98	1.65	31.99	1.64	16.44	1.29
7	17.53	1.75	14.49	1.72	26.28	1.95	15.42	1.52
8	32.29	1.26	35.19	1.86	39.28	1.48	19.77	1.18
9	22.33	2.17	20.98	2.33	36.80	2.61	21.57	1.77
10	21.79	1.68	19.34	1.74	27.33	2.00	15.17	1.68
11	36.61	5.78	41.69	5.81	43.66	4.19	21.67	2.35
12	26.99	2.26	27.06	2.15	39.09	2.29	21.82	1.79
13	37.52	1.51	43.76	1.88	47.78	1.49	23.98	1.20
14	39.94	3.99	50.24	2.93	54.98	3.75	27.24	1.99
15	27.13	4.10	46.83	8.59	46.85	7.28	24.80	5.27
16	33.49	1.30	37.30	2.18	43.16	1.51	22.03	1.52
17	26.57	1.72	38.72	3.05	43.94	1.98	22.75	1.76
18	19.71	36.89	35.86	35.33	0.00	0.00	0.00	0.00
19	.02	.15	4.49	15.00	0.00	0.00	2.84	11.05

Table 1. Cluster means and standard deviations for each of the nineteen clusters by Landsat Multispectral Scanner (MSS) bands for ISOCLAS block 2. Note the spurious means and standard deviations for clusters 18 and 19, indicating that these two clusters will not be reliable for further use.

Table 2. Band 7/band 5 ratios and color assignments for ISOCLAS block 1

Band 7/Band 5 Ratio*	Numerical Order	Cluster	Color Assignment Group
2.4534	1	5	Lavenders & Reds
2.1284	2	7	
2.0276	3	9	
1.6127	4	12	
1.5688	5	10	Browns & Oranges
1.3381	6	3	
1.2037	7	1	
1.1812	8	16	
1.1751	9	17	Yellows
1.1751	10	6	
1.1484	11	2	
1.1236	12	8	Greens
1.1032	13	4	
1.0960	14	13	
1.0844	15	14	Blues
1.0592	16	15	
1.0396	17	11	
------	18	--	Black
------	19	--	

*The actual equation for the Band 7/Band 5 ratio is:

2 x (Band 7 mean scene brightness value of cluster n) ÷ (Band 5 mean of scene brightness value of cluster n) where n goes from 1 to 17 inclusively.

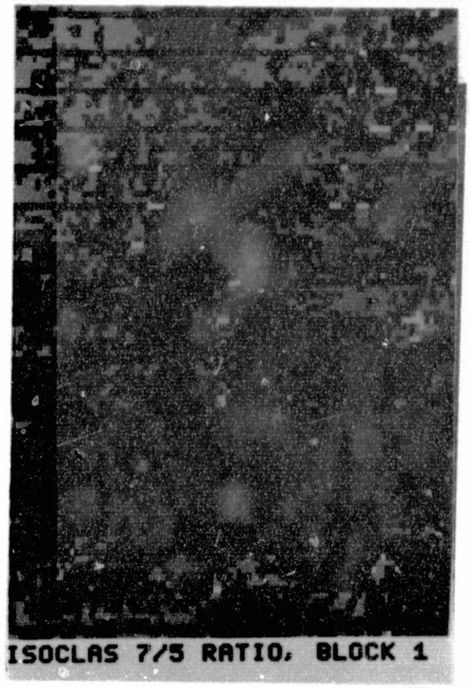

Figure 4. Band 7/band 5 ratio display of ISOCLAS block 1 based on Landsat data

43

Table 3. List of 7/5 ratios and clusters identified on type ISOCLAS block 1 for each vegetation-terrain class.

Vegetation/Terrain Class	Cluster	Band 7/Band 5 Ratio
High density eastside conifer	5	2.4534
	7	2.1284
Low density eastside conifer	9	2.0276
Brush/Chaparral	10	1.5688
Sagebrush/Bare Soil	12	1.6127
	2	1.1484
	4	1.1032
	8	1.1236
	16	1.1812
Sagebrush	1	1.2037
	3	1.3381
	6	1.1751
Bare Soil	11	1.0396
	13	1.0960
	14	1.0844
	15	1.0592

g. Once all of the training sites have been processed in this manner, each site should be ground checked to verify the classification. Using the Landsat imagery that has been clustered, the aerial photography, and topographic maps, each preliminary classification can be checked and verified or classification amended, as appropriate. Figure 5 shows a display of a final unsupervised classification of a single training site.

4. Selection of training class statistics

a. Each cluster has a single mean and standard deviation in terms of Landsat spectral values assigned to it, for each training site. Since it is possible that certain clusters could be "confused" with each other, a statistical test is necessary to determine their "separability". A methodology for the determination of class separability based on the Scheffé method of multiple comparison has been applied to this analysis. Statistical analysis using the Scheffé method allows significance probabilities to be calculated for all cluster pairs. These probabilities are displayed in matrix form. Class pairs with significance probabilities below specific threshold values are considered to be separable for classification purposes. Thus individual clusters can be statistically compared to other clusters within a vegetation/terrain group and all other clusters in the vegetation/terrain classes. Table 4 represents an example of the Scheffé multiple comparison test run on all clusters determined to fall into a specific vegetation/terrain class. Cluster pairs determined to be separable are designated by the symbol "0". Cluster pairs determined to not be separable are designated by the symbol "+". The significance level for the particular application of the Scheffé multiple comparison test was set at $\alpha = .10$. Clusters form various vegetation/terrain groups (i.e., those falling in some broad band of classification; for example, the coniferous forest vegetation/terrain group may include red fir, mixed conifer, eastside pine, pure fir, etc.) are systematically compared to one another until (if possible) unique sets of clusters are found which represent all desired vegetation/terrain classes and are all separable using the Scheffé test.

b. The resultant set of clusters now represents each vegetation/terrain class desired for the watershed-wide classification. Table 5 lists the mean, standard deviation and co-variance for each selected cluster.

45

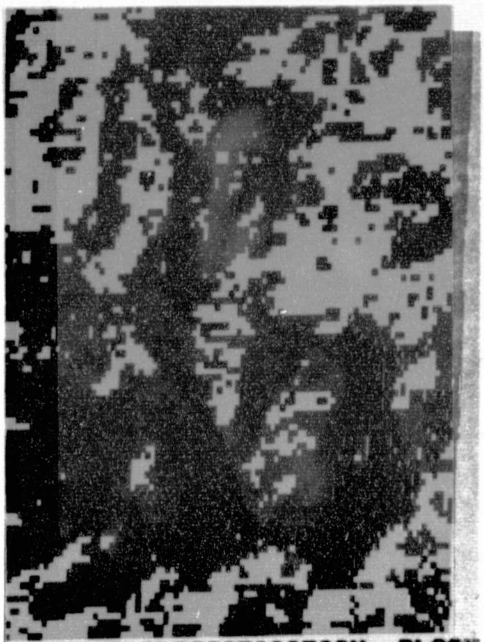

Figure 5. Classified ISOCLAS display of block 1 based on Landsat data

Identification Key

Color	Vegetation/Terrain Type
Brown	Bare Soil
Red	High Density Eastside Conifer
Green	Low Density Eastside Conifer
Yellow	Brush
Dark Blue	Sagebrush
Light Blue	Sagebrush/Bare Soil

Table 4. Scheffe multiple comparison test for brush and brush-related vegetation types. "0" indicates no confusion while "+" indicates confusion between class pairs at a significance level of .10.

	Class 1	Class 2	Class 3	Class 4	Class 5	Class 6	Class 7	Class 8	Class 9	Class 10	Class 11	Class 12	Class 13	Class 14	Class 15
Class 1	/	+	0	0	0	0	0	+	0	+	0	0	0	+	+
Class 2	+	/	+	+	+	+	+	+	+	+	+	0	0	+	+
Class 3	0	+	/	0	+	+	+	0	0	0	+	+	+	+	0
Class 4	0	+	0	/	+	0	0	+	+	0	+	0	0	0	+
Class 5	0	+	+	+	/	+	+	0	+	0	+	+	0	+	+
Class 6	0	+	+	0	+	/	+	0	0	+	0	+	+	+	0
Class 7	0	+	+	0	+	+	/	0	0	0	+	+	0	0	0
Class 8	+	+	0	+	0	0	0	/	+	+	0	0	0	+	+
Class 9	0	+	0	+	+	0	0	+	/	0	+	0	0	+	+
Class 10	+	+	0	0	0	+	0	+	0	/	0	0	+	+	+
Class 11	0	+	+	+	+	0	+	0	+	0	/	0	0	+	+
Class 12	0	0	+	0	+	+	+	0	0	0	0	/	0	0	0
Class 13	0	0	+	0	0	+	0	0	0	+	0	0	/	+	0
Class 14	+	+	+	0	+	+	0	+	+	+	+	0	+	/	+
Class 15	+	+	0	+	+	0	0	+	+	+	+	0	0	+	/

Cluster	MSS Band 4		MSS Band 5		MSS Band 6		MSS Band 7	
	Mean	STD	Mean	STD	Mean	STD	Mean	STD
1	30.37	1.25	31.68	1.75	35.95	1.62	18.19	1.13
2	28.34	1.05	27.98	1.65	31.99	1.64	16.44	1.29
3	21.79	1.68	19.34	1.74	27.33	2.00	15.17	1.68
4	36.61	5.78	41.69	5.81	43.66	4.19	21.67	2.35
5	34.67	1.55	39.02	1.55	43.65	1.32	22.81	1.19
6	21.10	2.14	14.45	1.41	64.66	1.82	42.94	1.68
7	34.34	1.53	39.90	1.86	48.43	1.64	26.13	1.36
8	36.45	1.54	42.43	1.56	46.60	1.99	24.43	1.66
9	24.95	2.29	25.83	1.95	44.22	2.23	27.54	1.57
10	31.60	1.39	34.68	1.92	38.97	1.79	20.46	1.66
11	21.73	2.12	20.13	2.44	20.10	1.39	25.81	1.04
12	22.70	2.56	21.86	2.43	23.13	2.25	10.80	1.83
13	17.13	1.66	11.88	1.80	28.96	1.37	17.63	1.13
14	17.36	1.71	12.43	1.72	32.91	1.52	20.64	1.07
15	26.49	2.28	26.49	2.29	43.90	1.61	26.06	1.77
16	17.98	1.98	12.48	1.23	43.69	2.53	28.63	2.35
17	17.47	1.72	13.32	2.04	31.41	1.51	19.68	1.35
18	18.81	2.08	13.63	1.90	51.63	3.17	34.30	2.27
19	32.23	3.60	38.82	2.81	43.63	2.91	22.92	2.38
20	15.72	1.69	10.00	.84	6.25	1.23	1.07	.65
21	16.30	1.74	11.92	1.71	23.71	1.76	14.37	1.41
22	14.73	1.17	6.73	.49	4.79	.93	1.04	.66
23	17.78	1.78	13.31	1.73	30.67	1.32	19.21	1.16
24	19.39	1.91	14.63	1.79	45.67	1.74	29.84	1.60
25	16.09	1.75	9.58	2.09	11.15	2.12	4.91	1.98
26	14.16	1.84	7.73	6.75	4.97	1.17	1.19	.67
27	22.86	1.78	19.73	1.68	37.34	2.10	21.64	1.38
28	19.39	2.12	14.22	2.14	31.76	1.24	18.86	1.11
29	25.53	2.30	24.49	2.06	40.65	1.77	23.01	1.32
30	28.89	4.24	25.85	4.44	29.48	3.60	13.77	2.83

Table 5. Cluster means and standard deviations for each of the thirty clusters by Landsat Multispectral Scanner (MSS) bands for the final CALSCAN training set.

5. Supervised classification of vegetation for the entire watershed

a. The cluster means, standard deviation, and co-variances for the set determined above are now used to drive the final, supervised classification of the watershed using digital Landsat spectral data. The computer compatible tape of the watershed boundary (mask) generated in Step 14 of the Geometric Correction and Watershed Boundary Determinations section (Appendix I) is now used to control the area on the Landsat data that is to be classified. The "raw" Landsat digital data in conjuction with the "mask" tape are now run through a supervised classification routine. The classification routine commonly used in conjunction with the classification of Landsat data is a discriminant analysis routine called LARSYSA. LARSYSA is a classification algorithm based on a maximum likelihood classifier developed at Purdue University. A similar version, based on LARSYSA, used at the University of California, is called CALSCAN. Both classifiers perform the same basic function, assignment of each pixel within the watershed to one of the training clusters selected from the unsupervised classification of the training sites. The final result for such a classification can be seen for the ISOCLAS test block in Figure 6, while the final watershed-wide classification is shown in Figure 7.

49

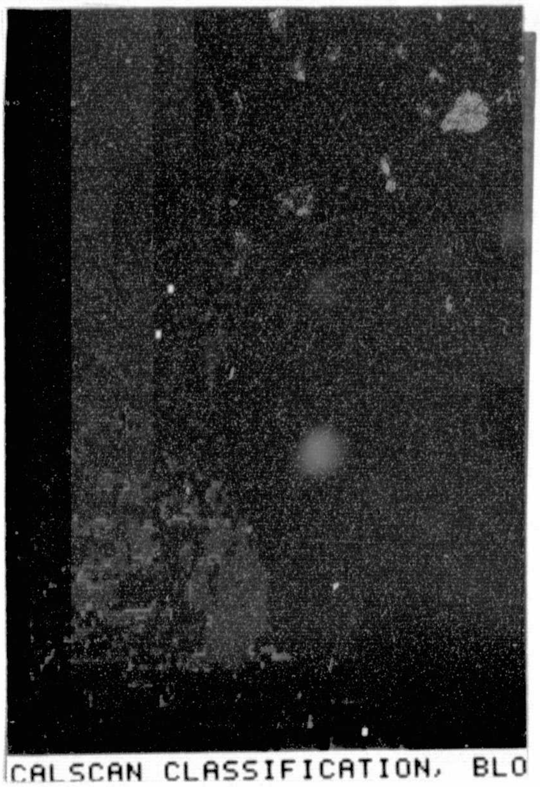

Figure 6. CALSCAN discriminant analysis classfication of block 1. The statistical training for this classification was derived form the ISOCLAS classification and applied to the Landsat raw digital data.

Identification Key

Color	Vegetation/Terrain Type
Lavender	Sagebrush
Purple	Sagebrush/Bare Soil
Off White	Bare Soil
Yellow	Mesic Grassland
Red	Mixed Conifer
Dark Green	Brush
Light Green	Xeric Brush

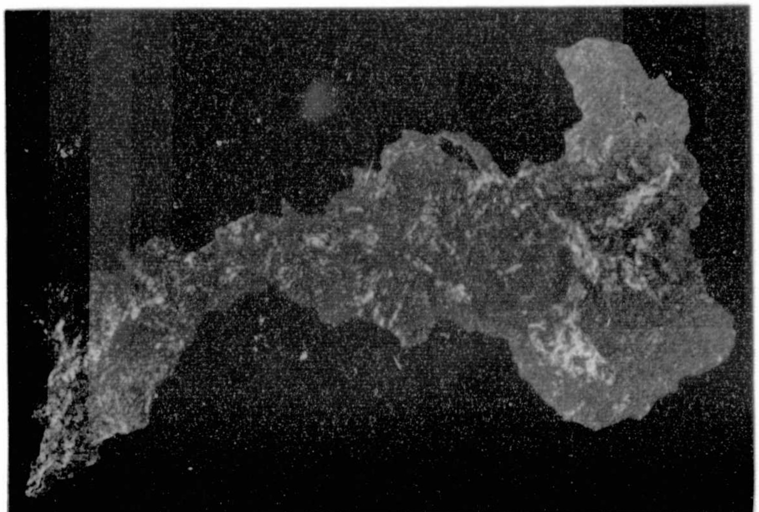

Figure 7. CALSCAN discriminant analysis vegetation/terrain classification of the Middle Fork of the Feather River Watershed.

Identification Key

Color	Vegetation/Terrain Type
Lavender	Sagebrush
Purple	Sagebrush/Bare Soil
Off White	Bare Soil
White	Rock
Orange	Agricultural
Yellow	Marsh/Mesic Grassland
Red	Mixed Conifer
Orange/Red	Red Fir
Light Blue	Riparian Hardwoods
Blue/Green	Mesic Brush
Dark Green	Brush
Light Green	Oakwood/Xeric Brush
Dark Blue	Water

APPENDIX III

STEPWISE PROCEDURE FOR TOPOGRAPHIC ANALYSIS

Topographic characteristics of the watershed are some of the major factors affecting the amount of solar radiation. These topographic characteristics include elevation, slope, and aspect. The following is a procedure for quantification of these parameters along with three different methods of control point selection and a set of algorithms for elevation interpolation and slope and aspect generation.

For a large portion of the country, digital terrain computer compatible tapes are available. These tapes may be obtained either from the Defense Mapping Agency (DMA), Topographic Center, or from the U.S. Geological Survey (USGS), Digital Elevation Model. If these digital tapes for the study area are available, the part of the following procedure for digitizing the elevation from USGS topographic maps may be eliminated. Otherwise, the following procedure will be adequate for preparation of elevation, slope, and aspect maps and digital tapes required for resource inventory and management.

1. Procedure for topographic analysis

   a. Acquire USGS topographic series maps, scale 1:250,000 so that the area analyzed is covered. (Note: the same maps used for the Geometric Control and Watershed Boundary Determination Section may be used for this phase of the work as well.)

   b. If the topographic maps used do not have the study area outlined on them, outline the area at this time.

   c. If there are two or more topographic maps needed to cover the study area, carefully trim and join the maps, taking care to maintain the planimetric accuracy as much as possible.

   d. If the topographic maps used do not have control points (for geometric correction purposes) located on them, see the Geometric Correction and Watershed Boundary Determination Section (Appendix I) of the Manual.

52

e. The selection of topographic control points is the next phase of the topographic analysis procedure. The actual technique used depends on the nature of the elevation, slope, and aspect generating algorithms used. Three methods for selection of control points are discussed in Section 2. A series of algorithms for elevation interpolation and slope and aspect generation is described in Section 3.

f. Each topographic control point is given x, y and z coordinate values. The x and y values are relative to the geometric correction points and are used for two-dimensional spatial location of the z or elevation value. The topographic control point and geometric control point networks, as located on the USGS topographic maps, are now digitized. This process assigns x and y values to all control points. The geometric control points should be digitized in a predetermined order so as to facilitate their accurate identification. The topographic control points should be digitized in such a fashion as to facilitate the assignment of a specific z (or elevation) value, to each control point.

g. To complete the digitizing process, a computer compatible tape (CCT) is generated for the topographic control points. The z value for each control point should be added to the digitized topographic control point data. This may be done on either the CCT or on punched cards (the x and y coordinates coming from the CCT with z values punched in manually).

h. Using the regression coefficients generated previously or that will be generated specifically for this analysis (for both counts see the Geometric Correction and Watershed Boundary Determination Section, Appendix I) in conjunction with the x, y and z values for each topographic control point, the x and y coordinates (in digitizing coordinate values) are transformed to Landsat-based coordinates.

i. The transformed x and y coordinates as well as the unchanged z value are now processed through an "interpolator" to assign a z (elevation) value to each Landsat pixel position. This "interpolation" of intermediate x y coordinate positions for elevation can be accomplished by a number of algorithms. In Section 3, one type of algorithm for elevation interpolation is described.

j. The interpolation is processed by a computer, the output usually being in the form of a CCT and supplementary paper output. The elevation interpolation may be displayed using the CCT on an interactive television display system. An example of the final product, using different colors for each elevational zone, can be seen in the case study.

k. The generation of slope and aspect maps is done by using another algorithm which uses the interpolated elevation values as the input data. An example of the output products of this algorithm can be found in the case study.

2. Selection of topographic control points

Three procedures will be shown in this section to give the user some idea of the possibilities for topographic control point selection. The ultimate decision for location of topographic control points will depend on the available computer system (and associated software routines) as well as the nature of the algorithms used for generating the elevation, slope, and aspect data.

Method a. This procedure involves the use of elevation contour isolines. Each isoline falling within the study area is digitized. By digitizing one elevation zone at a time, the data may be organized so that assignment of elevation values to digitized isolines is very simple and straightforward. If a computer compatible tape is used to store the digitized contour isolines, a separate file may be generated for each different elevation zone. Figure 1 shows a hypothetical distribution of control points using this technique. It should be noted that as few points as possible should be selected along each isoline to keep processing costs to a minimum. This method of control point selection is probably the most accurate and undoubtedly the most expensive due to the large number of control points usually selected.

Method b. The selection of topographic control points along ridge tops and valley bottoms is a commonly used procedure. Control points are located on ridge tops (including watershed boundaries, if they are

54

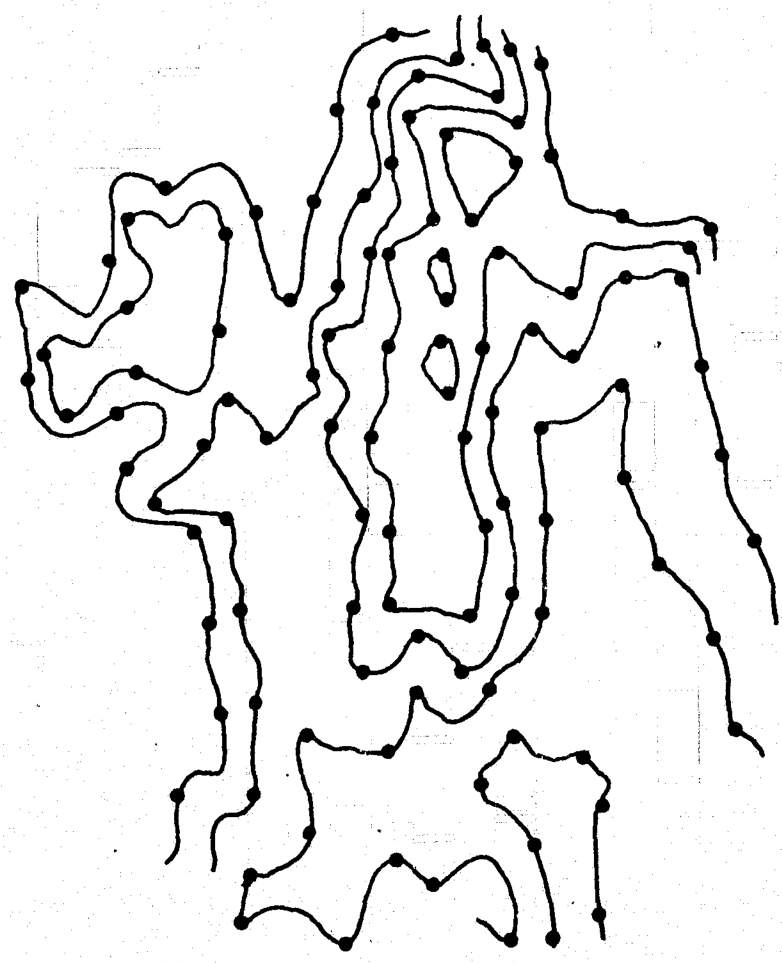

Figure 1. Example of topographic control point selection along contour isolines. If each set of points selected along a given isoline is filed separately, assignment of elevation values is eased.

to be used) and in the valley bottoms (generally along stream courses). Control points are selected at the ridge intersections and midway (approximately) down ridges running into valleys. Subsequently, control points are also located at stream intersections and midway up streams from their headwaters (Figure 2). The control points selected are digitized. The difficulties of this method involve the location of the ridge tops and valley bottoms, and the assignment of elevation values to each control point.

Method c. This method uses a predetermined grid which is laid over the study area. Each grid intersection is located as a control point and the elevation recorded. This system does not necessarily require the use of a digitizer due to the systematic nature of the control point network (however, a digitizer can be used). Again, the assignment of an elevation value to each control point is timely; however the nature of the control point selection procedure allows a tight control over the number of control points selected, thus helping to reduce costs.

Note: In order to assure as accurate values as possible for elevation slope, and aspect, control point selection should occur not only within the study area but also just beyond the boundaries. This assures that values along the actual study area boundary are reliable.

3. Sample algorithms used for elevation, slope, and aspect generation

The following formulas are those used by the Remote Sensing Research Program at the University of California at Berkeley, for topographic analysis. They are representative of those commonly in use.

56

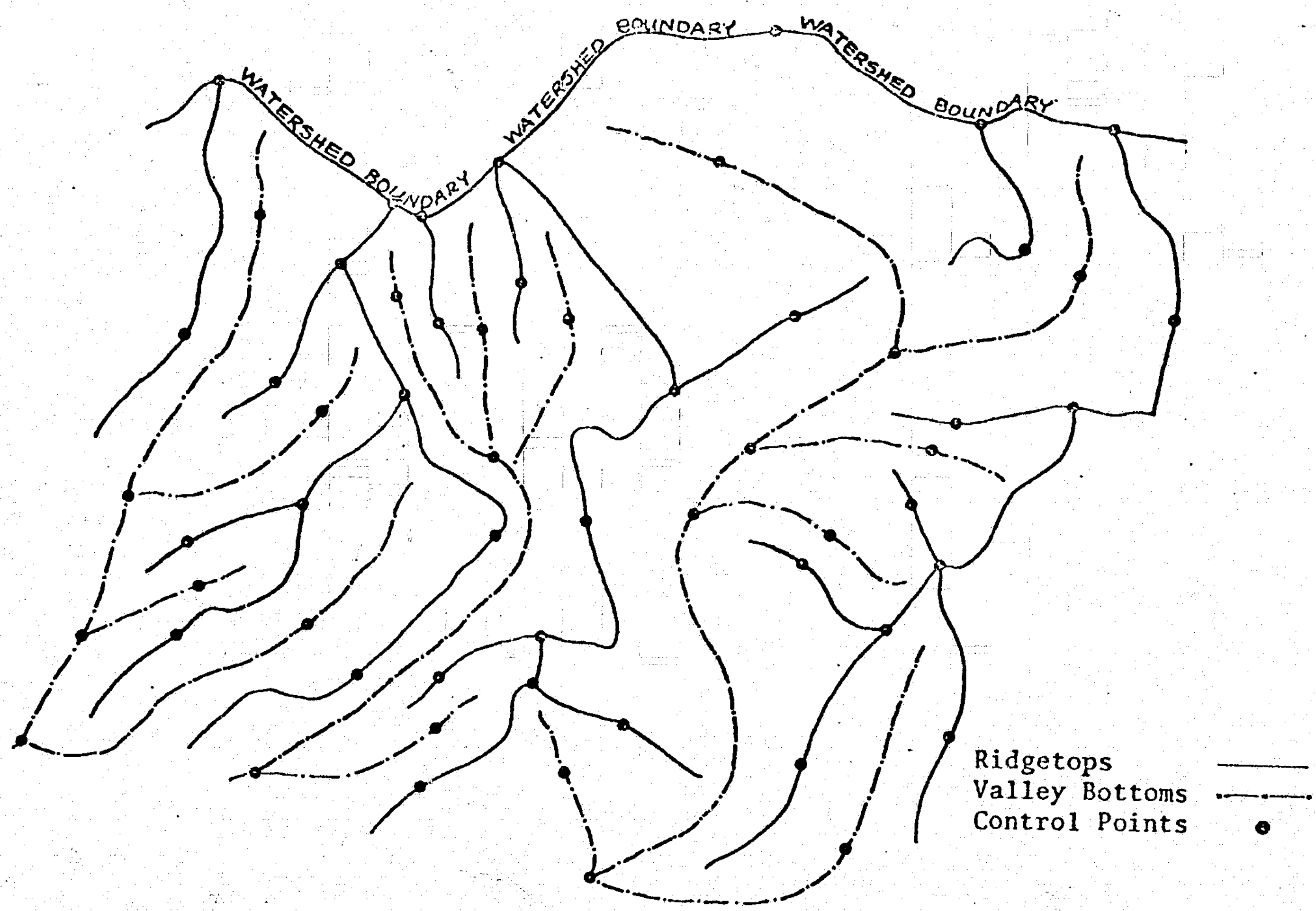

Figure 2. Location of control points on ridge tops and valley bottoms. Note the location of occasional control points along long stretches of ridge tops and valley bottoms.

The digitized values of control points are used to drive the elevation-determining algorithm,

$$E(x,y) = \frac{\sum_{i=1}^{n} \frac{Ei}{(\Delta i)^2}}{\sum_{i=1}^{n} \frac{1}{(\Delta i)^2}}$$

where: Δi = the distance from (x,y) to control point i,
Ei = the elevation of control point i,
n = the number of control points within range of (x,y)
$E(x,y)$ = the elevation of point (x,y).

which uses the x,y,z coordinates of the control points to assign a z coordinate (elevation) to each Landsat pixel. The actual z coordinate represents a zone of elevation per pixel rather than an absolute value.

Determination of a "normal" vector is necessary for pixel slope and aspect calculation. This "normal" vector is a directional variable that originates in the center of each pixel and locates a direction that is 90 degrees to the surface of the pixel. This vector is expressed in triple coordinates (n_x, n_y, n_z), where the center of the pixel is considered to be the origin (o, o, o), and the triple coordinates are the coordinates in three dimensions (x, y, z).

For determining slope and aspect, the "normal vector for a pixel is computed by using the pixel's position relative to the pixels to the right and below. The "normal" vector, $\vec{n}$, is then the cross product of the two vectors in x (the pixel to the right) and y (the pixel below) directions.

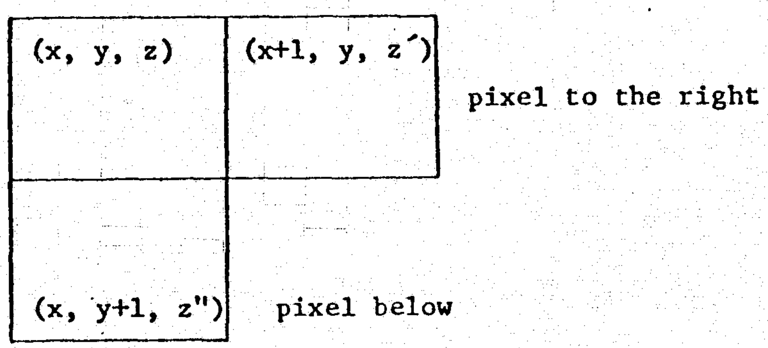

Using the vector's cross-product formula, the normal vector is

$$\vec{n} = (x + 1, y, z - z') \times (x, y + 1, z'' - z)$$

$$= \{[(x + 1)(y+1) - xy] - [(x+1)(x''-z) - x(z - z''],$$

$$[(n + 1)(y+1) - n\, y]\}$$

Once the "normal" vector, $\vec{n}$, is computed, the slope is calculable since it is the angle between the normal vector and the vertical vector (o, o, 1), 0, subtracted from $\frac{\pi}{2}$ in radians. Therefore

$$\theta = \text{arc cos } \left(\frac{n_\delta}{\|\vec{n}\|}\right) \qquad \text{and}$$

$$\text{slope} = \frac{\pi}{2} - \theta \quad \text{in radians, where}$$

$$\|\vec{n}\| = n_x^2 + n_y^2 + n_z^2$$

then slope is converted to percent.

The aspect is determined from the (x,y) projection of the normal vector. The degrees away from true North will determine the aspect,

$$\phi = \arctan \left(\frac{n_y}{n_x}\right), \text{ where}$$

ϕ is the angle from the x-axis in radians.

This is then converted to degrees and added to 90 degrees to give the aspect in degrees from the true North direction.

APPENDIX IV

PREPARATION OF CLIMATIC DATA MAPS FOR USE IN RADIATION AND EVAPOTRANSPIRATION MODELS

This appendix entails three sections: 1) collection and interpolation of climatic data based on ground meteorological stations data; 2) acquisition and processing of NOAA-4 satellite thermal data; and 3) a complete version of a computer algorithm for geometric correction and temperature calibration for NOAA-4 satellite data. Section 3 was originally provided by NOAA's National Environmental Satellite Service and was modified by UC Davis, Department of Electrical Engineering (Algazi group). One may develop his own algorithm based on the technique described in Section 3 and geometric package programs available from the NOAA-NESS office.

1. Collection and interpolation of data from ground meteorological stations

   a. Identification and selection of ground meteorological stations

      Subsequent to the delineation of the watershed boundary (described in Appendix I) on a useable map base (preferably a USGS quadrangle, the scale of which will depend on the size of the watershed) one should consult the publication titled "Climatological Data" provided by the National Oceanic and Atmospheric Administration's (NOAA) Environmental Data Service. This publication is provided on a monthly basis, state-by-state, and includes daily and long term average meteorological information with varying degrees of specificity. Provided within the publication is a map of the particular state that is of concern. All of the stations that provide data to the Environmental Data Service are indicated, as are the types of information they collect.

      With this information, the number and type of stations within the study area may be selected.

   b. Registration of the ground meteorological station data

      In order to prepare the climatological information for use in a Landsat based study, the information must be made compatible to the satellite data coordinate system. To accomplish this, the meteorological stations being used should be plotted on an acceptable map base (preferably a USGS quadrangle). Next, the

60

Universal Transverse Mercator (UTM) coordinates for each station should be determined from the map. Now, through use of the regression equations developed during the geometric correction of the original Landsat data, the Landsat coordinates may be calculated for each ground meteorological station. The climatological data is now registered to the satellite data base and may be used in direct conjunction with raw Landsat data or other data sources based on the Landsat coordinate system.

c. Recording and coding of ground meteorological station data

The climatological data derived from each of the ground meteorological stations, as well as important information such as date of data acquisition, station name, UTM coordinates, Landsat coordinates, and elevation, should be noted and recorded in a useable format. A convenient way to accomplish this is by the use of computer cards. Under a format developed by the user, all information collected about each station may be recorded on one or more computer cards. The information is now in an acceptable format for use in a data base computer routine such as RSRP's MAPIT program or an interpolation algorithm.

d. Climatic data interpolation

Since climatic data representing the entire watershed is collected from a number of point sources, there is a need to expand this data base so that climatic information will exist for each Landsat pixel (picture element). To accomplish this, an interpolation algorithm* was developed at RSRP that will mathematically generate data values for each pixel based on the ground station data (i.e. temperature, humidity, precipitation, evaporation, etc.). Upon completion of interpolations for each of the climatic variables of concern, the data is ready to be used as input into data base programs such as RSRP's MAPIT, or simulation models for short-wave, long-wave, or net radiation and evapotranspiration estimation.

*See following page for interpolation algorithm equation.

*The interpolation algorithm is described by the following equation:

$$D(x,y) = \frac{\sum_{i=1}^{n} \frac{D_i}{(D_i)^2}}{\sum_{i=1}^{n} \frac{1}{(D_i)^2}}$$

where:

D_i = the distance from the Landsat pixel being considered (x,y) to the ground meteorological station (i) expressed in terms of Landsat pixels.

D_i = the data value associated with the ground station.

n = the number of ground station locations within range of the pixel being considered (x,y).

D(x,y) = the calculated data value of the pixel (x,y) based on n ground station locations.

The derived value D(x,y) represents the two coordinates of a three dimensional (x,y,z) computer data base (such as MAPIT), registered perfectly to the x,y Landsat coordinate system.

e. Use of prepared climatic data in simulation models

After registration and interpolation of the climatic data, the information is ready for use as input into a number of simulation routines. Among these are models for estimating short-wave, long-wave, and net radiation and a number of models for evapotranspiration estimation. The output of such models is written onto magnetic tape and line printer class maps. The digital data on magnetic tape may be used to generate a visual product such as with RSRP's film writing device known as IGOR (Image Ganged Optical Reproducer), or as input into higher level simulation models, such as the water yield model developed by the joint Federal-State River Forecast Center.

f. Generation of final products

Upon completion of the data preparation and model

62

simulation activities, there is often the need to transform the derived data into a presentable form. Digital information, as it is derived from the solar radiation and evapotranspiration models, may be used as input into a film writing device such as IGOR. Selection of a logical sequence of colors to represent the different classes of digital information aids in the production of a meaningful and visually pleasing product. Following this, concise descriptive labels and a statistical summary should accompany each visual product to aid in its interpretation and effectiveness.

2. NOAA-4 satellite thermal data processing

Under the present climatic stations network, areal distribution of temperature for radiation models may be obtained adequately from ground meteorological stations. Data obtained form the NOAA-4 satellite offers an alternate method for generating a temperature map for a large area. The following text gives a) a brief summary of relevant information about the NOAA-4 satellite; b) an outline of required computer system facilities for implementing this procedure; and c) a step-by-step procedure developed by the Remote Sensing Research Program (RSRP) for NOAA-4 thermal data processing utilizing digital tapes obtained from the National Environmental Satellite Service (NESS) of NOAA. The algorithm used for part of the data processing (geometric correction and temperature calibration) has been provided by NESS and modified by grant participants in the Department of Electrical Engineering at UC Davis.

a. A brief description of the NOAA-4 satellite

The NOAA-4 is an environmental satellite in a sun-synchronous near-polar orbit. This satellite is an evolution of the NOAA series satellites launched by NASA and administered by NOAA after becoming operational. It is equipped with various sensors and scanners for obtaining meteorological data. The data used in this procedure was obtained by a Very High Resolution Radiometer (VHRR), a two-channel scanner which detects energy in the visible spectrum (.6 to .7 micrometers), as well as the thermal infrared (10.5 to 12.5 micrometers). The satellite orbit has an inclination of about 102°, an altitude of about 1450 km, and a period of 115.0 minutes. Its daytime pass over the earth is in a general Northeast to Southwest direction crossing the equator at an angle of 78° at approximately 9:00 AM local solar time. The VHRR scans west to east, from horizon to horizon, at the rate of 400 lines per minute. Its spatial resolution at the satellite subpoint is about 0.8 km.

b. Required system capabilities

The following computer facilities are required for implementation of the procedure:

1) A magnetic tape unit

2) A disk pack

3) A video display system capable of displaying 8-bit data as a black-and-white image, with some means of obtaining the coordinates of points in the image.

The software requirements include:

1) A program for reading the NOAA tape and generating a disk file for corrected or uncorrected imagery (See Appendix V)

2) A program for displaying the image on a television monitor

3) A means for obtaining the relative coordinates of a point in the displayed image

4) A set of algorithms for implementation of various required mathematical equations on the data file

5) A program for linear regression performance

6) A program to produce a histogram of the data values

7) A program to transform the data files to the desired coordinates

With the exception of a), which is given in Appendix V, almost all of the software programs should exist within any software package for an image analysis and display system.

64

c. NOAA data acquisition

The computer compatible tapes for both visible and thermal data can be obtained from NESS headquarters in Washington, D.C. The data for this study was obtained form grant participants at UC Davis who had copied 1600 bpi NOAA tapes to 800 bpi tapes, with a slight change in format. A written description of the important information for geometric correction was received along with the tapes. This information included satellite altitude, midpoint of the image, format of the tape, and the raw coordinates of one or two reference points.

d. Location of the area of interest on the raw thermal data:

1) If possible, estimate coordinates of the area of interest from the coordinates of a known reference point given in the written description.

2) Create a raw (uncorrected) file which includes the desired area. For the first trial, it is suggested that the image be reduced by a factor of four or more, and the starting coordinates adjusted accordingly, to allow a large margin for error.

3) Display the file and locate the area of interest. If it is not in the display, re-estimate starting coordinates and repeat Step 2.b.

4) Determine the coordinates (pixel and line numbers with respect to the beginning of the tape) of the upper left corner of the area of interest, and also determine the size of the area.

5) Using the new coordinates, repeat Steps b and c without reducing the image.

6) On the new display, choose a reference point, preferably near the center of the image, which can be accurately located on a map. Determine its coordinates with respect to the tape file, and determine its exact latitude from a planimetric map. Estimate the relative coordinates of the reference point (pixel) in the desired geometrically corrected output image.

e. Creation of a geometrically corrected image of the study area

Use the parameters determined in c.2. and the satellite height and period data to create a geometrically corrected image. The meanings of the parameters required by the NOAA program for geometric correction are as follows:

SIZEX - line length of output image in pixels

DELTAX - sampling distance along a line of input image

SIZEY - number of lines in output image

DELTAY - sampling rate of lines in output image

RAWX1 - x-coordinate of reference pixel with respect to beginning of tape file

RAWY1 - y-coordinate of reference pixel with respect to beginning of tape file

HEIGHT - height of satellite in kilometers at time of image acquisition

PERIOD - period of satellite (115.0 min.)

REFLAT - latitude of reference pixel

IMAGX1 - relative x-coordinate of reference pixel in output image

IMAGY1 - relative y-coordiante of reference pixel in output image

A complete description of the geometric correction algorithm is given in Section 3 of this appendix.

f. Creation of a histogram of the data values on the geometrically corrected image of the study area

Inspect the histogram to determine the range of valid data values. A temperature range of 0^{o} - $40^{o}C$ would correspond roughly to a data value range of 120-200.

g. NOAA data enhancement

The NOAA satellite data will probably have some visible banding (bad data lines primarily due to temperature variations of the sensor at the time of scanning) and "noise" (extremely high or low values inconsistent with all surrounding pixels). These two problems are handled separately. The corrected data is in each case generated as a new band appended to the data file. The banding is assumed to be the result of variation in the IR sensor, which could cause data values in adjacent scan lines to be inconsistent with each other, i.e. the same values could represent different ground temperature values. Values within one line are assumed to be consistent, since the amount of time required for one scan of the study area is small compared to the time between scans. Since each scan line cuts across a diverse terrain, the line averages are expected to vary smoothly, and sharp deviations are probably the result of sensor variations.

The procedure developed for reducing banding effects is the following:

1) Compute the mean M_n of all pixels in line n with values within the range of normal data.

2) For each line (n), compute an adjusted mean A_n, obtained from the sequence M_n by "smoothing". For this project, A_n was taken to be simply an average of the means of the five lines centered on n, weighted by binomial coefficients:

$$A_n = \sum_{k=-2}^{2} C_{5,k+3} M_{n+k}$$

3) Increment the value of every point in line n by the interger closest to $(A_n - M_n)$. In the data to which this procedure was applied, there was only one change of 3 units, about 7% of the lines were changed by ± 2, and about 45% by ± 1. A change of 2 units is approximately equivalent to one degree of centigrade temperature.

There may be some apparent noise in the image. The following procedure was used to correct for noise. This technique may be applied by using either vertical or horizontal lines in the image. For each point in the smoothed image, the following is applied:

1) Obtain its smoothed IR value (V) from the data file

2) Obtain the values U and W which are the smoothed IR values for the closest preceding and following pixels, along a vertical or horizontal line, whose values are within the range of valid data.

3) If V is not a valid data point, or if V is more than some tolerance (T) outside the range of values determined by U and W, then replace V by (U+W)/2. The process does not depend critically on the tolerance T, unless it is too small or large. T=10 appears to be reasonable.

h. Determination of voltage wedge values and the space view average

The voltage wedge values and space view average are used for transforming the raw values to voltages. Compute average values using the header data for all the lines in the study area. The space view average, S, is in byte 12, and the wedge values W(0),...,W(5) are in bytes 13-18. Also note the IR value (byte 20), T1 (byte 21), and T2 (byte 22), for later use. Typical values of these parameters are: W(0)=216, W(1)=181, W(2)=144, W(3)=108, W(4)=70, W(5)=35, S=30, IR=150, T1=180, T2=186. See Appendix V for further details.

i. Transformation of raw values to voltage values

This is a special procedure developed for data acquired prior to September 1975, for which some of the calibration data was recorded incorrectly. Compute the voltages V(0),...,V(5) corresponding to the wedge values W(0),...,W(5) by V(I)=(W(5)-W(4)) + 5.8 + (I-5.0). To compute the voltage corresponding to a data line value, interpolate between the two closest voltage values.

j. Transformation of voltage values to temperature values

Following the procedure described in Appendix V, compute the values V_c and T_c. On the "Radiometer Radiance Calibration Curves" graph paper, plot 5.8v and 0°K, and V_c,T_c. Connect the two points by a straight line. Carefully read off 10-15 points in the range 0-40°C. Run a linear regression, taking as the dependent variable temperature, and as the independent variables voltage V, V^2, 1/(5.8=V) and

$(\ln(5.8-V))^{1.5}$. This choice of variables gives a good fit, with residual values of 0.1°C or less, except for an aberration in the graph at about 12-16°C, where residual values may be 0.2-0.3°C. Use the above-mentioned equation to generate temperature values in °C.

k. Transformation of temperature values to the desired coordinates

If it is necessary to transform the temperature map to different coordinates, the following procedure is recommended:

1) Display the temperature band on the display system

2) Locate likely control points and determine their coordinates fairly accurately. This can be quite difficult on NOAA data. Most good points will probably be on bodies of water.

3) Print out the temperature values for blocks (about 15x15) of pixels centered on these control points. Comparing the printout with a map or a displayed image of the area in the desired coordinates, trace out contour lines (e.g. lake shorelines) to locate the control points more precisely.

4) Using the pairs of coordinates determined above, run a linear regression between the NOAA coordinates as dependent variables, and the desired coordinates and their squares as independent variables.

5) Transfer all temperature values to the desired coordinates using the relationship established in Step d.

3. A computer algorithm for geometric correction

The following computer algorithm (see Figure IV-1) may be used for geometric correction. The temperature calibration is done according to the procedure developed by NOAA-NESS. A modified version of this procedure, developed by the personnel at UC Davis, is described on the pages following.

a. NOAA thermal calibration

NOAA has provided us with a procedure for converting the IR data into surface temperature, but for images acquired prior to September 1975, the required calibration data was incorrectly recorded on the header records, so the procedure does not work. The following is a modified procedure which has been shown to be reliable by the Department of Electrical Engineering at UC Davis.

b. Procedure

1) Determine the voltages corresponding to the voltage wedge values on the data records (see NOAA Tape Format, attached). Denoting the wedge values by W_i (i=0,...,5) with corresponding voltages V_i, and denoting the space view average by S, the relationship is:

$$V_i = \frac{W_5 - S}{W_5 - W_4} + 5.8 + (i-5)$$

Prepare the voltage wedge table:

Voltage Wedge Values	Voltage
W_0	V_0
W_1	V_1
W_2	V_2
W_3	V_3
W_4	V_4
W_5	V_5

2) Determine the voltages of the thermistors T_1 T_2 by interpolating between values in the voltage wedge table. This will establish voltages V_{T1} and V_{T2}.

3) Determine the temperature of the IR calibration target, denoting the temperature indicated by T_1 as T_{T1}, and by T_2 as T_{T2}:

70

$$T_{T1} = 3.60\ V_{T1} + 11.40^{\circ}C$$

$$T_{T2} = 3.57\ V_{T2} + 11.68^{\circ}C$$

Use the average of these values as the calibration temperature T_c.

4) Determine the voltage corresponding to the IR calibration target value using the voltage wedge table. Denote this value by V_c.

5) Plot on the graph labeled "Radiometer Radiance Calibration Curves" a point at 5.8v and $0^{\circ}K$, and a second point at V_c and T_c. Connect these two points by a straight line.

6) A data value is now converted to temperature by first determining the voltage by interpolating between values in the voltage table and then finding the temperature from the graph.

c. Thermal calibration example

The record header for 5-24-75 is:

Character:	12	13	14	15	16	17	18	19	20	21	22
Value(hex):	1E	D8	B5	90	6C	46	23	64	96	B4	BA
Value(decimal):	30	216	181	144	108	70	35	100	150	180	186

Step #1: $V_i = \dfrac{W_5 - S}{W_5 - W_4} + 5.8 + (i-5)$

$$= \frac{35-30}{35-70} + i + 0.8$$

$$= i + 0.657$$

The voltage wedge table:

Wedge Values	Voltages
$W_0=216$	$V_0=0.657$
$W_1=181$	$V_1=1.657$
$W_2=144$	$V_2=2.657$
$W_3=108$	$V_3=3.657$
$W_4=70$	$V_4=4.657$
$W_5=35$	$V_5=5.657$

Step #2: $V_{T1} = \frac{W_1 - T_1}{W_1 - W_2} + V_1 = \frac{181-180}{181-144} + 1.657 = 1.684v$

$$V_{T2} = \frac{W_0 - T_2}{W_0 - W_1} + V_0 = \frac{216-186}{216-181} + 0.657 = 1.514v$$

Step #3: $T_{T1} = 3.60\ V_{T1} + 11.40 = 17.46^{o}C$

$$T_{T2} = 3.57\ V_{T2} + 11.68 = 17.08^{o}C$$

$$T_c = \tfrac{1}{2}(T_{T1} + T_{T2}) = 17.3^{o}C$$

Step #4: $V_c = \frac{181-150}{181-144} + 1.657 = 2.49v$

Step #5: See attached graph (Figure IV-1)

Step #6: If the radiometric data value (D) is 188:

$$V_D = \frac{216-188}{216-181} + 0.657 - 1.46v$$

From the graph, $T_D = 36.8^{o}C$

72

```
PROGRAM NOAA

NOAA - A ROUTINE TO GENERATE THE RAW OR GEOMETRICALLY
       CORRECTED (STRETCHED) NOAA IMAGE FILE FROM DATA
       READ FROM A NOAA TAPE.  STRETCHING CORRECTS
       FOR PANORAMIC (EARTH CURVATURE) AND
       SKEW (EARTH ROTATION)ERRORS.

RSRP, U.C. BERKELEY, 6/14/78
ORIGINALLY ADAPTED FROM A PROGRAM BY U.C. DAVIS,
ELECTRICAL ENGINEERING DEPARTMENT

PARAMETERS :

  INPUT

    SIZEX = NUMBER OF PIXELS ALONG A LINE IN THE OUTPUT IMAGE FILE
    DELTAX = SAMPLING DISTANCE ALONG A LINE OF THE INPUT DATA
    SIZEY = NUMBER OF LINES IN THE OUTPUT IMAGE
    DELTAY = SAMPLING RATE OF LINES IN THE INPUT IMAGE
    HEIGHT = HEIGHT OF SATELLITE IN KILOMETERS
    PERIOD = ORBITAL PERIOD OF SATELLITE IN MINUTES
    RAWX1 = RAW REFERENCE PIXEL NUMBER ALONG A LINE OF INPUT IMAGE
    RAWY1 = RAW REFERENCE PIXEL LINE IN INPUT IMAGE
    REFLAT = LATITUDE OF REFERENCE PIXEL IN DEGREES
    IMAGX1 = LOCATION OF RAWX1 IN OUTPUT IMAGE
    IMAGY1 = LOCATION OF RAWY1 IN OUTPUT IMAGE
    RAW = 0 TO GENERATE RAW IMAGE FILE [(RAWX1,RAWY1) WILL BE
            LOCATED AT (1,1) IN OUTPUT FILE]
          1 TO GENERATE A GEOMETRICALLY CORRECTED IMAGE FILE

  PROGRAM

    RAWX0 = RAW PIXEL NUMBER OF THE FIRST PIXEL IN THE FIRST LINE
            OF THE INPUT IMAGE USED FOR COMPUTING OUTPUT PIXEL
            (1,1).  RAWX0 NEED NOT BE AN INTEGER.
    RAWY0 = RAW LINE NUMBER OF THE FIRST LINE USED FOR COMPUTING
            OUTPUT PIXEL (1,1)
    INTX0 = CORRECTED PIXEL NUMBER OF RAWX0 BEFORE TRANSLATION
            TO OUTPUT IMAGE
    INTX1 = CORRECTED PIXEL NUMBER OF RAWX1 BEFORE TRANSLATION
            TO OUTPUT IMAGE
    SYNC(1) = FIRST SYNC MARK FOUND
    SYNC(2) = SECOND SYNC MARK FOUND
    MID = PIXEL NUMBER OF MIDLINE OF INPUT IMAGE
    THETA = SATELLITE LATITUDE
    DELPHI = INCREMENTAL GEOCENTRIC ANGLE
    DEBETA = INCREMENTAL GEOCENTRIC SKEW ANGLE

    INCLUDE "NOAASPEC"
    DATA PI/3.141593/

GET PARAMETERS AND OPEN FILES

    CALL INPAR
```


Figure IV-1. Computer algorithm for geometric correction.

ORIGINAL PAGE IS
OF POOR QUALITY

```
      CALL IOPEN
C     SET UP REMEDYS HEADER
      DO 30 I=0,255
30    HEAD(I)=0
      HEAD(0)=1
      HEAD(1)=1
      HEAD(10)=1
      HEAD(11)=1
      HEAD(12)=SIZEX
      HEAD(13)=SIZEY
      HEAD(14)=256
      A(3)=1.0
      TAPE=1
C     FIND FIRST LINE DESIRED
      RAWY0=RAWY1-IMAGY1*DELTAY
      K1=-1     ; OUTPUT LINE NO. COUNTER
      IF(RAWY0.GE.0) GOTO 60
      DO 50 I=RAWY0,-1
      K1=K1+1
      CALL IPUTLN(K1)
50    CONTINUE
      RAWY0=0
60    IFMT=ITYPE(TAPE,DIN(0))
      DO 70 I=0,RAWY0
      NOBYTE=LINE(TAPE,DIN(0),IFMT)
70    IF(NOBYTE.EQ.0) GOTO 930
      IF(RAW.EQ.0) GOTO 225
C     FIND SYNC MARKS
      ACCEPT "PRINT LINE HEADERS? (1-Y,0-N): ",IHD
      J=0
      I=29
80    I=I+1
      I1=IFETCH(I,DIN)
      I2=IFETCH(I+3,DIN)
      IF(I1.GT.200.AND.I2.LT.50) GOTO 100
90    IF(J.GE.5) GOTO 110
      IF(I.GE.NOBYTE-4) GOTO 130
      GOTO 80
100   J=J+1
      SYNC(J)=I+3
      I=I+3
      GOTO 90
110   TYPE "MULT SYNC MARKS FOUND AT :",(SYNC(I),I=1,J)
      J=2
130   CONTINUE
      IF(J.GT.2) GOTO 110
C     FIND MIDPOINT OF INPUT PICTURE
```

```
      GOTO (940,140,150), J+1
140   MID=SYNC(1)+1455
      IF(SYNC(1).GT.1250) MID=SYNC(1)-1455
      GOTO 160
150   MID=(SYNC(1)+SYNC(2))/2.0

C  INITIALIZE CONSTANTS

160   S=106666.          ; SAMPLING RATE  SAMPLES/SECOND
      W=400.   ; SCAN RATE  REVOLUTIONS/MINUTE
      K=S*60./(2.0*PI*W)        ; SAMPLING CONSTANT  SAMPLES/RADIAN
      COSQ=0.20791169 ; ORBITAL INCLINATION  COSINE OF 78 DEGREES
      T=1440.  ; PERIOD OF EARTH ROTATION  MINUTES
      R=6371.  ; RADIUS OF EARTH  KILOMETERS
      DELPHI=2.0*(PI/W)*(1.0/PERIOD+COSQ/T)     ; RADIANS
      CONST1=(HEIGHT+R)/R       ; CONSTANT  UNITLESS
      ALPHA=(RAWX1-MID)/K       ; SCAN ANGLE OF REFERENCE POINT  RADIANS
      Z=ASIN(CONST1*SIN(ALPHA))         ; ZENITH ANGLE  RADIANS
      PSI=Z-ALPHA       ; GEOCENTRIC ANGLE OF REFERENCE POINT  RADIANS
      THETA=ASIN((SIN(REFLAT*PI/180.)+COSQ*SIN(PSI))/COS(PSI)) ; RADIANS
      DEBETA=2.0*(PI/(W*T))*SQRT(COS(THETA)*COS(THETA)-COSQ*COSQ)
      INTX1=(1.0/DELPHI)*(Z-ALPHA-IMAGY1*DEBETA*DELTAY)
      INTX0=INTX1-IMAGX1*DELTAX
      LASTX=(SIZEX-1)*DELTAX
      LINENO=0
      LASTNO=(SIZEY-1)*DELTAY

C   WRITE OUT PARAMETERS

      WRITE(12,501) SIZEX,DELTAX,SIZEY,DELTAY,HEIGHT,PERIOD,
     * RAWX1,RAWY1,REFLAT,IMAGX1,IMAGY1,INTX0,INTX1,
     * (THETA*180/PI),MID,SYNC(1),SYNC(2)
501   FORMAT(1H1,10X,"SIZEX=",I7,2X,"DELTAX=",I7,2X,"SIZEY=",
     * I7,2X,"DELTAY=",I7,//,10X,"HEIGHT=",F10.2,2X,"PERIOD=",
     * F10.2,2X,//,10X,"RAWX1=",I7,2X,"RAWY1=",I7,2X,"REFLAT=",F10.2,
     * //,10X,"IMAGX1=",I7,2X,"IMAGY1=",I7,2X,"INTX0=",F10.2,
     * 2X,"INTX1=",F10.2,2X,"THETA=",F10.2,//,10X,
     * "MID=",I7,2X,"SYNC1=",I7,2X,"SYNC2=",I7,///)

C   PROCESS IMAGE

170   K2=-1      ; POINTS TO PIX IN OUTPUT LINE

      CONST2=LINENO*DEBETA
      DO 190 J=0,LASTX,DELTAX
      INTX=INTX0+J
      ANGLE=INTX*DELPHI+CONST2
      RAWX=K*ATAN(SIN(ANGLE)/(CONST1-COS(ANGLE)))+MID

C   CHECK IF OUT OF BOUNDS IN X DIRECTION

      IF(RAWX.LT.0.OR.RAWX.GT.NOBYTE-2) GOTO 180

C   USE LINEAR INTERPOLATION
```

```
      IRAWX=IFIX(RAWX)
      V1=IFETCH(IRAWX,DIN)
      V2=IFETCH(IRAWX+1,DIN)
      DELTA=RAWX-IRAWX
      K2=K2+1
      IVAL=V1*(1-DELTA)+V2*DELTA
      CALL STORE(IVAL,K2,DATOUT)
      GOTO 190
180   K2=K2+1
      CALL STORE(0,K2,DATOUT)
190   CONTINUE
      K1=K1+1
      CALL IPUTLN(K1)
      IF(IHD.NE.1) GOTO 198
      DO 192 I=0,27
192   DATOUT(I)=IFETCH(I,DIN)
      WRITE(12,601) LINENO,(DATOUT(J),J=0,27)
601   FORMAT(1H ,I5,2X,28I4)
198   LINENO=LINENO+DELTAY
      IF(K1.GE.SIZEY-1) GOTO 990
      DO 200 I=1,DELTAY
      NOBYTE=LINE(TAPE,DIN(0),IFMT)
200   IF(NOBYTE.EQ.0) GOTO 210
      GOTO 170

C    FILL WITH 0 IF OUT OF BOUNDS IN Y OR TAPE HAS FMT ERR

210   IF(K1.GE.SIZEY-1) GOTO 990
      DO 220 I=0,SIZEX-1
220   CALL STORE(0,I,DATOUT)
      DO 223 I=K1+1,SIZEY-1
223   CALL IPUTLN(I)
      GOTO 990

C    RAW IMAGE

225   WRITE(10,511) SIZEX,DELTAX,SIZEY,DELTAY,RAWX1,RAWY1
511   FORMAT(1H ,6I6)
230   K2=-1
      DO 250 J=RAWX1,RAWX1+(SIZEX-1)*DELTAX,DELTAX
      K2=K2+1
      IF(J.LT.0.OR.J.GT.NOBYTE-1) GOTO 240
      IVAL=IFETCH(J,DIN)
      CALL STORE(IVAL,K2,DATOUT)
      GOTO 250
240   CALL STORE(0,K2,DATOUT)
250   CONTINUE
      TYPE K1,NOBYTE
      K1=K1+1
      CALL IPUTLN(K1)
      IF(K1.GE.SIZEY-1) GOTO 990
      DO 260 I=1,DELTAY
      NOBYTE=LINE(TAPE,DIN(0),IFMT)
260   IF(NOBYTE.EQ.0) GOTO 210
      GOTO 230
```

76

```
C    ERROR MESSAGES

930       TYPE "TAPE FORMAT ERROR"
          GOTO 990
940       TYPE "NO SYNC MARKS"
          GOTO 991
990       CALL WRBLK(2,0,HEAD,1,IER)
          CALL TIER("WRHD",IER)
991       CONTINUE
          CLOSE 1
          CLOSE 2
          CLOSE 3
          CALL RLSE("MT0",IER)
          CALL TIER("RLSEMT",IER)
1000      STOP
          END
```

ORIGINAL PAGE IS
OF POOR QUALITY

```
C     "NOAASPEC" - SPECIFICATION STATEMENTS FOR PROGRAM NOAA

         INTEGER SIZEX, DELTAX, SIZEY, DELTAY, RAWX1, RAWY1,
      *  IMAGX1, IMAGY1, TAPE, SYNC(5), BUF(256), RAWY0
         REAL INTX0, INTX1, K
         INTEGER RAW
         INTEGER DIN(0:7000), DATOUT(0:800)
         COMMON/COLD/ DATOUT
         COMMON/PARMS/ SIZEX, DELTAX, SIZEY, DELTAY, RAWX1, RAWY1,
      *  HEIGHT, PERIOD, REFLAT, IMAGX1, IMAGY1, PI, RAW
         COMMON/NAMES/ UNIT(0:3), PART(0:8), IPART(0:9), NPART(0:6)
         INTEGER UNIT, PART, HEAD
         COMMON/ARRAY/ HEAD(0:255)
         DIMENSION A(120)
         EQUIVALENCE (A(1), HEAD(16))
```

78

```
      SUBROUTINE INPAR

C     ACCEPTS PARAMETERS FOR NOAA

      INCLUDE "NOAASPEC"
      LOGICAL NOTOK

10    CALL CLHZL(0)
      IMAGY1=0
      TYPE "INPUT NOAA PARAMETERS<15>"
      ACCEPT "SIZEX = ",SIZEX
      ACCEPT "DELTAX = ",DELTAX
      ACCEPT "SIZEY = ",SIZEY
      ACCEPT "DELTAY = ",DELTAY
      ACCEPT "RAWX1 = ",RAWX1
      ACCEPT "RAWY1 = ",RAWY1

20    ACCEPT "ENTER 0 FOR RAW IMAGE, 1 FOR CORRECTED: ",RAW
      IF(RAW.EQ.0) GOTO 30
      IF(RAW.NE.1) GOTO 20
      ACCEPT "<15>","HEIGHT = ",HEIGHT
      ACCEPT "PERIOD = ",PERIOD
      ACCEPT "REFLAT = ",REFLAT
      ACCEPT "IMAGX1 = ",IMAGX1
      ACCEPT "IMAGY1 = ",IMAGY1

30    IF(NOTOK(0)) GOTO 10

      RETURN
      END
```

```
      SUBROUTINE IOPEN
C   OBTAINS DIRECTORY AND FILE NAMES,
C   CREATES AND OPENS FILE AND FILE.HD,
C   ACCEPTS TAPE FILE NUMBER AND OPENS TAPE FILE
C
C   TAPE OPEN ON CHAN 1
C   FILE.HD OPEN ON CHAN 2
C   FILE OPEN ON CHAN 3

      INCLUDE "NOAASPEC"
      LOGICAL NOTOK

      CALL WITCH
710   TYPE "<15>","ENTER DIRECTORY NAME"
      READ(11,521) NPART(0)
521   FORMAT(S10)
      CALL DIR(NPART,IER)
      CALL ERGO("PARTIN",IER,$710)

C     TELL THE USER WHAT'S UP

      TYPE " "
720   PAUSE LOAD TAPE ON UNIT 0, TYPE ANY KEY
      CALL INIT ("MT0",0,IER)
      CALL ERGO("INIT",IER,$720)
   11 CALL CLHZL(0)

C     GET THE TAPE FILE NO.
      UNIT(0)="MT"
      UNIT(1)="0:"

   30 TYPE "<15>","ENTER TAPE FILE NO. (0 IS 1ST): "
      READ(11,1000)UNIT(2)
 1000 FORMAT(S2)
      IF(NOTOK(0))GOTO 11
      CALL MTOPD(1,UNIT,1,IER)
      CALL ERGO("TOPEN",IER,$30)

C     GET A DISK FILE NAME FROM USER

730   DO 10 I=0,9
      IPART(I)=0
   10 CONTINUE

   92 TYPE "<15>","ENTER DISK FILE NAME, UP TO 10 CHARACTERS"
      READ(11,1100)PART(0)
 1100 FORMAT(S10)

      IF(NOTOK(0))GOTO 92

C     ADD THE .HD EXTENSION TO IPART

      CALL DOTHD(16,PART(0),IPART(0))
```

80

```
C         CREATE & OPEN THE .HD FILE

          CALL CFILW(IPART,2,IER)
          IF(IER.EQ.1)GOTO 4
          IF(IER.NE.12)GOTO 5
          TYPE "NAME ALREADY IN USE"
          GOTO 92
     5    IF(IER.NE.4)GOTO 6
          TYPE "INVALID NAME. ONLY A-Z, 0-9 AND $ ALLOWED"
          GOTO 92
     6    IF(IER.NE.13)GOTO 7
          TYPE "NO FILE WITH GIVEN NAME"
          GOTO 92
     7    CALL ERGO("CREATEHD",IER,$730)

     4    CALL OPEN(2,IPART,3,512,IER)
          CALL ERGO("HDOPEN",IER,$730)

C         CREATE AND OPEN THE DATA FILE

          CALL CFILW(PART,2,IER)
          CALL ERGO("CREATEDATA",IER,$730)
          CALL OPEN(3,PART,3,SIZEX,IER)
          CALL TIER("DTAOPN",IER)
          RETURN
          END
```

```
      INTEGER FUNCTION ITYPE(ICHAN,BUF)

      INTEGER BUF(1),IREC(4)
      COMMON/NAMES/ UNIT(0:3),IDUM(26)
      INTEGER UNIT

      I=0
10    I=I+1
      L=ITAPEM(5340,BUF,ICHAN,IER)
      CALL TIER("RDTP1",IER)
      IF(L.EQ.45.OR.L.EQ.3840.OR.L.EQ.5340) GOTO 20
      IF(I.EQ.4) GOTO 910
      GOTO 10

20    IREC(1)=L
      DO 30 I=2,4
      IREC(I)=ITAPEM(5340,BUF,ICHAN,IER)
      CALL TIER("RDTP2",IER)
30    CONTINUE

      IPT=1
      IF(IREC(1).NE.45.OR.IREC(2).NE.45) GOTO 40
      IPT=2
      GOTO 50

C   FORMAT 4

40    IF(IREC(IPT).NE.5340) GOTO 50
      ITYPE=4
      GOTO 990

C   FORMAT 1

50    IF(IREC(IPT).NE.3840.OR.IREC(IPT+1).NE.3840) GOTO 60
      ITYPE=1
      GOTO 990

C   FORMAT 3

60    IF(IREC(IPT).NE.3840.OR.IREC(IPT+1).NE.1500) GOTO 70
      ITYPE=3
      GOTO 990

C   FORMAT 2

70    IF(IREC(IPT).NE.45.OR.IREC(IPT+1).NE.3840.OR.IREC(IPT+2).
     * NE.6) GOTO 80
      ITYPE=2
      GOTO 990

80    IF(IPT.GE.2) GOTO 920
      IPT=2
      GOTO 40

910   TYPE "ERROR - AT LEAST 4 WRONG-LENGTH RECORDS"
915   PAUSE
      CALL BACK
920   TYPE "ERROR - CANNOT MATCH TAPE TO NOAA FORMAT"
      GOTO 915

990   ICOM=40000K+5-IPT
      CALL MTDIO(1,ICOM,BUF,ISTS,INCT,IER)
      CALL TIER("TPBS",IER)
      RETURN
      END
```

82

```
      INTEGER FUNCTION LINE(ICHAN,BUF,IFMT)

C   READS ONE LINE FROM NOAA TAPE
C   LINE = BYTE COUNT IN LINE READ

      INTEGER BUF(1)

5     LINE2=0
10    LINE1=ITAPEM(14000,BUF(1),ICHAN,IER)
      CALL ERGO("RDTP",IER,$10)
      IF(LINE1.LE.6) GOTO 10
      GOTO (20,30,30,20), IFMT

30    LINE2=ITAPEM(14000-LINE1,BUF((LINE1+3)/2),ICHAN,IER)
      CALL ERGO("RDTP2",IER,$10)
      IF(LINE2.LE.6) GOTO 30
20    LINE=LINE1+LINE2
      IF(LINE.LT.3800) GOTO 5

      RETURN
      END
```

```
INTEGER FUNCTION ITAPEN(NBYT,BUF,ICHAN,IER)

INTEGER BUF(1)
NWRD=0
CALL MTDIO(ICHAN,NWRD,BUF,ISTS,IWCT,IER)
CALL TIER("RDLN",IER)
ITAPEN=2*IWCT
RETURN
END
```

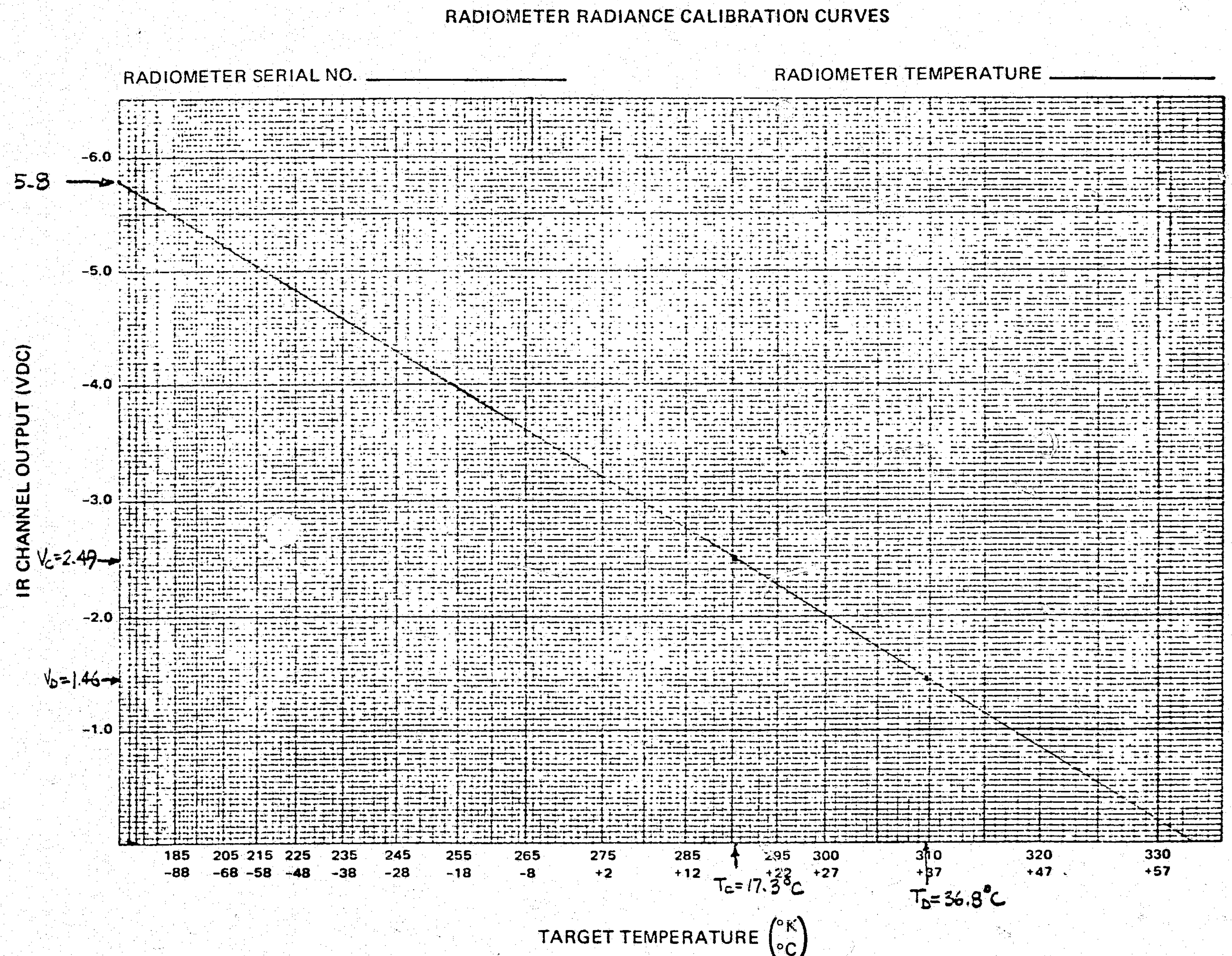

Figure IV-2. Calibration for 5-24-75.

APPENDIX V, CASE STUDY

IMPLEMENTATION OF THE REMOTE SENSING-AIDED PROCEDURE FOR ESTIMATING SOLAR AND NET RADIATION AS APPLIED TO THE MIDDLE FORK OF THE FEATHER RIVER WATERSHED

The stepwise procedure described in the procedural manual has been applied to a very diverse and large watershed in Plumas County in the Northern Sierra range of California known as the Middle Fork of the Feather River Watershed (MFFR). This watershed is approximately 2900 km^2 and is located at 39^o 30' North to 40^o 05' North latitude and 120^o 05' West to 121^o 25' West longitude. A Landsat color composite of the area with the watershed boundary on it is shown in Figure 1.

The areal distribution of all of the inputs to radiation models have been prepared and described models have been used to generate the final results. These results are net short-wave, net long-wave, and net radiation on the earth's surface for May 16, 1975. The input components consist of physiographic characteristics (elevation, slope, aspect, and albedo), together with climatic variables (cloud cover and temperature). Appendix II contains the results of this remote sensing-aided procedure for vegetation/terrain analysis as applied to the test watershed (MFFR). The vegetation map has been used to generate an albedo map of the watershed and is shown in Figure 2.

Climatic data required for this remote sensing-aided system for estimating evapotranspiration was not fully available within the MFFR watershed. The number of meteorological stations in this catchment is limited due to the sparsely populated nature of the area and the physical inaccessibility of a large portion of the watershed. Also, data pertaining to only a few types of climatic parameters have been taken at each station. There are only fifteen ground meteorological stations within the Middle Fork of the Feather River watershed which collect climatic data. These stations along with their latitudes, longitudes and elevations are listed in Table 1. The data types collected at these stations consist mostly of precipitation and temperature information. Very few of the stations collect wind data or report on atmospheric condition with reference to degree of cloud cover. The main climatic variable used in radiation models is the areal distribution of temperature. Two alternatives of interpolating temperature data based on ground meteorological stations (No. 1) and using NOAA-4 satellite thermal data (No. 2) were used to prepare the temperature data. Because of lack of adequate ground meteorological stations, 8b

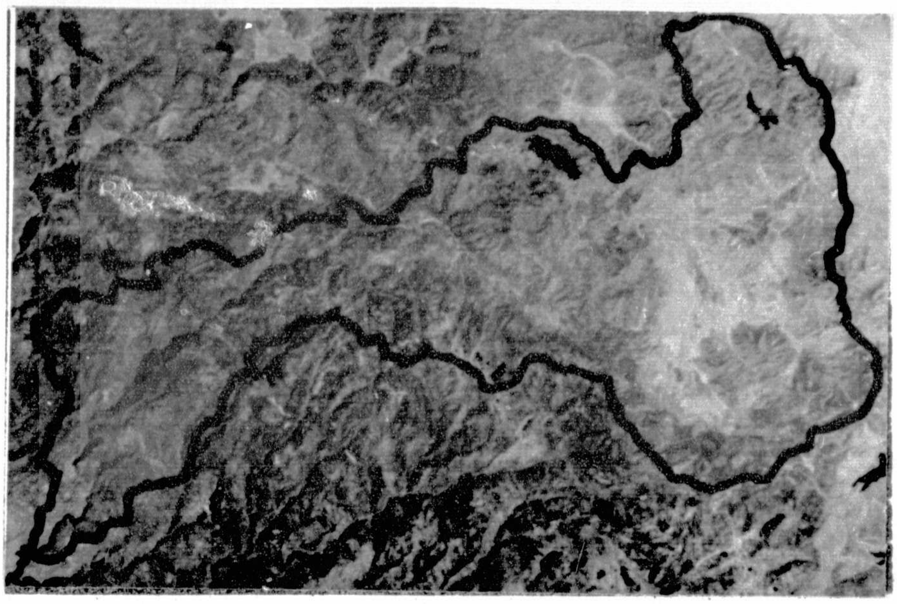

Figure V-1. Landsat color composite of the test area indicating the boundary limits of the Middle Fork of the Feather River Watershed.

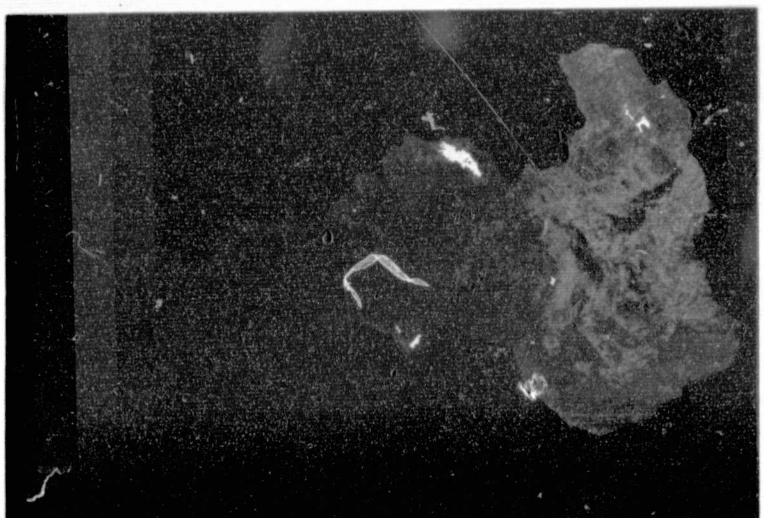

Figure V-2. Areal distribution of albedo for the Middle Fork of the Feather River Watershed, in percent, based on vegetation/terrain analysis

Identification Key

Color	Albedo in Percent
White	5
Dark Blue	9
Purple Blue	10
Yellow	11
Light Green	12
Green	13
Dark Green	14
Light Blue	15
Orange	18
Red	22
Brown	25

Table V-1. EXISTING GROUND METEOROLOGICAL STATIONS WITHIN AND SURROUNDING THE WATERSHED OF THE MIDDLE FORK OF THE FEATHER RIVER

Station Name	Longitude,W	Latitude,N	X	Y	Elev(ft)	Available Station Data for 1975*		
						Temp	Precip	Rel Hum
Brush Creek	$39^{\circ}41'$	$121^{\circ}21'$	642.50	4394.62	3560	—	✓	—
Bucks Creek Pump House	$39^{\circ}55'$	$121^{\circ}20'$	643.02	4419.02	1760	—	✓	—
Challenge Ranger Station			652.82	4371.76		✓	—	✓
Forbestown			649.53	4383.86	2900	✓	✓	—
Greenville Ranger Station	$40^{\circ}08'$	$120^{\circ}56'$	675.47	4445.19	3560	—	✓	✓
Mohawk Ranger Station	$39^{\circ}47'$	$120^{\circ}38'$	704.17	4351.06	4370	✓	✓	—
Oroville Ranger Station	$39^{\circ}32'$	$121^{\circ}34'$	603.69	4376.24	300	✓	✓	✓
Plumas Creek State Park	$39^{\circ}45'$	$120^{\circ}42'$	697.23	4403.10	5165	✓	✓	—
Portola	$39^{\circ}48'$	$120^{\circ}28'$	716.50	4408.93	4850	✓	✓	—
Quincy	$39^{\circ}55'$	$120^{\circ}57'$	675.94	4422.73	3408	✓	✓	✓
Sagehen Creek	$39^{\circ}26'$	$120^{\circ}14'$	737.53	4368.08	6337	—	✓	—
Sierra City	$39^{\circ}34'$	$120^{\circ}38'$	702.74	4381.86	4150	✓	✓	—
Sierraville Ranger Station	$39^{\circ}45'$	$120^{\circ}22'$	724.99	4384.61	4975	✓	✓	—
Vinton	$39^{\circ}49'$	$120^{\circ}11'$	740.64	4411.23	4950	✓	✓	—
Woodleaf Oroleve	$39^{\circ}31'$	$120^{\circ}11'$	656.52	4376.72	3340	—	✓	—

* ✓ = yes

— = no

alternative No. 1 is not recommended. However, a net radiation map based on the interpolated temperature values has been prepared and is shown at the end of this section.

Using the procedure described in Step 8.b of the procedural manual, a temperature map of the study area based on the NOAA-4 satellite thermal data and transferred to Landsat-based coordinates has been prepared. The date for this map was acquired as of 9:30 AM PST, May 16, 1975, and the temperature values range from +2°C to +41°C. This temperature map is shown in Figure 3.

Based on the procedure described in Appendix III, maps of elevation, slope, and aspect for the MFFR watershed have been prepared and are shown in Figures 4, 5, and 6, respectively. The elevation map is based on digitization of elevation contour isolines using USGS topographic series maps at a scale of 1:250,000.

A map of net radiation for the study area (using the interpolated values of temperature from ground meteorological stations for May 16, 1975) is shown in Figure 7. Another map of net radiation for the study area for May 16, 1975 (using temperature values based on NOAA-4 thermal data) is shown in Figure 8.

Based on the evaluation of results it is recommended to use the NOAA-4 thermal data, unless adequate ground meteorological stations exist within the study area, for preparation of temperature input for radiation models. Statistical summaries and percent distribution of the data over the study area can also be calculated. As an example, percentage distribution of net radiation values in ly/day for May 16, 1975 over MFFR watershed (areal distribution is shown in Figure 7) is shown in Table 2.

90

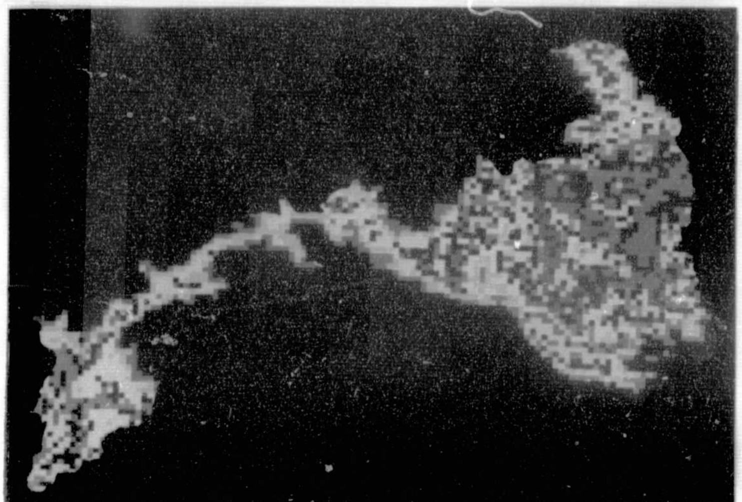

Figure V-3. Temperature map of the Middle Fork of the Feather River Watershed for May 16, 1975, based on NOAA-4 satellite infrared data.

Identification Key:

Color	Temperature in ^{o}F
Dark Blue	0 - 31
Blue	32 - 45
Purple	46 - 61
Blue Green	62 - 68
Green	70 - 78
Yellow Green	79 - 84
Yellow	85 - 88
Yellow Red	90 - 92
Red	93 - 96
Lavender	97 - 108

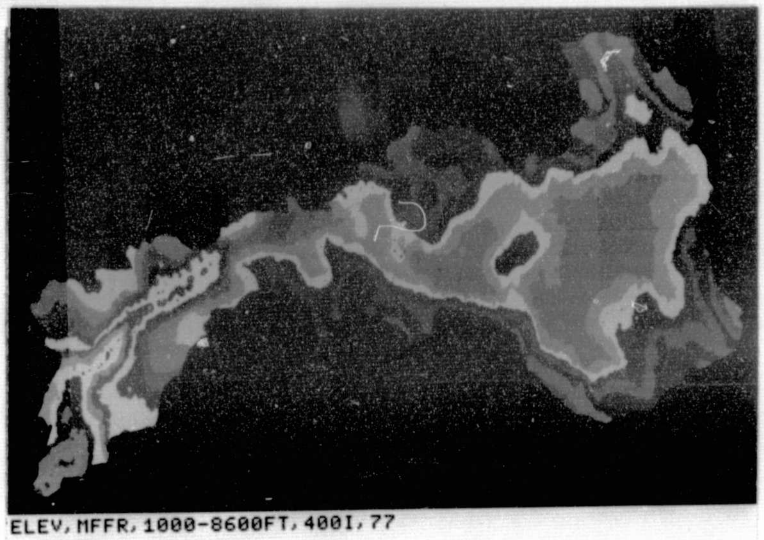

Figure V-4. Areal distribution of the elevation zones for the Middle Fork of the Feather River Watershed, in feet (MSL).

Identification Key

Color	Elevation in Feet
Red	1200
Orange	1600
Purple	2000
Brown	2400
Yellow	2800
Green	3200
Light Brown	3600
Light Yellow	4000
Yellow Green	4400
Dark Green	4800
Light Green	5200
Blue Green	5600
Dark Yellow	6000
Dark Blue	6400
Dark Purple	6800
Blue	7200
Purple	7600
Darker Purple	8000
Gray	8200

92

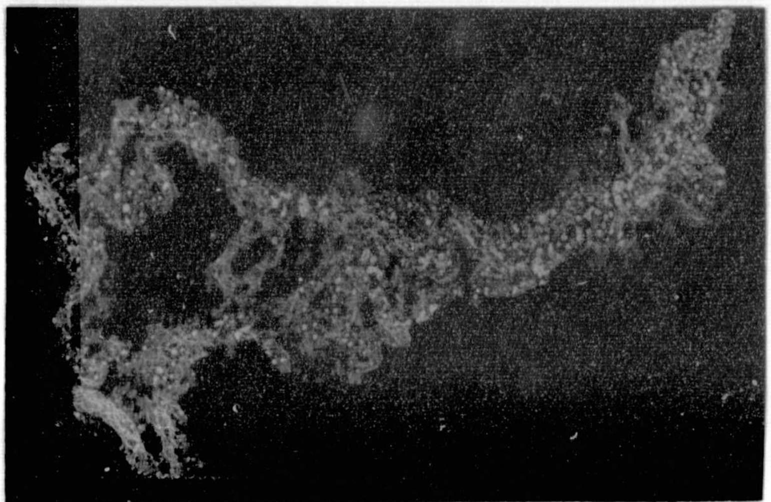

Figure V-5. Slope map of the Middle Fork of the Feather River Watershed, in percent.

Identification Key

Color	Slope in Percent
Black	Flat
Red	2-4
Blue	6-10
Green	12-20
Yellow	22-40
Dark Green	42-60
Purple	62-80
Blue Green	82-100
White	102-270

ORIGINAL PAGE IS
OF POOR QUALITY

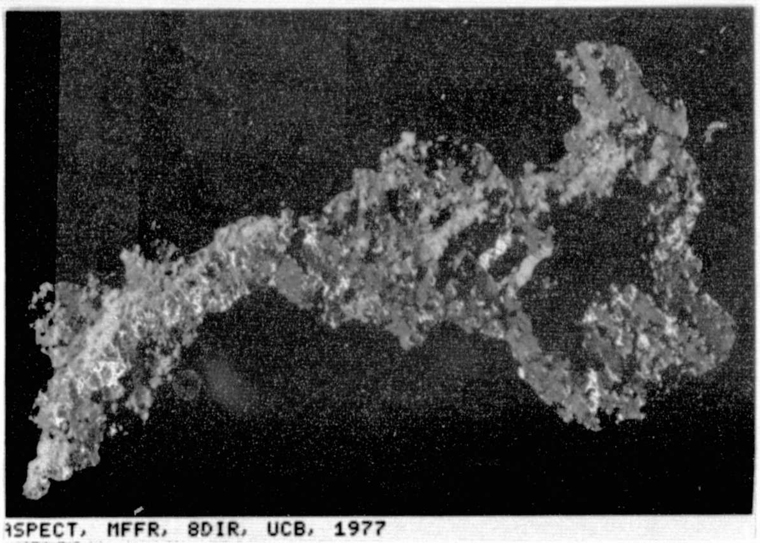

Figure V-6. Aspect map of the Middle Fork of the Feather River Watershed (N = North, S = South, E = East, W = West)

Identification Key

Color	Direction
Black	Flat
Red	N
Purple	NE
Orange	E
Yellow	SE
Light Green	S
Dark Green	SW
Blue	W
White	NW

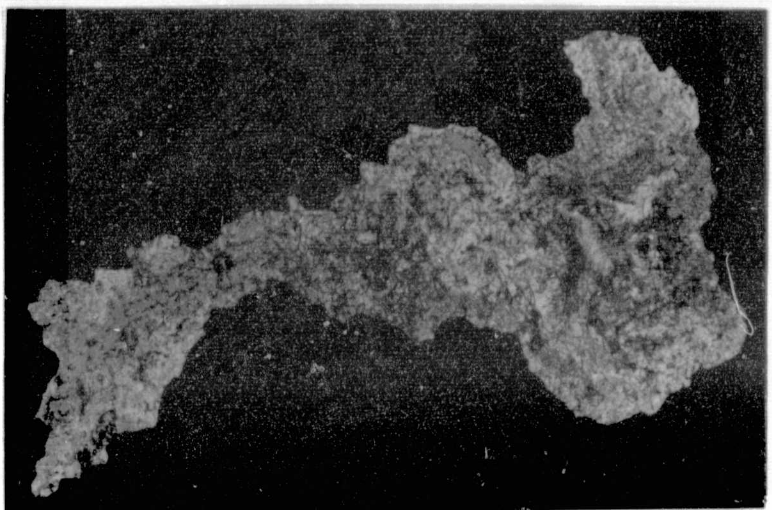

Figure V-7. Net radiation map of the Middle Fork of the Feather River Watershed for May 16, 1975, using interpolated temperature values of ground meteorological stations as an input.

Identification Key

Color	Net Radiation in ly/ day
Dark Green	10 - 200
Orange	210 - 350
Red	360 - 400
Blue	410 - 430
Yellow	440 - 450
Blue Green	460
Light Green	470 - 500
Purple	510 - 560

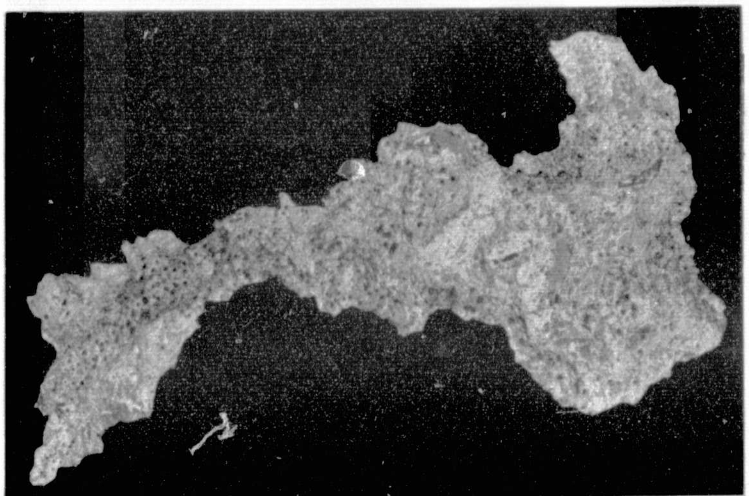

Figure V-8. Net radiation map of the Middle Fork of the Feather River Watershed for May 16, 1975, using temperature values based on NOAA-4 satellite infrared data as an input.

Identification Key

Color	Net radiation in ly/day
Dark Blue	0 - 250
Blue-Green	260 - 360
Yellow-Green	370 - 410
Green	420 - 430
Yellow-Brown	440
Yellow	450
Red-Brown	460
Yellow-Red	470
Lavender-Red	480
Red	490 - 600

Table V-2. Percentage distribution of net solar radiation values in ly/day for May 16, 1975, for the Middle Fork of the Feather River Watershed

Net Radiation	Percent
10-200	2.6
210-350	6.2
360-400	12.9
410-430	19.5
440-450	35.6
460	12.2
470-500	10.8
510-560	0.2

See Procedural Manual entitled, "Remote Sensing as an Aid in Watershed-Wide Estimation of Water Loss to the Atmosphere," pages I-12 through I-18 for references.

98

C-2

Procedural Manual

REMOTE SENSING AS AN AID IN WATERSHED-WIDE ESTIMATION OF WATER LOSS TO THE ATMOSPHERE

Principal Investigator: Robert N. Colwell

Principal Scientist
and Project Manager: Siamak Khorram

Project Scientists: H. Gregory Smith and
Edwin F. Katibah

NASA Grant NGL-05-003-404

Remote Sensing Research Program
University of California, Berkeley
May, 1978

REMOTE SENSING AS AN AID IN WATERSHED-WIDE ESTIMATION OF WATER LOSS TO THE ATMOSPHERE

INTRODUCTION

Water vapor is the principal participant in the many energy exchanges taking place in the atmosphere. These energy exchanges are responsible for the weather phenomena which serve as important links connecting the various phases of the hydrological cycle.

Quantification of the water flux mechanisms, viz. evaporation and evapotranspiration (which includes active plant water loss), is of importance in many scientific fields. They form one of the main components of the water budget, knowledge of which is indispensable for the solution of numerous water management problems. Reliable evaporation data are required for planning, designing and operating reservoirs, ponds, shipping canals, and irrigation and drainage systems. Evapotranspiration is especially important in arid zones where water must be used in the most efficient way possible. In addition, knowledge of the water requirement of crops depends partly on an accurate determination of the loss of water by evapotranspiration from cultivated fields.

Evapotranspiration data are used for estimating irrigation requirements, rainfall disposition, safe yield of ground water basins, water yields from mountain watersheds, stream flow depletion in river basins, and in vegetation management for fiber production.

In view of the overriding importance of evapotranspiration to accurate basin yield estimation and to other water consumpttive use determinations, any cost-effective, precise evapotranspiration estimation system would be of significant utility to a water manager. Remote sensing techniques may provide the key to such a system's data requirements. Its timely, spatial, and relatively inexpensive nature give rise to accurate, location-specific estimates of evapotranspiration.

Evapotranspiration estimates are incorporated in current water yield estimation procedures such as the joint Federal-State River Forecasting Center model. It is therefore the purpose of this section to lay the foundation for a remote sensing-aided methodology for accurate and efficient watershed evapotranspiration estimation.

10

Objective

The objective of this procedural manual is to describe a stepwise remote sensing-aided procedure developed by our Remote Sensing Research Program (RSRP) personnel for the watershed-wide estimation of potential evapotranspiration from water supply basins of interest. The results of this study are designed to be readily implemented in hydrologic models for water yield forecasts.

Definitions

Evaporation may be defined as the transfer of water vapor from a non-vegetative surface on the earth into the atmosphere. Evapotranspiration is the combined evaporation from all surfaces and the transpiration of plants. Except for the omission of a negligible amount of water used in the metabolic activities, evapotranspiration is the same as the "consumptive use" of the plants. The fact that the rate of evapotranspiration from a partially wet surface is greatly affected by the nature of the ground leads to the concept of potential evapotranspiration. Penman (1956) defines potential evapotranspiration as "the amount of water transpired in unit time by a short green corp, completely shading the ground, of uniform height and never short in water". Pruitt (1960) designated the term "potential maximum evapotranspiration" to describe the situation when advected (horizontal movement of energy through the atmosphere surrounding the plant) energy is present.

PROCEDURE

This procedure is composed of a series of mathematical models for evapotranspiration (ET) estimation and techniques for providing the required input information to these models. The ET values as well as all the input values to the models are in areal distribution (map) form. A complete description of a three level modeling technique and sampling design for providing the inputs to all three levels of models, as well as integrating the results, is given in Appendix I. The representative of level I models will be discussed in this manual. This representative model has been selected based on the comparison of the results of all level I models applied to a test watershed in Northern California. A modified version of Jensen and Haise model for daily prediction of potential evapotranspiration has been selected for this procedure. Due to lack of funding, application of level II and level III evapotranspiration models has been postponed.

1. Selection of study area and delineation of watershed boundary

   All the information for use in this procedure must be of a common register. In this case, the Landsat-base registration is recommended. Landsat multispectral scanner (MSS) data tapes of the watershed should be acquired and geometrically corrected. The watershed boundary should be determined and transferred onto the Landsat data base. The detailed description of the technique for geometric correction of Landsat data and boundary transformation of the watershed is described on pages I-1 through I-8 (i.e., in Appendix I of the Procedural Manual for Net Radiation Estimation).

2. Selection of a model for evapotranspiration estimation

The selected model is a modified version of the Jensen and Haise (1963) model. This model is defined as:

$$ETp = (0.014T - 0.37)\ R_n \qquad \text{where}$$

ETp = daily potential evapotranspiration in inches

T = mean daily temperature in $^{\circ}F$

R_n = daily net radiation on the Earth's surface in inches of water equivalent

3. Preparation of temperature map of the area as an input to the model

Lack of adequate ground meteorological stations, in general, creates a problem in satisfying the temperature data requirements. We have chosen two alternatives for solving this problem: (1) computer assisted interpolation of existing temperature data collected in ground meteorological stations; and (2) using the National Oceanic and Atmospheric Administration's NOAA-4 satellite Very High Resolution Radiometer (VHRR) data for generating the temperature map of the area.

Collection and interpolation of temperature values based on ground meteorological stations data entail the following steps:

a. Identification and selection of meteorological stations

b. Registration of the data

c. Recording and coding of the data

103

d. Temperature data interpolation

e. Use of the data in simulation models

f. Generation of final products

The detailed description and the techniques for the above-mentioned steps are given on pages IV-1 through IV-4 (i.e. in Appendix IV of the Procedural Manual for Net Radiation Estimation).

Acquisition and processing of NOAA-4 satellite thermal data entail the following steps:

a. Data acquisition

b. Location of the study area on the raw thermal data

c. Geometric correction of the data

d. Data enhancement

e. Transformation of voltage values to temperature values

f. Transformation of temperature data to the desired coordinates system

g. Preparation of final product

The detailed description and the techniques for the above-mentioned steps and a brief description of the VHRR scanner are also given in Appendix IV (pages IV-4 through IV-26 of this report).

4. Preparation of net radiation data as an input to the model

The methodology for net radiation estimation is based on a series of mathematical models and a remote sensing-aided information system designed to provide the needed input data for the models. The detailed stepwise procedure for net radiation estimation is discussed in a separate manual titled "Remote Sensing as an Aid in Watershed-Wide Estimation of Solar and Net Radiation" appearing before the evapotranspiration manual. The results of net radiation models are site- and time-specific and consider the effects of climatic variability as well as terrain condition such as elevation, slope, and aspect.

5. Calculation of potential evapotranspiration

Upon the completion of temperature and net radiation maps, by using the equation described in Step 2 one may calculate the areal distribution of potential evapotranspiration for the area of interest. The computer program used for calculation of potential evapotranspiration (ETp) is known as MAPIT. MAPIT is a program developed by RSRP personnel to create, analyze, and display maps and map-related data. One may use his own technique for calculation of evapotranspiration in map or any other form. An example of the results (potential evapotranspiration) as applied to the Middle Fork of the Feather River Watershed, Northern California (approximately 2900 km^2) for May 16, 1975, is shown in Figure 1. (For a description of the study area, see Appendix V of the Manual on Radiation Estimation.)

RSRP's film writing device known as the Image Ganged Optical Reproducer (IGOR) was used to generate the color-coded map shown in Figure 1. The temperature map and net radiation map used as inputs for generation of this ETp data are shown in Figures 3 and 8, respectively, in Appendix V (case study) of the Manual for Radiation Estimation. NOAA-4 satellite thermal data has been used for preparation of a temperature map as well as being used as one of the inputs for preparation of the net radiation map.

1.04

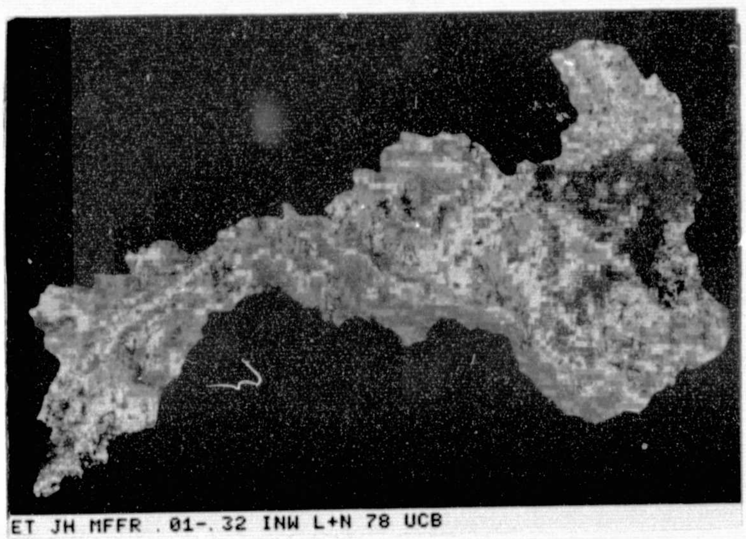

Figure 1 Potential evapotranspiration (ETp) map of the Middle Fork of the Feather River Watershed for May 16, 1975 using temperature values based on NOAA-4 satellite data as an input.

Identification Key

Color	ETp in inches of water
Red	0.00 - 0.05
Orange	0.06 - 0.11
Yellow-Orange	0.12 - 0.15
Yellow	0.16 - 0.19
Yellow-Green	0.20 - 0.22
Dark Green	0.23 - 0.24
Green	0.25 - 0.26
Blue-Green	0.27 - 0.28
Dark Blue	0.29 - 0.33
Blue	0.34 - 0.41

Appendix I

THREE LEVEL EVAPOTRANSPIRATION ESTIMATION MODELS WITH REMOTE SENSING-AIDED SAMPLING PROCEDURE FOR PROVIDING REQUIRED INPUT DATA FOR MODELS

The methodology for evapotranspiration (ET) estimation involves a multistage, multiphase sampling design employing three increasingly resolved levels of information to be used respectively in the three increasingly sophisticated levels of ET modeling.

The sampling technique for providing all the required information for ET models (see the recommended models for their required inputs) is discussed at the beginning and is followed by the three levels of ET modeling. Data sources include the entire spectrum of environmental data gathering programs and information banks currently operating. Data types are those which are required by all three levels of ET models.

1. Sampling technique

a. Primary sampling units

The first level is composed of Landsat and NOAA and topographic data. Vegetation-terrain and meteorological types of information are defined for a convenient base resolution element, in this case a small group of Landsat pixels. Based on this information associated with each base resolution element, an estimate of evapotranspiration is made for that location. The appropriate evapotranspiration equations, defined as level I models, perform adequately on this "least resolved" information available from the first data level.

After an estimate of evapotranspiration has been made for each base resolution element, the resolution elements (here 3x3, 4x4, or 5x5 blocks of pixels) are grouped into primary sampling units.

106

b. Secondary sampling units

Within each primary sampling unit (PSU) selected, a series of secondary sampling units (SSU's) are defined and photographed at large scale with light aircraft. The photographic SSU data along with nearby snow course and ground station calibrated meteorological satellite data will provide the second level of information resolution. At the SSU stage of the sampling design, much more specific information concerning local vegetation canopy, soil, and local climatic conditions will be available as opposed to that obtainable from information at level I. Thus level II evapotranspiration models employing more data types and more refined data are used to generate evapotranspiration estimates for each PSU.

c. Tertiary sampling units

A sample of two of the SSU's per PSU selected is then randomly (equal and/or unequal probability) chosen for further analysis on the ground. For each of these SSU's selected, detailed ground measurements are made of vegetation canopy geometry, color, etc., as well as of soil and litter-organic debris conditions. The detailed data from this third level of information will then drive evapotranspiration prediction models. Since estimates of evapotranspiration will be for the entire ground area of the SSU photo plot, this third stage unit (TSU) will actually comprise a double sample of the SSU's. The sampling concepts and terminology in the preceding discussion are summarized in Figure I-1.

d. Multistage equation

A multistage estimation equation is being used to integrate the data from levels I, II, and III for generating an estimate of watershed-wide evapotranspiration. This equation is shown in Figure I-2 and the definitions of its components are summarized in Table I-1. Based on this multistage equation, watershed-wide estimation of ET is calculated by first using the ground-based evapotranspiration estimates to calibrate the

Figure I-1 EVAPOTRANSPIRATION SAMPLE DESIGN TERMINOLOGY

Information Level	Sample Unit	Sample Design Level	Comments
1	PSU 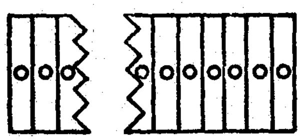	STAGE I Multistage portion of sample design	All PSU's in watershed have evapotranspiration estimates made based on a summation of evapotranspiration estimates for LANDSAT resolution elements occupying each PSU. A sample of the PSU's is selected for further sampling
2	PHOTO SSU 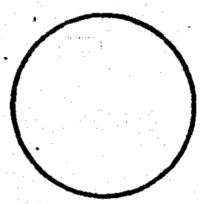	STAGE II PHASE 1 Multiphase or double sample portion of sample design	All SSU's within a selected PSU have evapotranspiration estimates made based on surface characteristics interpreted from the photography
3	GROUND SSU 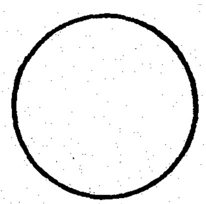	PHASE 2	Ground measurements resulting in ground-based evapotranspiration estimates are made for a sample of the photo SSU's

108.

Figure I-2 Multistage ET Estimation Equation and Corresponding Sample Frame

$$ET = \frac{1}{n}\sum_{i=1}^{n}\frac{1}{p_i}\left[\frac{1}{n_i}\sum_{j\in\{D\}}\frac{A_i}{a}\times\frac{y_{ij}}{p_{ij}}\right]$$

$$p_i = \frac{ET_i}{\sum_{i=1}^{n} ET_i}$$

$$p_{ij} = \frac{ET_{ij}}{\sum_{j\in\{D\}} ET_{ij}}$$

ET_i = ET based on level I data

ET_{ij} = ET based on level II data

$y_{ij} = ET_{ij}^{*}$ = ET based on level III data

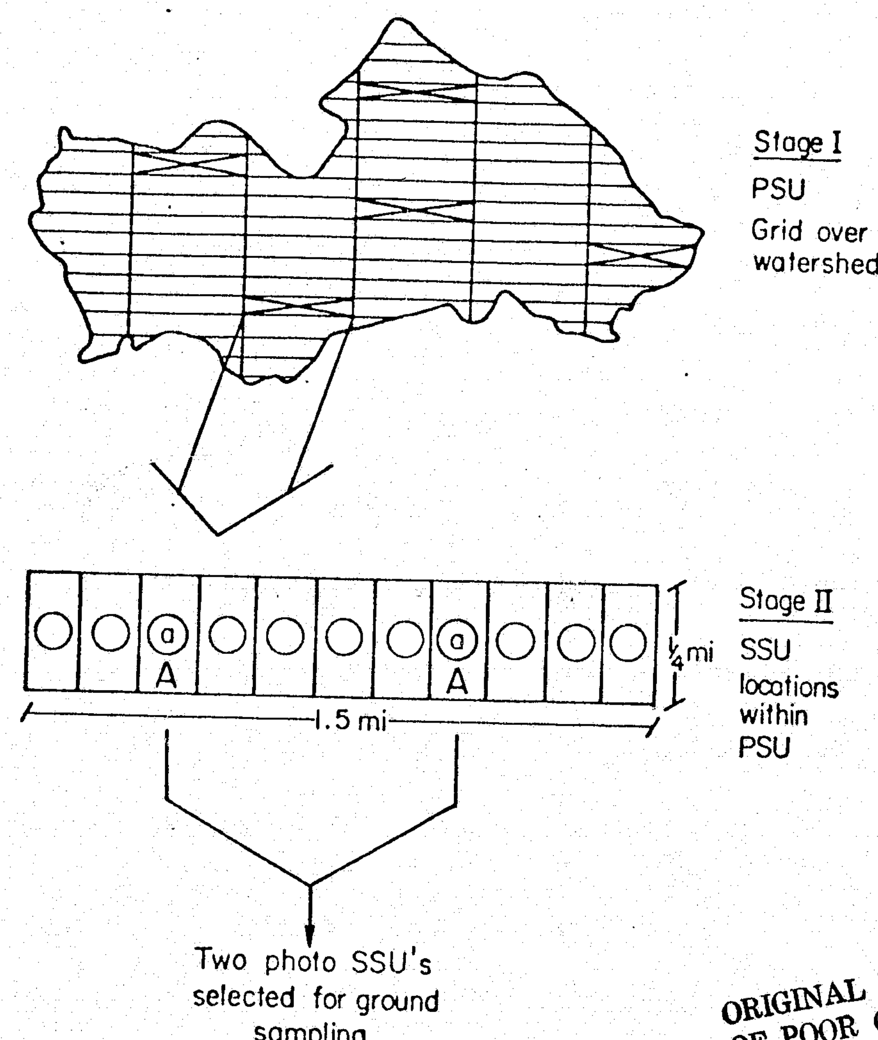

Table I-1 Description of Terms Used in the Multistage ET Estimation Equation in Figure 2.

n	=	number of PSU's sampled
p_i	=	probability of selection of the ith PSU
n_i	=	number of SSU's selected within ith PSU
$J \in \{D\}$	=	the set of SSU's selected in each sampled PSU
A_i	=	area of the section within which SSU is located
a	=	area of SSU
Y_{ij}	=	ground ET estimation for the jth SSU of the ith PSU
p_{ij}	=	probability of selection of jth SSU for ground measurement within ith PSU
ET	=	average evapotranspiration estimate for the entire watershed.

SSU estimate derived from photo data. The calibrated SSU estimates are then expanded to the PSU stage by utilizing the SSU selection weights developed earlier. Finally, PSU evapotranspiration estimates can be expanded, each over the appropriate stratum, and then to the entire watershed by applying the PSU selection weights (proportion of evapotranspiration in the given PSU relative to all other PSU's in the watershed) originally calculated. In this way, a cost-effective combination of an increasingly smaller sample of more precise and more extensive information levels can be utilized to give base-wide watershed estimates.

e. Description of the procedure for using multistage equations

First, the ground-based estimate of evapotranspiration, Y_{ij}, for the j^{th} SSU of the i^{th} PSU is inflated by division with p_{ij} (the proportion of evapotranspiration estimated from level II data to occur in the j^{th} SSU of the i^{th} PSU). After multiplication by the ratio of the average segment area (A_i) to its corresponding plot area (a), this inflated ground ET value represents an estimate of total evapotranspiration for the i^{th} PSU.

These PSU ET estimates are made for each ground measured SSU in the i^{th} PSU. Ground visited SSU's in a given subsampled PSU, are defined to compose the set D. Summing over these ET estimates for each SSU in the set D and then dividing by n_i, the number of SSU's in set D of the i^{th} PSU, then gives an average estimate of PSU evapotranspiration. The steps just described are indicated within the bracketed expression of the ET equation in Figure I-2.

Once an average evapotranspiration estimate has been derived from level I and level II data, for each of the small number of PSU's subsampled, then each such value must be inflated to a watershed-wide ET estimate. This is done, as shown in Figure I-2 by multiplying the bracketed quantity by $\frac{1}{p_i}$ There p_i represents the proportion of evapotranspiration in the i^{th} PSU based on level I information relative to the sum of evapotranspiration from all PSU's in the watershed. The watershed-wide evapotranspiration estimates thus gained for each PSU selected for sub-sampling are then summed. This sum is next averaged by dividing by n, the total number of PSU's selected for subsampling. The result is the total watershed-wide estimate of evapotranspiration.

Sampling theory allows a derivation of an estimate of variance for the above watershed ET estimate. Multiplying the resulting standard error by an appropriate Student's-t value gives a confidence interval half-width (a statistical statement of estimate precision) to be associated with the estimate.

The true value of evapotranspiration from the watershed is then expected to lie within plus or minus the confidence interval half-width of the ET estimate a given number of times out of a hundred (e.g. 90) with specified confidence probability (e.g. .95).

2. Recommended evapotranspiration models

a. Recommended level I ET model

A number of empirical and semi-empirical ET estimation models have been examined for this level. These models included Blaney-Criddle (1950), Hargreaves (1956), Turc (1961), and Jensen and Haise (1963) models. Based on the comparison of the results of the above-mentioned models with: 1) the pan evaporation data collected on the test site; and 2) expected values of ET for the test area, a modified version of the Jensen and Haise model was selected for the best performance. The test area was a catchment in the Sierra Nevada Mountains of northern California, known as the Spanish Creek Watershed (475 km^2).

The modified Jensen and Haise model is defined as:

$$ETp = (0.014\ T - 0.37)\ R_n \qquad \text{where:}$$

ETp = daily potential evapotranspiration in inches

T = daily temperature in ^{o}F

R_n = daily net radiation on the Earth's surface in Langleys

112

A complete stepwise procedure for this model is given in the main part of this manual.

b. Recommended level II ET models

The basis for the evapotranspiration models to be applied to the second level of information resolution is that of energy conservation, which is a proven law of thermodynamics. For this level, the energy-balance method will be combined with other methods for consideration of vegetation canopy effects and advected energy processes. The objective of the model applied at level II will be to capitalize on vegetation canopy, geometry-composition, and other surface data available from aerial photography to provide improved evapotranspiration estimates. The following models are being examined for application:

<u>Priestly and Taylor Model</u>

Priestly and Taylor used the equation:

$$E = \frac{\alpha}{L} \frac{(S)}{S+\gamma} (R_N - G)$$

for estimation of evapotranspiration over the surfaces where surface resistance was expected to be negligibly small. In this equation:

S = slope of saturation curve versus temperature

γ = psychrometric constant

R_N = net radiation

G = heat flux into the soil

α found to be 1.26

This estimate of α is the overall mean of land and water surface.

<u>McNaughton and Black Model</u>

The best potential evapotranspiration relationship that was suggested by McNaughton and Black is

$$PE = \frac{1.05}{L} \frac{S}{S+\gamma} (R_N - G) + 0.17\ GIL \quad \text{where:}$$

PE = potential evapotranspiration

L = latent heat of water

S = slope of saturation curve versus temperature

γ = psychrometric constant

R_N = net radiation

G = heat flux to the soil

GIL = gross interception loss

Modified McIlroy and Slatyer

The following equation was used by McIlroy and Slatyer to estimate actual evapotranspiration (E).

$$E = \frac{E(pot)}{1 + \frac{\gamma}{s+\gamma} \times \frac{h}{h_i}}$$ where:

γ = psychrometric constant

s = slope of saturation vapor pressure curve versus temperature

h = transfer coefficient

h_i = molecular diffusion of water vapor through stomata

$\frac{h}{h_i}$ = the canopy effect on the amount of actual evapotranspiration

This equation will be modified to use some other terms for the canopy effect.

Linacre Model

A semi-empirical method of evapotranspiration was derived by Linacre (1967) through the combination of Penman's method and solar radiation equations. Linacre considered the forest canopy as impeding the loss of water by means of two resistances: the canopy resistance, r_c, which is a function of canopy structures and their properties, and aerodynamic resistance, r_a, which is a function of the canopy-atmosphere interface. The combined equation is:

$$LE = \frac{\Delta Q_n + C_p \cdot \rho \cdot \frac{s}{r_a}}{\Delta + \gamma + \gamma \frac{r_c}{r_a}}$$ where:

Q_n = difference between downward and upward radiation fluxes

C_p = specific heat of air at constant pressure

ρ = air density

γ = psychrometric constant

s = saturation deficit

Δ = change of water vapor pressure with temperature in ambient conditions

The variables to be estimated for input to the level II models are much more canopy and ground specific than those required for level I. In general, input variables to be applied in level II must be determined more precisely and more frequently as well. Data requirements include temperature, humidity, and wind value profiles in the soil surface-vegetation zone. Wind friction velocity, rainfall, ground cover, and topographic data may also be considered. These canopy data requirements will be fulfilled in large part through large scale photographic measurements collected form photo second stage sampling units and calibrated by corresponding ground data. Canopy-top meteorological data will be obtained as in level I, viz., through meteorological satellite data calibrated by ground station information and by microclimatic functions extrapolating satellite and ground data values to SSU's of interest. Vertical meteorological variable profiles within the canopy will be generated form canopy-top data according to canopy geometry functions.

c. Recommended level III ET models

The third information resolution level in the remote sensing-aided evapotranspiration estimation system will allow application of the practical as well as the most sophisticated models. The approach may be to select and develop those evapotranspiration estimation equations which are most rational and physical in terms of the actual processes involved. Based on the desired accuracy and need, a combination of empirical, energy balance and aerodynamic methods are recommended for examination at this level.

115

For instance, this model(s) may be based on a combination of methods using radiation energy and temperature as primary variables (e.g. Jensen and Haise equation) and on methods considering vegetation canopy effects and aerodynamic resistance (e.g. Priestly and Taylor equation; McNaughton and Black equation). This new model(s) could be constructed so as to take best advantage of the data gained through remote sensing and ground sampling.

The following list includes the references for both procedural manuals on radiation and evapotranspiration:

REFERENCES

Abdel-Aziz, M.H., Taylor, S.A., and Ashcroft, G.L., 1964, Influence of advective energy on transpiration, Agr., J., 56:139.

Avery, C.C., and L.J. Fritschen, 1971, Hydrologic and energy budgets of stocked and non-stocked Douglas-fir sites as calculated by meteorological mehtods, Research Completion Report, College of Forest Resources, University of Washington, 131 pp.

Black, T.A. and K.G. McNaughton, 1972, Average Bowen-ration methods of calculating evapotranspiration applied to a Douglas-fir ofrest, boundary-layer meteorol. 2: 466-475.

Blaney, A.F. and K.H. Morin, 1942, Evaporation and consumptive use of water empirical formula, Trans. American Geophysical Union 23: 76-83.

Blaney, H.F. and W.D. Criddle, 1950, Determining water requirements in irrigated areas form climatological and irrigation data, U.S. Soil conserv. Service Tech. Paper 96, 48 pp.

Brown, H.E. and J.R. Thompson, 1965, Summer water use by aspen, spruce, and grassland in western Colorado, Journal of Forestry, 63(10): 756-760.

Budyko, M.E., 1963, Evaporation under natural conditions, Israel Program of Scientific Translations.

Buell, M.F. and J.T. Ballard, 1972, Evaporation from lowland vegetation in the New Jersey Pine Barrens, Report No. B-006-N.J., N.J. Water Resources Research Institute.

Burgy, R.H. and Z.H. Papazafiriou, 1971, Vegetative management and water yield relationships, biological effects in the hydrological cycle, pp. 315-331, The Third International Seminar for Hydrology Professors.

California Division of Forestry and U.S. Forest Service, 1962, California wildland fire danger rating handbook.

Chindasnguan, C., 1966, Estimation of pan evaporation in northeast region of Thailand by using various formulas based on climatological data. Master of Science Thesis, Utah State Univ., Logan, Utah.

Christiansen, J.E., 1966, Estimating pan evaporation and evapotranspiration from climatic data, methods for estimating evapotranspiration, Irrigation and Drainage Specialty Conference, ASCE, Las Vegas, Nev.

117

Cochran, W.G., 1963, "Sampling techniques", Second Edition, John Wiley & Sons, Inc., New York, 410 pp.

Cowan, IR., 1968, Estimation of evaporation using meteorological data, in Land Evaluation Papers of CSIRO Symposium organized in cooperation with UNESCO, G.A. Steward, ed., pp. 291-311, McMillan.

Department of Water Resources, 1974, Solar radiation measurements in California, DWR, State of California, 20 pp.

Dilley, A.C. and I. Helmond, 1973, The estimation of net radiation and potential evapotranspiration using atmometer measurements, Agric. Meteorol., 12: 1-11.

Dyer, A.J. and W.O. Pruitt, 1962, Eddy-flux measurements over a small irrigated area, Jour. Applied Meteorol. 1: 471-473.

Dylla, A.S. and D.C. Muckel, 1964, Evapotranspiration studies on native meadow grasses, USDA-SWC, Rq.

Federer, C.A., 1970, Measuring forest evapotranspiration-theory and problems, USDA Forest Ser. Res. Paper NE: 165.

Frank, C.E. and R. Lee, 1966, Potential solar beam irradiation on slopes, Rocky Mountain Forest and Range Experiment Station, p. 117.

Fritschen, L.J. and P. Doraiswamy, 1973, Dew: An addition to the hydrologic balance of douglas fir, Water Resources Research, Vol. 9, No. 4, pp. 891-894.

Fritz, S., 1948, The albedo of the ground and atmosphere, Bull. Am. Meteorol. Soc. 29: 303-312.

Gangopadhyaya, M, Chairman, G.E. Harbeck, Jr., T.J. Nordenson, M.H. Omarond, V.A. Uryavev, 1966, Measurement and estimation of evaporation and evapotranspiration, WMO Tech. Note No. 83.

Gary, H.L., 1972, Rime contributes to water balance in high-elevation aspen forests, Journal of Forestry, 20(2): 193-197.

Geiger, R., 1971, The climate near the ground, Harvard University Press, Cambridge, Mass., pp. 10-15, 57, 153, 205, 225, 227, 259, 262, 371, 531, 535.

Geotz, Billingsley, Elston, Lucchitta, and Shoemaker, 1973, Geologic applications of ERTS images on the Colorado Plateau, Arizona, in Third Earth Resources Technology Satellite-1 Symposium, Goddard Space Flight Center, Washington, D.C., Vol. 1, Section A, pp. 719-744.

Grootenboer, Jan, 1973, op. cit., The influences of seasonal factors on the recognition of surface lithologies from ERTS-1 imagery of the Western Transvaal, pp. 643-655.

Hall, D.J. and G.H. Ball, 1967, A clustering technique for summarizing multivariate data, Behavioral Science, Vol. 12.

Hall, D.J. and G.H. Ball, 1965, ISODATA, a novel technique for data analysis and pattern classification, Technical Report, Stanford Research Institute, Menlo Park, California, May.

Hargreaves, G.H., 1956, Irrigation requirements based on climatic data, Paper 1105, Journal of the Irrigation and Drainage Division, ASCE, Vol. 82, No. IR-3.

Hargreaves, G.H., 1966, Consumptive use computations from evaporation pan data, Journal of Irrigation and Drainage Specialty Conference, ASCE, Las Vegas, Nev.

Hounam, C.E., 1971, Problems of evaporation assessment in the water balance, Report No. 13, WMO, No. 285.

Jensen, M.E. and R.E. Howard, 1963, Estimating evapotranspiration from solar radiation, Paper 3737, Proc. ASCE, J. Irrig. and Drain. Div. 89(IR4): 15-41.

Jensen, M.E., 1966, Empirical methods of estimating or predicting evapotranspiration using radiation, ASAE Conference Proc. Evapotrans. and its Role in Water Resour. Manag., Chicago, pp. 49-53.

Johnston, R.K.T. and R.D. Doty, 1969, Soil moisture depletion and estimated evapotranspiration on Utah Mountains watershed, USDA Forest Service Research Paper INT-67.

Katibah, E.F., Areal extent of snow estimation using Landsat-1 satellite imagery, Chapter 2 in An Integrated Study of Earth Resources in the State of California Using Remote Sensing Techniques, Annual Progress Report for NASA Grant NGL 05-003-404, Robert N. Colwell, Principal Investigator, 1 May 1975.

Khorram, S., Derivation, description, and definition of input parameters for current evapotranspiration estimation equations, in An Integrated Study of Earth Resources in the State of California Using Remote Sensing Techniques, Space Sciences Laboratory Series 16, Issue 2, University of California, Berkeley, 1974, 24 pp.

119

Khorram, S., 1974, Evaluation of current models for evapotranspiration estimation, Chapter 2b in An Integrated Study of Earth Resources in the State of California Using Remote Sensing Techniques, Semi-Annual Progress Report for NASA Grant NGL 05-003-404, Space Sciences Laboratory Series 16, Issue 2, University of California, Berkeley, December, 20 pp.

Khorram, S., Radiation theory applied to hydrological modeling Chapter 2b in An Integrated Study of Earth Resources in the State of California Using Remote Sensing Techniques, NASA Grant NGL 05-003-404, Annual Progress Report, Space Sciences Laboratory, Series 16, Issue 34, University of California, Berkeley, May 1975, 11 pp.

Khorram, S. and R.W. Thomas, Watershed-wide estimation of water loss to the atmosphere using remote sensing techniques, Fifth Annual Remote Sensing of Earth Resources Conference Proceedings, Tullohoma, Tennessee, 1976, 16 pp.

Khorram, S. and R.W. Thomas, Development of a remote sensing-aided evapotranspiration estimation system, Workshop for Environmental Application of Multispectral Imagery Proceedings, U.S. Army Engineering Topographic Laboratories, Fort Belvoir, Virginia, 1975, 13 pp.

King, K.M., 1966, Mass transfer-profile method., ASAE Conference Proc. Evapotrans. and its Role in Water Resour. Manag., Chicago, pp. 38-41.

Kutilek, M., 1971, Direct methods of soil moisture estimation for water balance purposes, WMO/IHD Project, WMO No. 286.

Kirkby, M.J., Infiltration, throughflow, and overland flow, Chapter 5 in Richard J. Chorley (Ed.) Introduction to Fluvial Processes, Methuen & Co. LTD., London, 1971, pp. 85-97.

Lang, A.R.G., 1973, Measurement of evapotranspiration in the presence of advection by means of a modified energy balance, Agr. Meteorol. 12: 75-81.

Leaf, C.F., 1969, Aerial photographs for operational streamflow forecasting in the Colorado Rockies, in Proceedings of the 39th Western Snow Conference, pp. 19-28.

Leeper, C.W., 1950, Thornthwaite climate formula, Australian Jour. Agr. Sci. 16: 2-6.

Lewis, D.C. and R.H. Burgy, 1967, Water use by native vegetation and hydrologic studies, Annual Report, Department of Water Science and Engineering, University of California, Davis, 53 pp.

Lewis, D.C., 1968, Annual hydrologic response to watershed conversion from oak woodland to annual grassland, Water Resources Research, Vol. 4, No. 1: 59-72.

Linacre, E.T., 1967, Climate and the evaporation from crops, ASCE, IR4: 61-79.

Linacre, E.T., 1968, Estimation of net-radiation flux, Agr. Meteorol., 5: 49-63.

Linacre, E.T., 1973, A simpler empirical expression for actual evapotranspiration rates -- a discussion, Jour. Agr. Meteorol., 11 (1973); pp. 451-452.

Lumley, J.L. and H.A. Panofsky, 1964, The structure of atmospheric turbulence, Interscience Publishers, 139 pp.

Millington, R.J. and D.P. Peters, 1971, An experimental study of eddy diffusion coefficients, evapotranspiration and water use efficiency, UILU-WRC-71-0048, Research Report No. 48.

Monin, A.S. and A.M. Obukhov, 1954, Principle law of turbulent mixing in the air layer near the ground USSR Acad. Nauk. Geophys. Inst. No. 24 (Translated from Russian, 1954).

Palayasoot, P., 1956, Estimation of pan evaporation and potential evapotranspiration of rice in the Central Plain of Thailand by using various formulas based on climatic data, Master of Science Thesis, Utah State University, Logan, Utah.

Pasquill, F., 1950, Some further considerations of the measurement and indirect evaluation of natural evaporation, Quart. J. Roy. Meteorol. Soc. 76: 287-301.

Patil, B.B., 1962, A new formula for the evaluation of evaporation, Master of Science Thesis, Utah State University, Logan, Utah.

Penndorf, R., 1956, Luminous reflectance (visual albedo) of natural objects, Bull. Am. Meteorol. Soc., 37: 142-144.

Penman, H.L., 1948, Natural evaporation from open water, bare soil, and grass, Proc. Roy. Soc., (London) A. 193: 120-145.

Philip, J.R., 1963, Comments on paper by Monteith, in Environmental Control of Plant Growth, L.T. Evans, ed., Academic Press, p. 111.

Pike, J.G., 1964, The estimation of annual runoff from meteorological data in a tropical climate, J. of Hydrology, Vol. 11, No. 2: 116-123.

Priestley, C.H.B. and R.J. Taylor, 1972, On the assessment of heat flux and evaporation using large-scale parameters, Mon. Wea. Rev., 100: 81-92.

Pruitt, W.O., 1964, Cyclic relations between evapotranspiration and radiation, Trans. ASAE 7: 3,271-75; 280.

Pruitt, W.O. and F.J. Lourence, 1968, Correlation of climatological data with water requirements of crops, 1966-68 Report, Dept. of Water Science and Engineering, University of California, Davis, 57 pp.

Pruitt, W.O., 1971, Factors affecting potential evapotranspiration; biological effects in the hydrological cycle, The International Seminar for Hydrology, pp. 82-102.

Rabchevsky, G.A., 1970, Hydrologic conditions viewed by the nimbus meteorological satellites, First Western Space Congress, Santa Maria, California.

Raj, Des, 1968, Sampling theory, McGraw-Hill Book Company, San Francisco, 302 pp.

Rosenberg, N.J., H.E. Hoyt, and K.W. Brown, 1968, Evapotranspiration review and research, University of Negraska, MP 20.

Rouse, W.R. and R.G. Wilson, 1972, A test of the potential accuracy of the water-budget approach to estimating evapotranspiration, Agr. Meteorol., 9: 421-446.

Rutter, A.J., 1966, Studies on the water relations on Pinus sylvestris in plantation conditions, J. Appl. Ecol., 3: 393-405.

Seginer, I., 1967, The affects of albedo on the evapotranspiration rate, Agr. Meteorol. G: 5-31.

Sellers, W.D., 1965, Physical climatology, University of Chicago Press, Chicago.

Shiau, S.Y. and K.S. Davar, 1973, Modified penman method for potential evapotranspiration from forest regions, J. Hydrol. (Amsterdam) 18(314): 349-365.

Slatyer, R.O. and I.C. McIlroy, 1961, Practical Micrometeorology, CSIRO Australian and UNESCO.

Slatyer, R.O., et al., 1970, Estimating evapotranspiration: an evaluation of techniques, Australian Water Resource Council, Hydrolog. Series No. 5.

Stenhill, G., 1969, A simple instrument for the field measurement of turbulent diffusion flux, Journal of Applied Meteorology, pp. 509-513.

Swift, L.W. and K.R. Knoerr, 1973, Estimating solar radiation on mountain slopes, Agr. Meteorol. 12: 329-336.

Tanner, C.B., 1963, Plant temperatures, NOTE, Agron. J. 55: 210-211.

Tanner, C.G. and W.L. Pelton, 1960, Potential evapotranspiration estimates by the approximate energy balance method of Penman, J. Geophys. Research, Vol. 65, No. 10.

Thom, A.S., 1972, Momentum, mass and heat exchange of vegetation, Quart. J. R. Met. Soc., 98: 124-134.

Thomas, R.W. and G.A. Vasick, 1975, Application of the Scheffé method of multiple comparison to determination of class separability, Internal Information Note, Remote Sensing Research Program, University of California, Berkeley.

Turc, L., 1961, Estimating irrigation water requirements, potential evapotranspiration, Ann. Agron., 12(1): 13-49.

Van Bavel, C.H.M., 1966, Combination (Penman type) methods, ASAE Conference Proc. Evapotrans. and its Role in Water Resour. Manag., Chicago, pp. 38-41.

Van Bavel, C.H.M., 1966, Potential evaporation, the combination concept and its experimental verification, Water Resour. Res., 2: 455-467.

Wiesnet, D.R, and D.F. McGinnis, 1973, Hydrological application of the NOAA-2 very high resolution radiometer, Proc. No. 17: 179-190.

World Meteorological Organization, 1966, Measurement and estimation of evaporation and ET, WMO Tech. Note No. 83.

Yamaoka, Y., 1958, The total transpiration from a forest, Trans., Am. Geophys. Union, Vol. 39, No. 2: 266-271.

Yeh, G.T. and W. Brutsaert, 1971, A solution for simultaneous turbulent heat and vapor transfer between a water surface and the atmosphere, Boundary-Layer Meteorology 2: 64-82.

Ziermer, R.R., 1963, Summer evapotranspiration trends as related to time following logging of high elevation forest stands in Sierra Nevada, Master of Science Thesis, University of California, Berkeley, California.

Procedural Manual

REMOTE SENSING AS AN AID IN DETERMINING THE AREAL EXTENT OF SNOW

Principal Investigator: Robert N. Colwell

Principal Scientist
and Project Manager: Siamak Khorram

Project Scientist: Edwin F. Katibah

Contributor: Melinda Shackleford

NASA Grant NGL-05-003-404

Remote Sensing Research Program
University of California, Berkeley
May, 1978

TABLE OF CONTENTS

Remote Sensing As An Aid In Determining The Areal Extent Of Snow

ILLUSTRATIONS

TABLES

REMOTE SENSING AS AN AID IN DETERMINING THE AREAL EXTENT OF SNOW

INTRODUCTION

The term "areal extent of snow" pertains to the surface area of the terrain in a specified watershed that is covered with snow at a given time or seasonal state.

For many years the need for an improved method of estimating snow areal extent has been recognized by hydrologists and others concerned with the prediction of water runoff and the estimation of water yield, watershed-by-watershed. Among the methods showing greatest promise is the one dealt with in this Procedural Manual. That method seeks to make maximum use of modern remote sensing techniques, including those which result in the acquisition of aerial and/or space photography of the watershed at suitably frequent intervals. Because of an advantage known as the "synoptic view," it is possible on space photography, and even on high-altitude aerial photography to cover vast watershed areas with only a very few frames of photography. As will presently be seen, this advantage can be of great importance to those wishing to use such photographs as an aid in determining the areal extent of snow.

Of the several remote sensing-based techniques that have been developed for estimating snow areal extent, only two will be mentioned here since they appear to be both representative and highly promising. The first is based merely on the delineation of the apparent snowline on the photographs. The delineated portions of the photographs are then measured in such a way as to provide an estimate of the areal extent of the snow-covered area. This technique is described fully by Barnes and Bowley (1974).

A second technique has been developed which utilizes a two-stage sampling scheme to arrive at an estimate of the snow-covered area. The procedure for employing this technique is described herein. As will presently be seen, the technique employs as much ancillary (i.e., non-remote sensing-derived) information as possible to aid in the accuracy of the final estimate. Furthermore, the design of the model that is employed when this technique is used is such as to largely eliminate final estimate discrepancies, even when two or more photo interpreters are used as a team, since a statistical evaluation of each photo interpreter's results is made. The method, overall, is sufficiently simple and inexpensive to permit it to be used in addition to, rather than instead of, more conventional methods, thereby providing additional confidence in the final estimate of snow areal extent on which operational decisions must be made, in any given instance, by the hydrologist or other resource manager.

128

When this second method is used by a competent image analyst, in addition to his determining the total area that is covered with snow, he also derives detailed locational information of great value, i.e., he determines the exact portions of the watershed that are snow-covered and differentiates them from the snow-free areas. This can be of great advantage in relation to his desire to make accurate estimations of water yield and water runoff rates because the rate of snow depletion for a given portion of the watershed obviously is a function of its slope, aspect, vegetative cover, and other locally-variable factors.

PROCEDURE

The procedure described here for estimating areal extent of snow is based upon a two-stage analysis of remote sensing imagery. The first stage entails the use of Landsat* color composite imagery, while the second stage employs low-altitude, large-scale aerial photography. The following description provides a step-by-step guide to the use of this method in estimating the areal extent of snow:

Step 1. Prior to the start of the winter season (i.e., the season when the snowpack is to be measured) all of the projected dates when Landsat will be overflying the area of interest during the snow survey period should be systematically listed. In compiling this list one should keep in mind that there is sidelap of about 20 to 30 percent (depending upon the latitude of the area) between the 115-mile swath that is covered by Landsat on one day and that which the same vehicle covers on the following day. Therefore, this factor needs to be considered as the list is being made of all possible dates for the acquisition of Landsat imagery of the area of interest.

Step 2. During the snow-survey period, on each date when a Landsat overflight of the area of interest is about to be made under what is predicted to be suitably cloud-free conditions, by prior arrangement steps should be taken to procure nearly simultaneous low-altitude aerial color photography of preselected flight lines, thereby acquiring the previously mentioned "second stage sample." An optimum scale for such photography is approximately 1/30,000, and 35mm negative color film is preferred.

Step 3. The second stage photography procured in Step 2, above, should be promptly processed and from it standard "3R" prints (i.e., size 3-1/2" x 5") should be made.

---

* The term "Landsat" applies to various unmanned earth resources technology satellites (formerly called "ERTS"), each of which provides images of the surface of the Earth on an 18-day sun-synchronous cycle (0930 local sun time, approximately) from an altitude of approximately 570 miles and covering a swath width of approximately 115 miles.

Step 4. As promptly as possible after the corresponding Landsat overflight has been made, and again by prior arrangement (in this case normally with the EROS Data Center at Sioux Falls, South Dakota) black-and-white MSS (multispectral scanner) transparencies should be obtained from bands 4, 5 and 7 covering the entire watershed area of interest. The standard 9"x9" transparencies produced by the EROS Data Center are preferred. In addition, either at the time when the first of this snow-season Landsat photography is being acquired, or at some earlier date, an additional summertime (snow-free) set of Landsat imagery also should be acquired for comparative analysis, as indicated below (see Step 15).

Step 5. In each instance, on the Landsat imagery that has been acquired the boundary of the watershed or other area of interest should be delineated.

Step 6. For each of the frames of Landsat imagery required in making the delineation of Step 5, a simulated color infrared color composite should be made, using the three bands (4, 5 and 7) to make a "triple exposure" on negative color film in the manner described in Appendix II of this procedural manual.

Step 7. From the resulting negative color composites, reflection prints (rather than transparencies) should be made to a size of approximately 8"x10". In those instances where more than one Landsat frame is required to cover the area of interest, the Landsat frames originally selected (and the corresponding areas copied and printed from them) should overlap each other sufficiently to provide complete coverage of the entire watershed or other area of interest.

Step 8. Either at the time when the first of the wintertime Landsat sets of imagery is obtained, or prior thereto, a set of acetate overlays each about 9"x9" in size and gridded at various intervals into squares,[1] should be prepared. In any given instance the size of the grid should be governed by time, accuracy, and cost constraints. Obviously, in most instances as grid size decreases, the accuracy, cost and time factors all increase.

Step 9. Through the use of geographic features that are readily located on Landsat imagery, each successive frame of such imagery should be indexed so that the gridded acetate overlay can be registered in exactly the same way with respect to each of the frames that cover a given area.

Step 10. Similarly, the grids, as they appear on the Landsat frames of imagery, should be transferred to the low-altitude photos (i.e., the stage two photos taken at large scale with 35mm color film) and then labelled in such a manner that any grid unit (i.e., any image sample unit) can be easily located there and readily cross-referenced to the corresponding Landsat imagery.

---

1. See: Table II-1 Summary of Image Sample Unit (ISU) Optimization Data, page II-1

130

Step 11. The indexed grids as they now appear on the low-altitude photography should be interpreted for areal extent of snow. Generally four to six snowcover classes should be used, based on the proportion of the grid that appears to be snow-covered. An example using six classes could be: Class 1, 0-9 percent; Class 2, 10-25 percent; Class 3, 25-50 percent; Class 4, 50-75 percent; Class 5, 75-90 percent; Class 6, 90-100 percent. (It has been found that, due to the large amount of detail visible on the large scale prints, it is a fairly easy task for each grid unit to be placed in a specific class with a high degree of certainty.)

Step 12. This set of classified grid units should now be divided into a training and a testing set. The training set should be located on the gridded acetate overlays to the Landsat imagery and should include a wide range of snow appearance types covering the range of snowcover classes.

Step 13. The interpretation set-up should now be constructed. It should consist of a coincident image viewing device, such as a mirror-stereoscope or a transfer scope, the set of 8"x10" Landsat summer color composite prints, for which the determination of snow areal extent is to be made, and the set of classified grid units, as seen on the low-altitude aerial photography, corresponding to the gridded winter color composite prints.

Step 14. As the detailed interpretation of the Landsat winter photos begins, one 8"x10" summer Landsat print should be placed under the stereoscope (or transfer scope) along with the corresponding scene on the gridded winter Landsat print set. The prints should be adjusted so that conjugate images can be fused by the photo interpreter (i.e., so that all common features can be made to coincide with each other, one image viewed with each eye), thus allowing the interpreter to assess both the snow areal extent and the vegetation/terrain conditions in each grid unit.

Step 15. The interpreter should next engage in the task of training himself to recognize different snowcover condition classes within grid units based on: (a) underlying vegetation/terrain features (as seen on the summer Landsat print), (b) the snowcover visible on the gridded winter Landsat print, and (c) the appearance and subsequent classification of the grid units as seen on the low-altitude aerial photography. By viewing through the coincident image device and observing how each grid unit in the training set appears during the winter and summer, and by then referring to the training set grid units on the low-altitude aerial photography, the interpreter can effectively complete this training task in very short order.

Step 16. Once trained, the interpreter should then proceed to classify each grid square (image sample unit) on the winter Landsat print (in terms of the snow areal extent class to which it belongs) according to his synthesis of the information available as he perceives it on the summer and winter Landsat prints.

Step 17. After all of the winter dates of imagery have been classified, the interpreter's initial interpretation results are ready for the testing phase. Therefore, at this point the results of the grid classification (as made on the low-altitude aerial photography testing set) should be compared to the results obtained by the interpreter in all applicable grid units. A ratio estimator statistic, as described in detail in Appendix I of this Procedural Manual should then be applied. This statistic will provide the adjustment calibration necessary to correct the interpreter's initial interpretation results.

Step 18. Once the true value for the snow areal extent has been estimated using the population ratio estimator, two other statistical tests can be applied to clarify the final result. The confidence interval concept can be used to give an idea of the range of the final snow areal extent value. A Chi-square test can be applied to test the snowcover class width selection. Both of these tests are discussed in detail in Appendix I.

Note: It is apparent from the foregoing that, even if this procedure is highly successful, its end product is merely an accurate determination of the areal extent of snow, together with an accurate delineation of each portion of the watershed area according to the snowcover class to which it belongs. This is an essential step leading to a prediction of water runoff and the estimation of water yield. The remaining steps are discussed in other procedural manuals.

132

Appendix I

A SPECIFIC CASE STUDY

The following case study describes uses that our RSRP personnel have made of the foregoing procedure for the Feather River Watershed, California.

On April 4, 1973 the majority of the Feather River Watershed (located in the central Sierra Nevada Mountains, California) was imaged in a virtually cloud-free condition by the Landsat satellite. In order to document the existing ground conditions in greater detail than that provided by the satellite imagery, a photographic mission was flown over the watershed on April 6, 1973. Four transects were flown using a motorized 35mm camera to acquire photography at a scale of approximately 1:30,000 on the negative (Figures 3 and 4).

Landsat imagery from August 13, 1972 was chosen for use as the vegetation/terrain base for the snowpack analysis procedures. The August 13 and the April 4 Landsat images of MSS bands 4, 5, and 7 were photographically combined to produce simulated color infrared enhancements (Figures 3 and 4).

The simulated color infrared enhancement of the August 13, 1972 Landsat scene was photographically reproduced to give a 16" x 20" color print of approximately 1:250,000 scale. The April 4, 1973 Landsat color infrared enhancements were enlarged to precisely the same scale as the August 13, 1972 imagery and printed to give overlapping 8" x 10" prints.

An acetate grid (each grid block equalling approximately 2,000 meters on a side at a scale of approximately 1:250,000) was attached to the vegetation/terrain Landsat image. The grid blocks, termed image sample units (ISU), were transferred to the large scale photography where applicable. The image sample units on the large scale aerial photography were coded as shown in Table I-1.

Table I-1

Snowcover Condition Classes Used for Areal Extent of Snow Estimation

Code	Snowcover Class	Midpoints
1	No snow present within ISU	0
2	0-20% of ISU covered by snow	.10
3	20-50% of ISU covered by snow	.35
4	50-98% of ISU covered by snow	.74
5	98-100% of ISU covered by snow	.99

The interpreter then engaged in the training phase to familiarize himself with the imagery and image classification technique. Once trained, the interpreter proceeded to classify all the image sample units on the 8" x 10" Landsat color print for the winter dates. A more detailed description of this process will be found in the Procedural Manual.

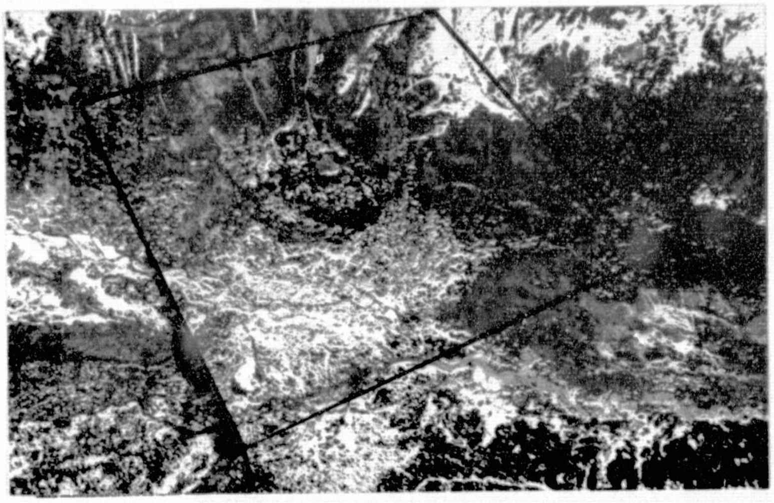

FIGURE I-1

Low altitude aerial photographs of the snowpack taken from a light aircraft using a 35 mm camera. The scale of the negative is approximately 1:30,000. The grid shown on the photograph represents an image sample unit, (ISU), also located on the Landsat color composite imagery (see Figure I-4). The image sample unit shown represents a snowcover class of 3 (See Table I-1).

134

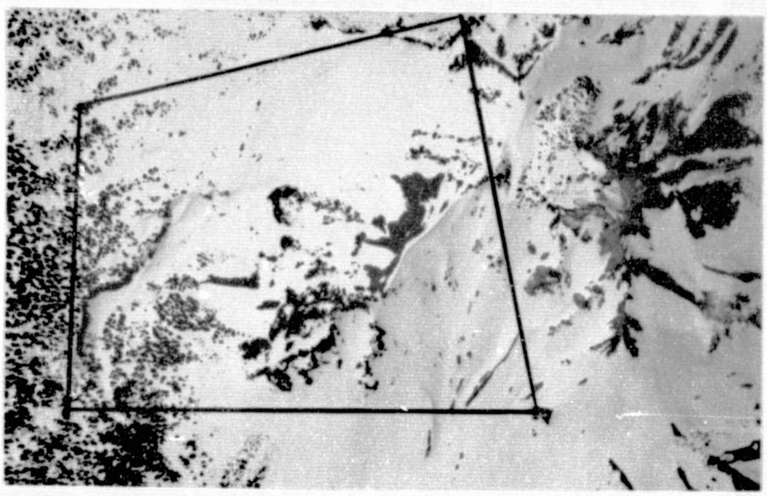

FIGURE I-2

Low altitude aerial photograph of the snowpack similar to Figure I-1 however representing a snowcover class of 4 (See Table I-1).

ORIGINAL PAGE IS
OF POOR QUALITY

FIGURE I-3

August 13, 1972 Landsat color composite image showing the Feather River and the Spanish Creek Watersheds.

136

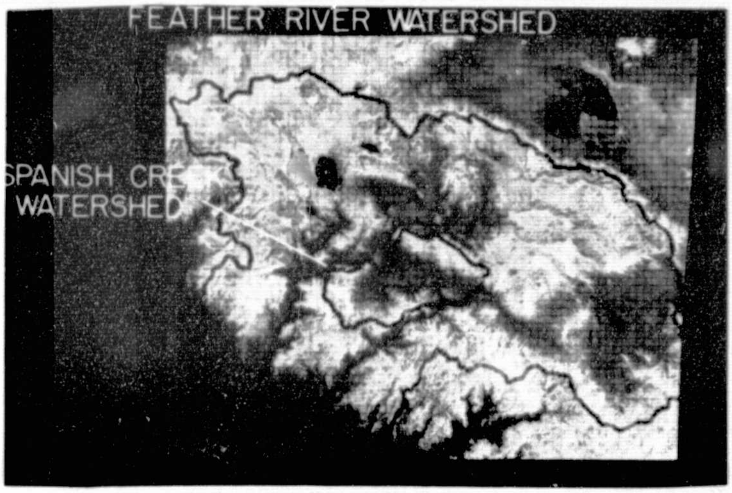

FIGURE I-4

April 4, 1973 gridded Landsat color composite image showing the Feather River and Spanish Creek Watersheds. The grids define the image sample units, each being approximately 400 hectares in size.

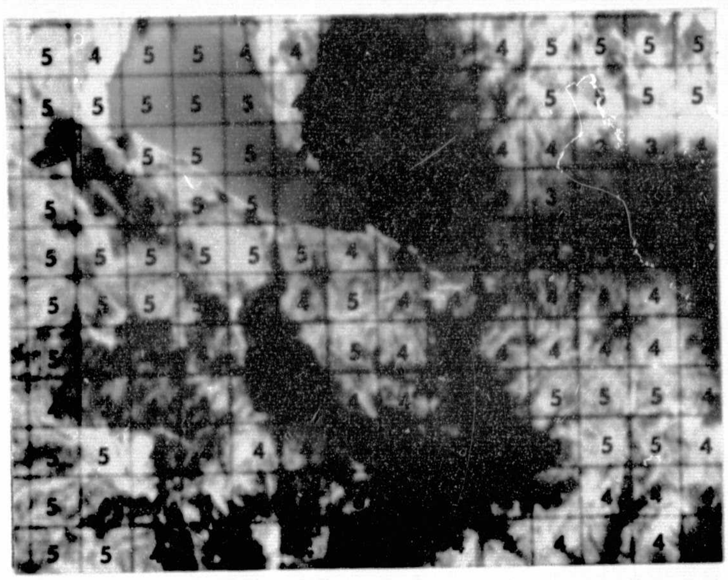

FIGURE I-5

A portion of the April 4, 1973 Landsat color composite image showing the snowcover class interpretations on an image sample unit basis.

The classified imagery was then subjected to statistical analysis. The following are the results from the April 4 Landsat areal extent of snow analysis.

	Snowcover (Condition) Class				
	1	2	3	4	5
Total number of ISU's classified per class	403	289	214	453	859

To derive the approximate number of hectares in each class, the image sample unit totals per class were multiplied by the number of hectares per image sample unit (400) with the results indicated below:

	Snowcover (Condition) Class				
	1	2	3	4	5
Hectares	$.161 \times 10^6$	$.116 \times 10^6$	$.856 \times 10^5$	$.181 \times 10^6$	$.344 \times 10^6$

Then to establish the approximate amount of actual snow-covered area per class, the number of hectares/class were multiplied by the snowcover class midpoints (from Table I-1) for each class, as indicated below in the following tabular summary:

	Snowcover (Condition) Class				
	1	2	3	4	5
Snowcover condition class midpoint	0	.10	.35	.74	.99
Hectares of snow per class	0	$.116 \times 10^5$	$.300 \times 10^5$	$.134 \times 10^6$	$.340 \times 10^5$

By adding the "hectares of snow per class" values, the "total surface area of snow" in hectares was established. Thus for the April 4, 1973 Landsat date the estimate of snow areal extent was found to be 515,772 hectares. This value, however, may be biased by any errors which occurred during the classification of the Landsat image sample units for snow areal extent. The uncorrected areal extent of snow estimate can be "corrected" by comparing the interpreter classification results with a series of preselected, preclassified image sample units, chosen for testing purposes from the large scale aerial photographs.

Interpretation results not falling in a given snowcover condition class for both the large scale aerial photographic and Landsat image data represent a misclassification of image sample units by the interpreter (Table I-2). Thus it can be seen that 13 out of a possible 80 image sample units were misclassified. This misclassification error can then be represented by a statistic, the population ratio estimator (Cochran, 1959), which will be used to correct the initial areal extent of snow estimate of 5.1582×10^5 hectares derived from the Landsat image classification.

The statistical approach is defined as follows:

(Equation 1.0) $\hat{Y}_r = X\hat{R}$ = the final, corrected areal extent of snow estimate

(Equation 1.1) where: $X = \sum_{j=1}^{N} X_j$ = the uncorrected Landsat areal extent of snow estimate

given that: X_j = the Landsat interpretation estimate of snow areal extent, per image sample unit, by snowcover class

j = the index for all Landsat image sample units

N = the total number of Landsat image sample units classified for snow areal extent

(Equation 1.2) where: $\hat{R} = \overline{Y} \div \overline{X}$ = the population ratio estimator

(Equation 1.3) given that: $\overline{Y} = \left(\sum_{i=1}^{n} y_i\right) \div n$ = the average snow areal extent value for the large scale photographic image sample unit estimates

(Equation 1.4) $\overline{X} = \left(\sum_{i=1}^{n} x_i\right) \div n$ = average snow areal extent value for the Landsat image sample unit estimates

and that: n = the total number of image sample units used in the testing phase

i = sampling index

y_i = large scale photography snow areal extent estimate for image sample unit i

x_i = Landsat snow areal extent estimate for image sample unit i

ORIGINAL PAGE IS
OF POOR QUALITY

Since the uncorrected Landsat areal extent of snow estimate (X) has been calculated to be 5.158 x 10^5 hectares, the value for the population ratio estimator, R, must be determined to solve for the final, corrected Landsat areal extent of snow estimate, $\hat{Y}_r$, (from the equation $\hat{Y}_r = X\hat{R}$). Table I-2 represents an expanded version of Table 2 designed to facilitate the calculation of the population ratio estimator, $\hat{R}$. The table has been enlarged to include listings of snowcover condition class/image sample unit, specific large scale photography estimates of snow areal extent, and Landsat areal extent of snow estimates.

y_u = large scale aerial photography estimate of snow areal extent per image sample unit by snowcover condition class (in hectares)

$$= \begin{bmatrix}\text{snowcover condition class} \\ \text{midpoint}\end{bmatrix} \begin{bmatrix}\text{number of hectares} \\ \text{per image sample unit}\end{bmatrix}$$

and; x_u = Landsat snow areal extent estimate per image sample unit by snowcover condition class (in hectares)

$$= \begin{bmatrix}\text{snowcover condition class} \\ \text{midpoint}\end{bmatrix} \begin{bmatrix}\text{number of hectares} \\ \text{per image sample unit}\end{bmatrix}$$

f_u = image sample unit interpretation frequencies

u = index for table containing the results of the testing phase

Additionally,

n = the number of image sample units used in the testing phase, i.e.,

(Equation 1.5)
$$n = \sum_{u=1}^{1} f_u = 80$$

where: u = index for Tables I-2 and I-3.

and k = the number of interpretation result blocks in Tables I-2 and I-3=11.

$\hat{R}$, the population ratio estimator, can now be calculated by solving for $\overline{Y}$ and $\overline{X}$ from the data presented in Table I-3. Thus if

(Equation 1.6)
$$\sum_{i=1}^{n} y_i = \sum_{u=1}^{k} f_u \, y_u$$

ORIGINAL PAGE IS
OF POOR QUALITY

(Equation 1.7) and $$\sum_{i=1}^{n} x_i = \sum_{u=1}^{k} f_u y_u$$

then $$\overline{Y} = \sum_{i=1}^{n} y_i \div n$$ (Equation 1.3)

(Equation 1.8) $$= \sum_{u=1}^{k} f_u y_u \div n$$ (from Equation 1.6)

(Equation 1.9) $$= \sum_{u=1}^{k} f_u y_u \div \sum_{u=1}^{k} f_u$$ (from Equation 1.5)

and $$\overline{X} = \sum_{i=1}^{n} x_i \div n$$ (Equation 1.4)

(Equation 2.0) $$= \sum_{u=1}^{k} f_u \div n$$ (from Equation 1.7)

(Equation 2.1) $$= \sum_{u=1}^{k} f_u x_u \div \sum_{u=1}^{k} f_u$$ (from Equation 1.5)

Therefore (from Table I-3 and equations 1.9 and 2.1).

$$\overline{Y} = \frac{(0)(6)+(40)(1)+(40)(10)+(296)(1)+(40)(2)+(140)(6)+(296)(2)+(140)(1)+(296)(12)+(296)(6)+(396)(33)}{6+1+10+1+2+6+2+1+12+6+33}$$

$$= \frac{20784}{80}$$

$$= 259.80$$

and

$$\overline{X} = \frac{(0)(6)+(0)(1)+(40)(10)+(40)(1)+(140)(2)+(140)(6)+(140)(2)+(296)(1)+(296)(12)+396(6)+396(33)}{6+1+10+1+2+6+2+1+12+6+33}$$

$$= \frac{21132}{80}$$

$$= 264.15$$

Consequently, the population ratio estimator (Equation 1.2) is calculated to be:

$$\hat{R} = \overline{Y} \div \overline{X} \qquad \text{(Equation 1.2)}$$

$$= 259.80 \div 264.15$$

$$= .9835$$

Finally, to solve for $\hat{Y}_r$ (the final, corrected areal extent of snow estimate), the population ratio estimate, $\hat{R}$, is multiplied by the uncorrected Landsat areal extent of snow estimate, X (Equation 1.0). Thus,

$$\hat{Y}_r = X\hat{R} \qquad \text{(Equation 1.2)}$$

$$= (\ 515{,}772 \qquad) \ (.9835) \text{ hectares}$$

$$= 507{,}278 \text{ hectares}$$

Once the actual areal extent of snow has been estimated, $\hat{Y}_r$, it may be useful to know where the true value for the areal extent of snow lies. The confidence interval is useful for this purpose. The statistical approach is as follows, using the 95% level of confidence as an example:

Y_r = the true value for the areal extent of snow

The confidence interval around Y_r can be expressed as the probability that

(Equation 2.2) $$\left[\hat{Y}_r - t_{n-1,\ .025}\sqrt{V(\hat{Y}_r)} \leq Y_r \leq \hat{Y}_r + t_{n-1,\ .025}\sqrt{V(\hat{Y}_r)}\right] = .95$$

(Equation 2.3) where $$V(\hat{Y}_r) = \frac{N(N-n)}{n(n-1)}\left[\sum_{i=1}^{n} y_i^2 + \hat{R}^2 \sum_{i=1}^{n} x_i^2 - 2\hat{R}\sum_{i=1}^{n} x_i\, y_i\right]$$

= sample variance

where $$\sum_{i=1}^{n} Y_i^2 = \sum_{i=1}^{k} f_u(Y_u^2)$$

and $$\sum_{i=1}^{n} X_i^2 = \sum_{i=1}^{k} f_u(X_u^2)$$

A summary of all the major results from the statistical analysis described previously for the April 4, 1973 snow analysis date is contained in Table VIII-4.

The final statistical test that was employed in this analysis was used to determine the suitability of the snowcover condition class widths as selected from step 11 in the procedure and Table 1-2. This test was to determine if the values in the snowcover classes from the Landsat image data came from the same statistical probability distribution as the values in the snowcover classes from the large scale aerial photographic data. If they came from the same distribution it could be expected that the areal extent of snow estimation procedure would provide good results. If these indicated that the two data sets came from different distributions, then new class widths should be selected and the areal extent of snow estimation procedure should be rerun. To perform such probability distribution "likeness tests," a Chi-square statistic was used:

(Equation 2.4) $$x^2 \sim \sum_{i=1}^{k} \frac{(O_i-E_i)^2}{E_i}$$

where O_i = the observed values

E_i = the expected values

k = the number of snowcover condition classes

i = index.

The values in the snowcover classes from the large scale photo data were designated as the expected values (E_i), since they were assumed to be "ground truth." The values in the snow cover classes from the Landsat image data were designated as the observed values (O_i).

The results of the Chi-square test for the April, 1973 statistical testing data (Table I-5) are shown in Table I-2. The results indicate that the two data sets do come from the same statistical probability distributions; thus it can be assumed that the snowcover class widths used for the areal extent of snow analysis are adequate.

144

Table I-2

Interpretation results of the testing phase, areal extent of snow estimation for the April 4, 1973 Landsat and April 6, 1973 large scale aerial photographic data.

Landsat Image Data: Snowcover Condition Class	Large Scale Aerial Photographic Data: Snowcover Condition Class 1	2	3	4	5
1	6	1			
2		10		1	
3		2	6	2	
4			1	12	
5				6	33

Key to Table I-2

$\boxed{f_u}$

where: f_u = Image sample unit interpretation frequencies

u = Index for the table.

ORIGINAL PAGE IS
OF POOR QUALITY

Table I-3

Interpretation results of the testing phase, areal extent of snow estimation for April 4, 1973 Landsat and April 6, 1973 large scale aerial photographic data. Also included is a listing of uncorrected large scale aerial photographic and Landsat image estimates of snow areal extent per image sample unit by snowcover class.

		Large Scale Aerial Photographic Data				
		Snowcover Condition Class				
		1	2	3	4	5
Landsat Image Data — Snowcover Condition Class	1	0 0 6	40 0 1			
	2		40 40 10		296 40 1	
	3		40 140 2	140 140 6	296 140 2	
	4			140 296 1	296 296 12	
	5				296 396 6	396 396 33

Key to Table I-3

	y_u
x_u	f_u

where: x_u = Landsat snow areal extent estimate per image sample unit by snowcover condition class (in hectares)

y_u = Large scale photography snow areal extent estimate per image sample unit by snowcover condition class (in hectares)

f_u = Image sample unit interpretation frequency

u = Index for the table.

Table I-4

Summary of Statistical Results
Areal Extent of Snow Estimation
April 4, 1973

Landsat estimate of the areal extent of snow (in hectares)	X	515,772
Population ratio estimator	$\hat{R}$	.9835
Estimate of the true areal extent of snow (in hectares)	$\hat{Y}_r$	507.278
Standard deviation of the areal extent of snow estimate (in hectares)	$\sqrt{V(\hat{Y}_r)}$	12,659.29
Confidence interval (95%) around the true value for the areal extent of snow (in hectares)		$482,040 \leq Yr \leq 532,517$
Total number of image sample units inventoried on the Landsat imagery	N	2,218
Average surface area of an image sample unit (in hectares)		400
Total number of hectares inventoried		887,200
Total number of image sample units sampled for the statistical testing procedure	n	80

Table I-5

Chi-square Test for April 4, 1973 Data

<u>Null Hypothesis</u>: Ho: The observed values (O_i) come from the same distribution as the expected values (E_i)

<u>Alternative Hypothesis</u>: Hi: The observed values do not come from the same distribution as the expected values

<u>Significance Level</u>: 5%

<u>Test Statistic under the Null Hypothesis</u>: $\sum_{i=1}^{k} \frac{(O_i-E_i)^2}{E_i} \sim X^2_{k-1}$;

where k-1 = the degrees of freedom

Full Class Data Summary

Class	O_i	E_i	$\frac{(O_i-E_i)^2}{E_i}$
1	7	6	.1667
2	11	13	.3077
3	10	7	1.2857
4	13	21	3.0476
5	39	33	1.0909

$$\sum_{i-1}^{k} = 5.8992$$

Conclusion: The null hypothesis is accepted since the calculated value of 5.8992 is less than the table value of 9.49.

148

APPENDIX II

PROCEDURE FOR OPTIMAL IMAGE SAMPLE UNIT SIZE ESTIMATION

The operational application of the image sample unit areal extent of snow estimation technique is heavily dependent on the size of the image sample unit used.

It was expected that the smaller the ISU size the smaller the standard deviation (and variance) of the corrected areal extent of snow estimate. Conversely, as the size of the ISU's decreased, it was suspected that interpretation time (also known as cost!) would increase. In an effort to give prospective users a starting point when deciding on what image sample unit size to use, a simple test was developed to find some optimal image sample unit size (i.e. minimized standard deviation and interpretation time). The test would compare interpretation time and standard deviation of the corrected areal extent of snow estimate for three different image sample unit sizes. One interpreter was used throughout the test to minimize - or at least standardize - bias in the final results.

Three image sample unit sizes (204, 459, and 815 hectares each) were used on a single Landsat winter date. Interpreter training, classification, and testing were carried out as described in steps 15, 16 and 17.

The estimated values of the areal extent of snow along with their standard deviations and interpretation times for each image sample unit size, are summarized in Table II-1.

Table II-1 Summary of Image Sample Unit (ISU) Optimization Data.

Image Sample Unit Size (in hectares	Standard Deviation of the estimate (in hectares)	Interpretation Time (in hours)
204	9,981.36	6.75
459	16,864.54	6.00
815	24,439.40	5.50

As expected standard deviation decreases and interpretation time increases with image sample unit size. By plotting the data it was determined that an image sample unit size of 365 hectares was the point where both standard deviation and interpretation were minimized as shown in Figure II-1

It should be noted that the image sample unit size of 365 hectares is to be considered a maximum size for 2 reasons:

(1) The interpreter who analyzed the three image sample unit sizes was previously inexperienced in this type of interpretation. The largest ISU size was interpreted first and the smallest last. It can be expected that the interpretation time for each succeeding ISU size was reduced due to the experience gained on the operation of the interpretation system design. Thus, it seems reasonable that as more experience is gained, the intepretation time for any ISU size would be reduced, lowering the "interpretation time versus ISU size" curve. Consequently, the value of 365 hectares for an "optional" ISO size could conceivably be reduced by increasing interpreter experience.

(2) While the results illustrated in Figure II-1 , indicated an optimal ISU size for minimizing standard deviation and interpretation time, the image sample unit size may de decreased even further if more time can be spent in the interpretation phase.

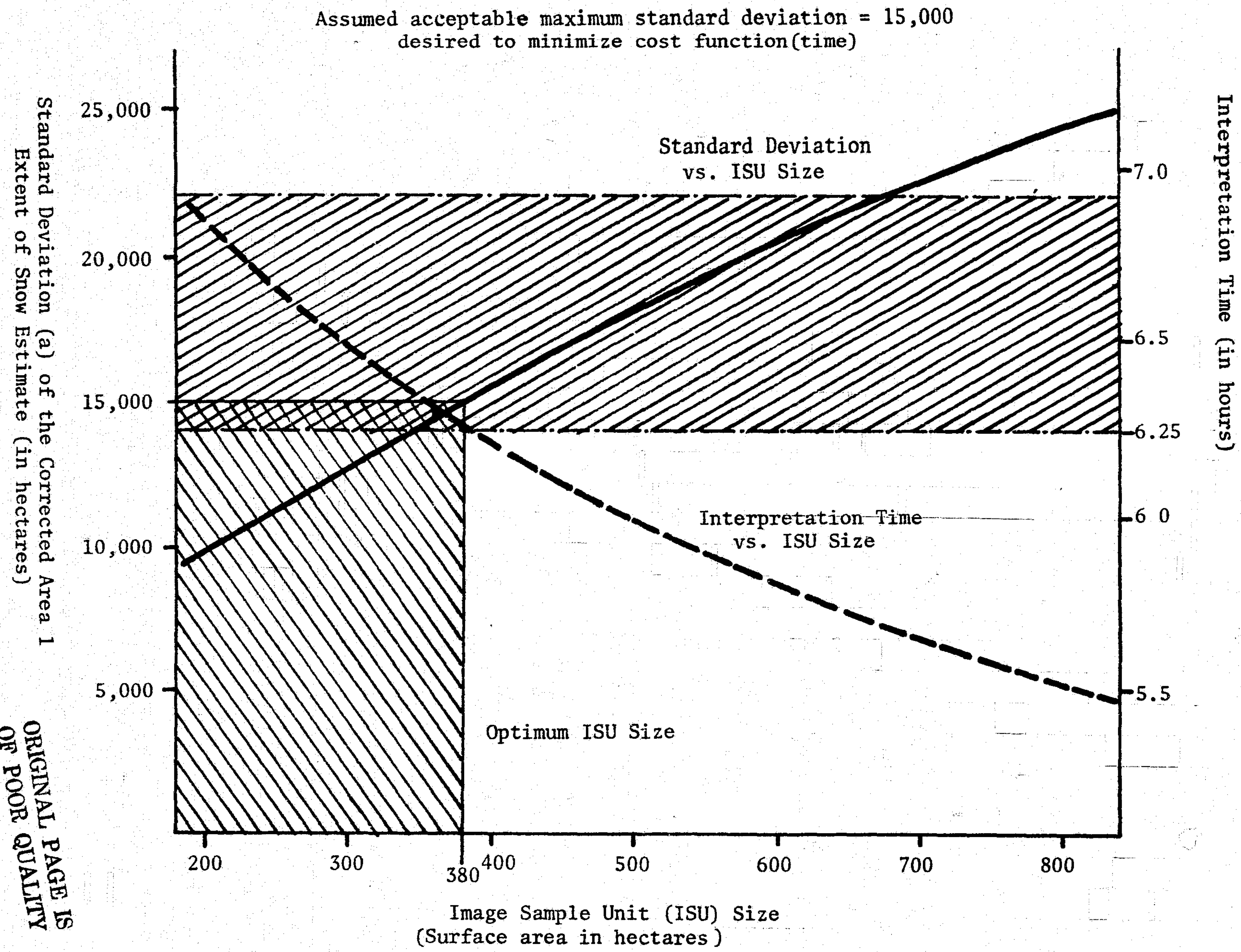

Figure II-1 Determination of Optimal ISU Size

ORIGINAL PAGE IS OF POOR QUALITY

Appendix III

PROCEDURAL MANUAL FOR THE PHOTOGRAPHIC CONSTRUCTION OF LANDSAT COLOR COMPOSITE IMAGERY

INTRODUCTION

The value of color composites has long been recognized as an aid to the interpretation of Landsat imagery. The technique described in this technical brief demonstrates how Landsat color composite imagery can be constructed from Landsat positive black-and-white transparencies conveniently and inexpensively.

COLOR COMPOSITE THEORY

Typical color reversal and color negative films consist basically of three light sensitive layers. These layers react individually to blue, green, and red light, each layer corresponding to a particular dye, dependent upon film type, as indicated below:

Light Sensitivity	Color reversal film Dye layers activated	Color negative film Dye layer activated
Red	Yellow and Magenta	Cyan
Green	Yellow and Cyan	Magenta
Blue	Magenta and Cyan	Yellow

If, for instance, color negative film is exposed to blue light, the blue sensitive layer of the film is activated while the other layers remain unaffected. This blue-sensitive layer corresponds to a final yellow dye image and hence the results will appear yellow on the negative.

When color reversal film is exposed to blue light, the blue sensitive layer of the film is activated; however, during processing the two remaining sensitivity layers corresponding to the magenta dye (green sensitive) and the cyan dye (red sensitive) are either chemically or mechanically exposed. The originally exposed blue sensitive layer becomes non-functional and the resulting image appears blue due to the combination of magenta and cyan dyes. The reactions of color reversal and negative film to red and green light can be explained similarly since red is produced by a combination of yellow and magenta dyes and green is produced by a combination of cyan and yellow dyes.

152

The photographic construction of Landsat color composites relies on the three-layer sensitivity of color film and on the different densities of any given feature as it appears on the various Landsat black-and-white bands. Each of the different Landsat black-and-white bands chosen to make the color composite is photographically copied onto the same sheet (or frame) of color film, each band through a different colored filter (in essence a multiple exposure). Figure III-1 illustrates the set-up used to produce Landsat color composites. Depending on which filter is used with each band of imagery different color renditions may be produced, hopefully enhancing different features.

MATERIALS AND EQUIPMENT

LANDSAT BLACK-AND-WHITE IMAGERY

The construction of Landsat color composites commonly uses Multispectral Scanner (MSS) imagery of bands 4, 5, and 7, usually in the 9½ inch positive transparency form (although the 70 millimeter positive transparencies may also be used). MSS Band 6 is also used for some composites as well as available Return Beam Videcon (RBV) positive imagery. Furthermore, just as a color composite can be formed by combining bands of imagery acquired on a single date, so it also can be formed by combining several dates of imagery acquired in a single band, or any combination of multiband/multidate images.

FILTERS

Eastmak Kodak Wratten filters are suggested for use in the construction of color composites due to their optical quality and the large variety of colors and sizes available. To produce a simulated false-color infrared color composite image (Figures I-3 and I-4), Wratten filter number 25 (tricolor red), 47B (tricolor blue), and 58 (tricolor green) can be used.

FILTER RELATED ACCESSORIES

Eastmak Kodak filter frames provide a convenient way to mount the Wratten filters. The filters so mounted can be easily inserted into a commercially available filter holder which mounts, via adapters, to the filter-threaded receptacle in the front of most enlarging lenses.

PHOTOGRAPHIC LIGHT SOURCE

The light source is used to provide the light which will be transmitted through the Landsat bands during the exposure process. Basically, the light source may be of two common types; incandescent or flourescent and electronic strobe. Incandescent or flourescent illumination in the form of a "light table" may be the most convenient form to use initially. One of the problems encountered with using a light table is its relatively low light output, necessitating long exposures times. One way of countering this is by using an electronic strobe light box which could give decidely greater light output and thus shorter exposures.

REGISTRATION SHEET

The registration sheet is used to register the individual Landsat bands with respect to one another. It also serves as a convenient base for introducing grids, watershed boundaries or other data directly on the color composite. The material used for the registration base should be translucent (frosted preferably), dimensionally stable and have a surface amenable to scribing.

SCRIBING TOOLS

The scribing tools consist of a scriber and a metal straight edge. The scriber can be constructed by inserting a drafting compass needle in an engineering drafting pencil while the metal straight edge may simly be a metal engineering scale. The scribing tools are used to transfer the Landsat registration marks onto the registration sheet.

CAMERA SYSTEM

A large variety of cameras and related accessories ranging in format from 35 millimeter to much larger image sizes can be used to construct Landsat color composites. The only requirement is that the camera be capable of making accurate multiple exposures on a single sheet or frame of film. The most convenient camera used to develop this system was found to be a type of copy camera which utilizes a leaf shutter system allowing as many exposures as desired on a single sheet or frame of film. A camera system of this type is desirable due to its ability to accept film formats from 35 millimeters to 4 x 5 inches.

The camera lens used for making color composites should be of very high quality. Since the construction of color composites utilizes most of the light-sensitive spectral range of conventional color film, the lenses used should be color corrected. The lenses should be of very high uniform edge-to-edge resolution and contrast to assure that no information is lost throughout the image area.

EXPOSURE METER

An exposure meter should be used to determine how much exposure should be given to each of the Landsat black-and-white images in making the color composite. The meter used should have a locking needle, a wide sensitivity range and a narrow acceptance angle so that selective area measurements can be made.

FILM TYPES

If reflection prints are to be made of the color composite, it is most convenient to use a fine grain negative color film such as Kodak Vericolor II Type S. If positive color transparencies are desired (e.g. for projection purposes) the use of either Kodachrome or Ektachrome film is appropriate, depending on the film format used.

154

PROCEDURE

The following step-by-step description will detail the procedure used to construct a Landsat color composite.

Step 1. Tape one band of a Landsat black-and-white set of imagery for a specific date to a light table in proper viewing position.

Step 2. Tape a sheet of the registration base material over the Landsat image so that the four registration marks (+) in the corners of the Landsat image are completely covered by the overlying sheet.

Step 3. Transfer the registration marks to the registration base material using the scriber and the metal straight edge. The scribed line should be narrow in width and extend beyond the actual Landsat registration marks to facilitate the actual registration process.

Step 4. The registration sheet should be labeled with the latitude/longitude and date of the Landsat imagery from which it was made. This information is placed on the same edge as observed on the Landsat image below so that the Landsat black-and-white bands may be oriented correctly during the registration process.

Step 5. The completed registration sheet is removed and placed in proper position on the light table or flash box and taped down.

Step 6. One of the Landsat bands to be used for making the composite is taped down in register over the registration sheet. The registration marks and the information line are used to register and orient the two, relative to one another.

Step 7. The camera system is focused upon this registered image and locked into position.

Step 8. An exposure measurement of the Landsat band is then made on the ground glass focusing screen of the camera with the lens set at a fixed aperture, usually maximum. This reading is recorded. The other Landsat bands to be used are then placed one at a time on the registration sheet with the image projected onto the focusing screen and the exposure measurement for each is recorded again at the same fixed aperture.

Step 9. The exposure measurements for the Landsat bands are averaged and refered to exposure graphs (which are explained in the next section).

Step 10. The camera/lens exposure controls are then set according to the exposure graphs.

Step 11. The film on which the composite is to be made is then loaded in the camera.

Step 12. One at a time, the Lands-t bands are placed on the registration sheet and exposed through the appropriate filter. The film is not advanced or removed until all exposures have been made.

Step 13. The film is then processed normally yielding the final color composite.

EXPOSURE DETERMINATION

In determining the proper exposure to give each of the Landsat black-and-white images the separate bands are assumed to be matched separation positives. The actual deviation from this assumption is generally so slight that it may be ignored in most if not all cases.

Since no two light source systems developed to construct Landsat color composite imagery will have equal light outputs, the graph used to determine proper exposure must be empirically established. The following describes the determination of the exposure graph necessary for proper exposure calculation. Since each exposure graph can be calculated for one particular color composite type (i.e., band/filter combination) only, the following description will deal with the construction of a simulated false color infrared composite. To make this particular rendition Landsat band 7 is exposed through a Wratten 25 (Red) filter, band 5 through a Wratten 58 (Green) filter and band 4 through a Wratten 47B (Blue) filter.

To empirically determine the exposure graphs for the various band/filter combinations, a series of color composites are constructed at different overall exposures. Each series of color composites has exposure values measured for each band as per step 8 under "procedures". The values measured are averaged for each set and then plotted versus the actual overall exposure found to give an acceptable color composite. All light measurement values are taken with the lens set at a fixed aperture. This aperture will always be used for the through-the-lens exposure measurements of each band. This is necessary to provide a consistent index system for reference to the exposure graphs.

The averaged exposure measurements taken from the individual Landsat bands are plotted on the x-axis versus Exposure Values (EV) on the y-axis. EV refers to equal light intensities; hence equal combinations of shutter speed and aperture which yield the same exposure to the film. For example, EV 13 equals 1/30 second at f/15, 1/60 second at f/11, 1/125 second at f/8, 1/250 second at f/5.6, etc. Figure III-2 illustrates the appearance of such an exposure graph.

Due to the different optical densities of the filters used to construct a color composite, different exposures are needed for each band/filter combination. These different densities can be refered to as filter factors. The filter factor for a given filter changes with the film type as well as the light source; consequently filter factors must be calculated for each film type/light source combination. One practical way of calculating specific filter factors is to photograph a transparent gray scale through each of the filters for which the filter factor is to be determined. These will produce individual exposures through the filters onto color film, either positive or negative. Several exposures are taken through each filter, advancing or changing the film after each exposure. All exposures must be recorded for the final determination of the filter factors. For each filter an exposure is found which best reproduces the gray scale (i.e. all gray levels are

156

clearly distinguishable from each other) by examining the color film. In all cases each individual gray level should have the same optical density for all of the filter types used. This is best done through the use of a densitometer but can be done visually if necessary. A comparison of the exposures used for the various filters to obtain equal densities gray level-by-gray level, will give the filter factors for each filter. These filter factors may then be translated into EV's to give the relative exposure differences for the filters used.

To establish the exposure graphs for the various band/filter combinations, a series of color composites are constructed, all at different overall exposures. Each composite so constructed must have the filter factors (in terms of individual exposure differences) included. If, for example, for a specific film/light source combination, it is determined that a Wratten 47B filter requires 1 EV more exposure than a Wratten 58 filter, (which requires itself ½ EV more exposure than a Wratten 25 filter to obtain equal density levels) then a series of exposures can be made using these differences. For the first composite the overall exposure might be EV13 through the Wratten 47B filter, EV 14 through the Wratten 58 filter, and EV 14.5 through the Wratten 25 filter. For the second composite overall exposure might be EV14 through the Wratten 47B filter, EV 15 through the Wratten 58 filter, and EV 15.5 through the Wratten 25 filter and so on. Since the individual filters require different but equal relative exposure differences maintained during the construction of the composites, color balance is kept stable, but overall composite density is not. Thus the best composite density from this series of different overall exposures can be determined. By plotting the exposures used for each filter in the best composite constructed, one group of points may be plotted on the exposure graph for this particular band/filter combination. Once two groups of points, each representing a good color composite overall exposure for a specific band/filter combination have been plotted, the graph can be completed.

CONCLUSIONS

Several critical points are worth mentioning again to assure that the color composites are correctly constructed:

1. During the actual photographic construction, several exposures are made on the <u>same</u> sheet or frame of film; the film is not removed or advanced during these exposures.

2. All exposure measurement values of the various bands are made through the camera/lens assembly on the ground glass using a fixed aperture. This aperture may change depending upon the actual responses of the various bands during the copying process.

3. The individual exposure measurements of the bands to be used are mathematically averaged and then referred to the exposure graph for the exposure setting of each band/filter combination.

157

ORIGINAL PAGE IS
OF POOR QUALITY

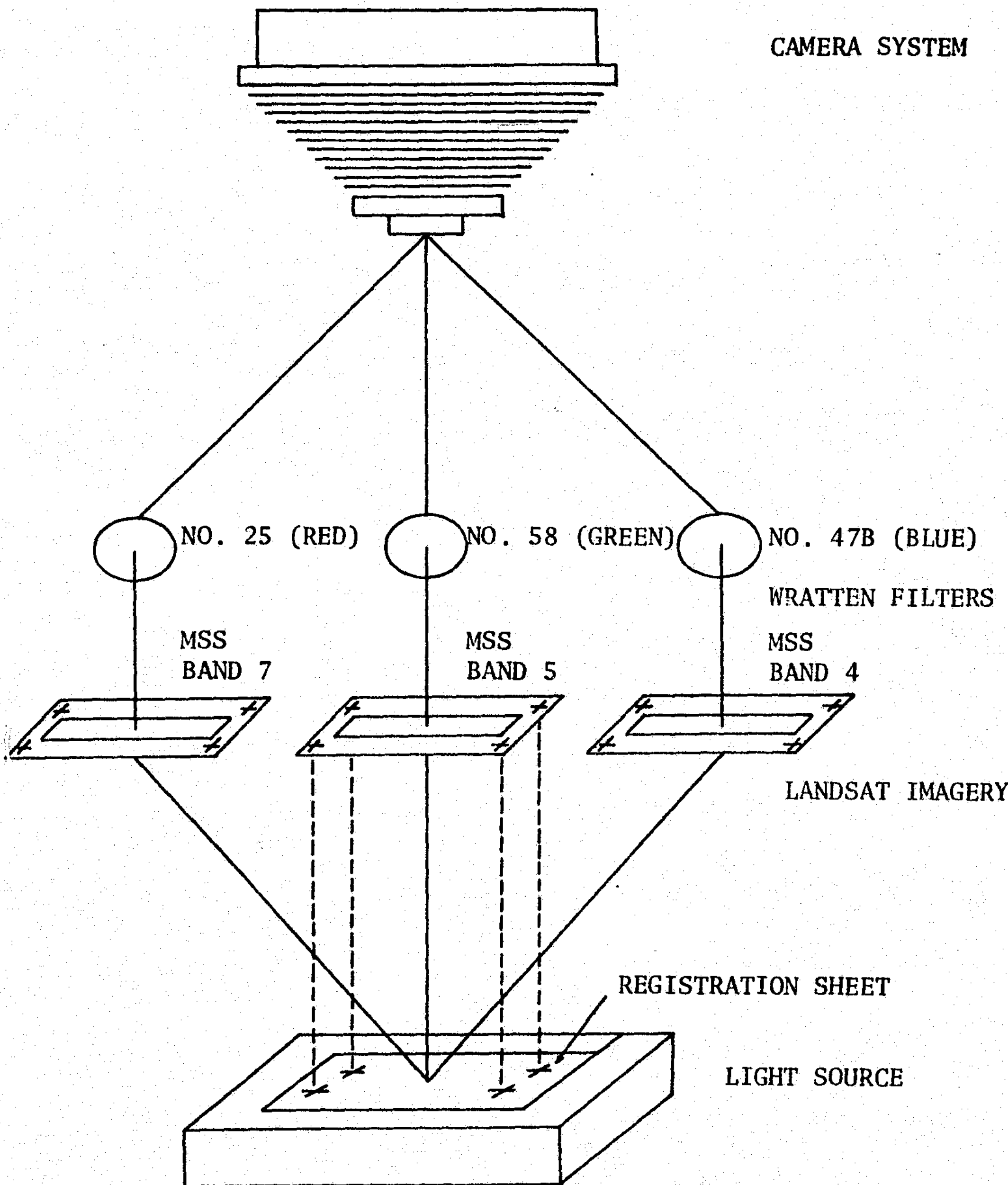

Figure III-1 This schematic diagram illustrates the photographic technique for constructing color composite images. A camera, color film, colored filters, LANDSAT imagery, a registration sheet and a light source are employed. Note that all three bands are placed separately on the registration sheet for copying. The band/filter combinations shown in the diagram above are used to produce simulated false color infrared composites. Different band/filter combinations will produce differently colored composites.

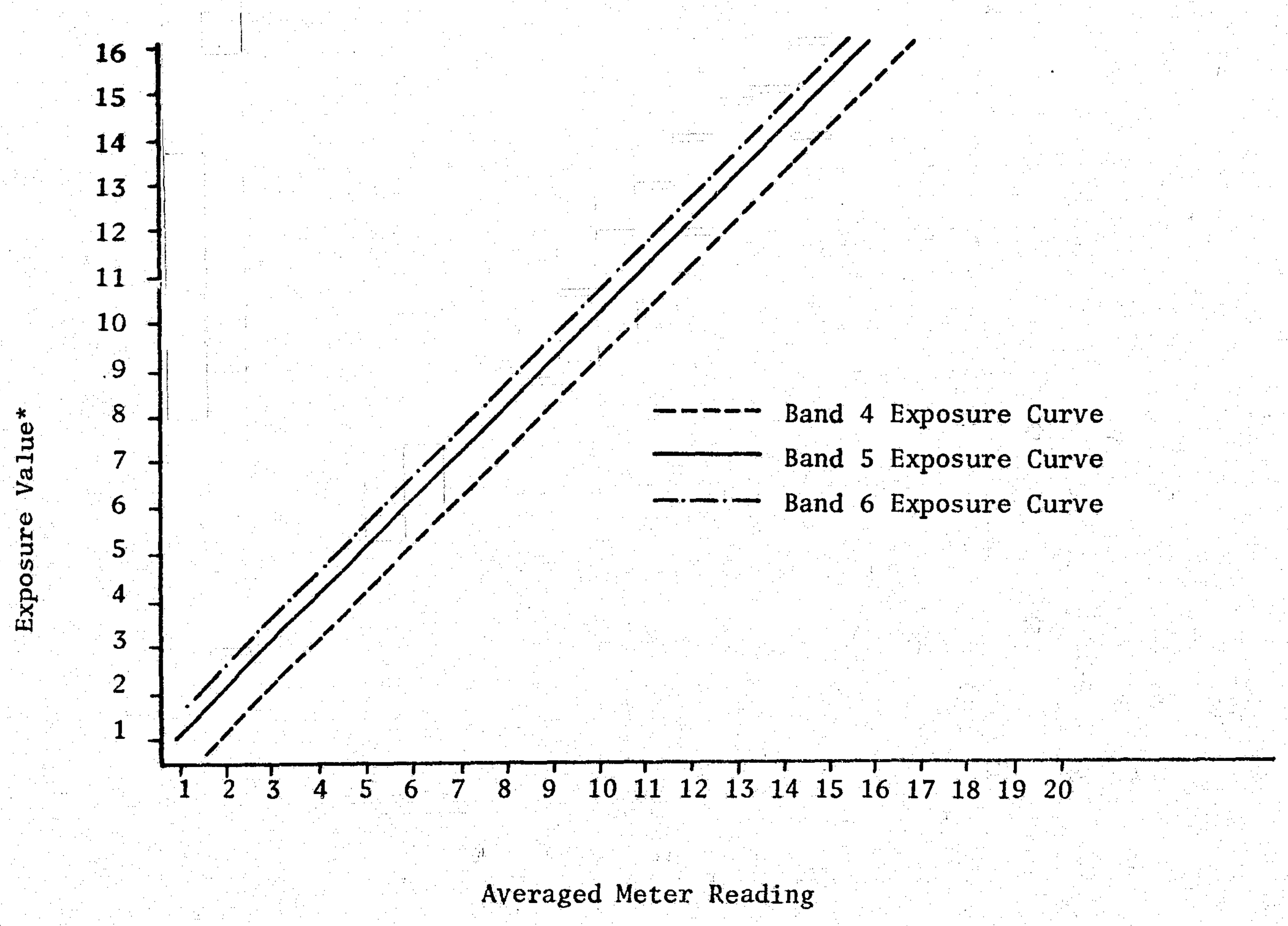

Figure III-2 Example exposure data for the construction of a simulated false-color infrared three band color composite using a conventional light table or a flashbox. LANDSAT MSS Band 4 is combined with a Wratten 47B filter, Band 5 with a Wratten 58 filter, and Band 7 with a Wratten 25 filter. Different exposure curves must be derived for different film speeds and/or different band/filter combinations, as explained in the text.

*Exposure values (EV) are those unique combinations of shutter speed and aperture which yield the same exposure. For instance EV 13 represents the combinations 1/125 second at f/8, 1/60 second at f/11, 1/30 second at f/16, etc.

REFERENCES

Barnes, J. C. and C. J. Bowley, 1974, "Handbook of Techniques for Satellite Snow Mapping", Environmental Research & Technology, Inc., Concord, Massachusetts, 95 pgs.

The author wishes to express a special thanks to Melinda Shackleford for her contribution to this procedural manual.

157

Procedural Manual

REMOTE SENSING AS AN AID IN DETERMINING THE WATER CONTENT OF SNOW

Principal Investigator: Robert N. Colwell

Principal Scientist
and Project Manager: Siamak Khorram

Project Scientists: Randall W. Thomas and
James M. Sharp

NASA Grant NGL-05-003-404

Remote Sensing Research Program
University of California, Berkeley
May, 1978

Procedural Manual

REMOTE SENSING AS AN AID IN DETERMINING THE WATER CONTENT OF SNOW

1.0 Introduction

This procedural manual describes the use of Landsat data in combination with conventional ground snow course data to provide an estimate of watershed or subbasin snow water content. The technique is designed to be implementable in operational water runoff forecasting models incorporating, as one variable, an estimate of snow water content (expressed as a depth of water or as a dimensionless index). Developed and tested in the Northern Sierra Nevada Range in California (Thomas and Sharp 1975), the method may find its greatest utility in mountainous situations characterized by significant winter snowpack buildup. Only a small initial capital investment is necessary and personnel requirements need not be substantial. The technique is designed to complement current snow measurement methods by providing spatial information on snow water content. Consequently it permits more accurate estimates to be made on a basin or subbasin basis. However, successful application of the method does require relatively cloud free weather following winter storms during which sufficient Landsat coverage can be obtained of the watershed(s) of interest.

Normally, snow water content estimates are obtained directly from ground-based snow course or snow sensor measurements. The procedure described herein introduces a stratified double sampling approach that relates the ground-based estimates to snow areal extent data gathered from Landsat imagery. The resulting relationships enable low-cost remotely sensed data to characterize statistically the spatial and temporal variability of specific snow depletion environments sampled with ground snow course data. In this manner satellite data can be used to determine the weight assigned to a particular snow course measurement and also to provide more frequent assessment of snow water content.

For determining snow areal extent, this technique utilizes the Landsat-based procedure described in our *Snow Areal Extent Procedural Manual* as the remote sensing input. However, non-Landsat remotely sensed data types also could provide useful

161

information to characterize the spatial variability, watershed-wide with respect to snow water content. For example, meteorological satellite data could be used with the *Snow Areal Extent Procedure* to provide more frequent (daily) information, although of lower spatial resolution. The technique can also be refined by the user, if desired, to include machine processing of the satellite data.

2.0 General Approach

The following provides an overview of the remote sensing-aided snow water content estimation procedure.

Sample Design and Measurement

A stratified double sample method is used to develop a basin-wide estimate of snow water content. Under this approach, snow water content information for the whole watershed, as obtained inexpensively on a sample unit basis from Landsat data, is combined with that gained from a much smaller and more expensive sample of ground-based measurements at snow courses (see Figure 1). The result is a basin-wide estimate of snow water content based on Landsat data calibrated by regression on ground snow course data. Since much of the watershed snow water content variation is accounted for by information gained from the Landsat sample stage, an overall estimate of basin snow water content is possible at more precise levels (i.e., lower sampling error) than available for the same cost from conventional snow course data alone.

The sequential sampling and measurement process proceeds by first locating a sample grid over the watershed. Snow areal extent estimates are quickly made for each sample unit by manual techniques (see *Snow Areal Extent Procedural Manual*) for the previous snowpack buildup dates and then for the specific forecast date. The snow areal extent data is then combined by a linear equation to generate an index parameter that is correlated with snow water content information specific to the forecast date for each sample unit. This linear model is designed to reflect the relationship between snow areal extent and snow depletion behavior, and is specific to the watershed being studied. Some users may choose to develop more complex, physically realistic areal extent-to-water content transformations.

By specifying the precision (sampling error) and level of confidence desired in the basin-wide snow water content estimate and by considering measurement costs in relation to the available budget, one is able to calculate the necessary ground subsample size. Ground snow water content measurements are then allocated to Landsat-based snow water content-index classes (strata) according to weighted random stratified sampling procedures.

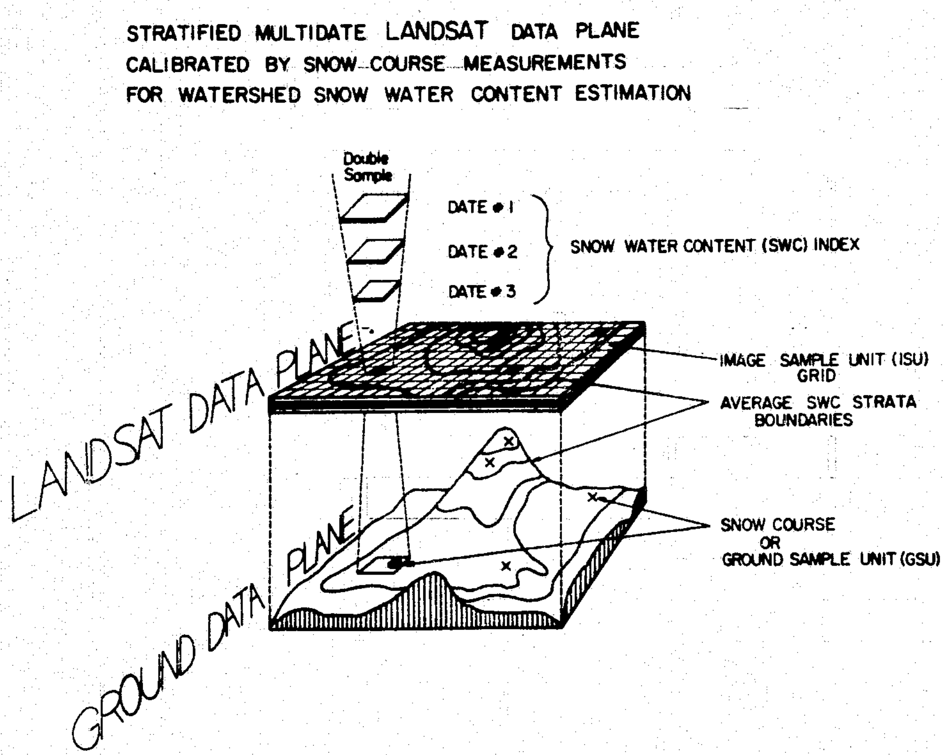

Figure 1. Stratified multidate Landsat data plane calibrated by snow course measurements for watershed snow water content estimation.

163

Regression relationships are developed between the Landsat snow water content index data and the ground snow water content measurements. These equations are then used to correct all Landsat-based data by ground values of snow water content. The ground corrected values of Landsat-based snow water content information in each stratum or class are added to give a total basin-wide estimate of snow water content, together with an associated confidence interval around the estimate.

Results and Their Applications

The Landsat-aided snow water content estimation procedure is designed to generate an estimate of total watershed snow water content and an associated statement of precision for a given forecast period. The estimate may then be related by regression equations directly to basin water yield for a given period. Alternatively, the statement may be used as another predictor variable in current snow survey or river forecast equations. Grid overlays, when placed either on watershed maps or directly on Landsat imagery, give a location-specific estimated snow water content index for each sample unit. Such information can be used to produce improved hydrologic modeling procedures incorporating this spatial data.

Performance Criteria

Performance criteria for this procedure consist of 1) the precision (sampling error) and accuracy of the estimate of snow water content over the watershed versus the cost of making the estimate; 2) the timeliness of the estimate; and 3) the value of any in-place map information regarding snow water content that can be produced through use of the procedure.

3.0 Detailed Description of the Method

The stepwise procedure for estimating snow water content with the aid of remote sensing is described below:

Step 1: An overall plan is first developed which will facilitate adoption of the remote sensing-aided snow water content estimation procedure by the user. This implementation plan should consider 1) available budget; 2) requirements for either training or obtaining image interpreter(s); 3) type of products desired, e.g., watershed and/or sub-watershed estimates or in-place snow water content maps; 4) performance requirements in terms of estimate precision and satellite image acquisition-to-forecast turnaround time requirements; 5) interface of the snow water content procedure with current user forecasting methods; and 6) startup equipment (stereoscopy, photographic laboratory facility) and labor requirements.

Step 2: Color composites are prepared from Landsat imagery and/or from other satellite imagery types (e.g., weather service), and the appropriate image sample unit (ISU) grid placed over each watershed of interest. In the performance of this step, black-and-white Landsat transparencies are obtained (e.g., from the EROS Data Center) and transformed into a simulated infrared color composite by a sample photographic procedure described in the *Snow Areal Extent Procedural Manual*. In the color-combining process, an ISU grid is randomly placed over a base-date image to cover the watershed of interest. The base date Landsat transparencies should be a summer image clearly depicting watershed geomorphological and vegetative features obtained before the first winter in which this technique is applied. Grids on all succeeding Landsat transparencies subjected to the color-combination process should be aligned with that on the base date image. In addition, watershed boundaries as plotted on 1:250,000-scale US Geological Survey topographic map sheets should be transferred to the color composite images via optical rectification devices (if available) or by ocular inspection.

A complete description of the boundary and sample grid overlay is given in the *Snow Areal Extent Procedural Manual*. Square image sample units each 400 hectares in size, are recommended. This size is large enough to stabilize variance and small enough to give location-specific snow water content-related information at reasonable cost. The user may choose to modify these image sample unit dimensions as experience is gained with the estimation procedure.

Step 3: The snow areal extent is then estimated for each Landsat ISU for previous season(s) or current season snow buildup dates. Each ISU should be interpreted manually to determine its average snow areal extent cover class according to the snow environment-specific technique described in the *Snow Areal Extent Procedural Manual*. Previous dates of imagery used should include: 1) one of the images covering the average date of maximum snow accumulation in an average snow year; 2) at least one image from an early season snow date in the current snow season; and 3) if possible, another image from a date well into the snow season representing average snow distribution for that date. As will be discussed later in Step 5, these previous snow season images are used to maximize the correlation between the satellite-derived snow water content indices and ground

165

measurements of snow water content for any given sample unit on the forecast date in question.

Step 4: Snow areal extent is estimated by ISU for the Landsat snow season forecasting date of interest, again using the procedure described in the *Snow Areal Extent Procedural Manual*. The length of the delay that can be tolerated between image acquisition by the satellite and imagery receipt by the user will depend on the use of the snow water content estimate. A very short turn-around time (hours) will be required for weekly or sub-weekly water yield forecasts, but longer times usually will be satisfactory for monthly or seasonal forecasts.

Step 5: Snow areal extent data is next tranformed to snow water content index values by Landsat ISU. Snow water content is estimated from the following first order, time-specific model, designed to reflect physical snow depletion behavior in a given melting environment:

$$x_i = \sum_{j=1}^{J} (M_{ij}) \, (G_j) \, K_i \qquad \text{where:}$$

x_i = estimated Landsat snow water content index for image sample unit i, correlated to corresponding actual ground snow water content data;

M_{ij} = midpoint of the snow cover class (see *Snow Areal Extent Procedural Manual*) for image sample unit i on date j as obtained by interpretation of Landsat imagery; midpoint is expressed on a scale of 0.00 to 1.00;

G_j = weight (related to snow depletion zone behavior characteristics) assigned (0.00 to 1.00) to a past M_{ij} according to the date of the current estimate;

K_i = the number of times out of J' that sample unit i has greater than zero percent snow cover; and

J = total number of snow season dates used.

J' = number of current snow season dates used.

The basic assumption of this simple model is that the greater the sum of areal snow extent over all dates used and the more often snow is present, the higher will be the expected snow water content. This model is most appropriate in mountainous environments. Each user may want to specify a more sophisticated and more physically realistic model for his own watershed(s).

Definition of the weighting factor, G_j, will be watershed specific. Generally, weights should approach 1.00 as the dates of imagery approach the date of forecast. The justification of the weighting relationship is that successively more recent climatic events have progressively more importance in determining the actual snow water content on the forecast date in question. To insure reasonably high correlation between x_i and corresponding ground snow water content values, at least three snow season dates are usually considered ($J \geq 3$). Of these, one or two dates of Landsat imagery would be required during the early snow accumulation season. Occasionally, J may be only two, such as when the first date consists on an April 1st snow water map, based on the past year's Landsat data, and the second represents the current early snow season date in question. In all cases the sample unit grids on all dates must be in common register with respect to a base date grid location. Starting weight suggestions are: 0.25 for the previous year image that is representative of an average maximum snow accumulation date; 0.50 for the early snow season date; 0.75 for dates occurring a month or two before the forecast date; and 1.00 for the forecast date and for all dates occurring within one or two months prior to the forecast date.

Step 6: All ISU's in the watershed(s) of interest should be classified into snow water content strata. Strata are defined by dividing the range of ISU snow water content index values for a mid-snow season forecast date (e.g., April 1) into two or three natural groupings (seen by plotting snow water content index versus the number of ISU's). If no natural groupings are present, then the range of ISU snow water content index values should be divided into two or three ranges having approximately equal numbers of ISU's in each stratum. ISU's are assigned to the stratum having the snow water content index range that includes the snow water content index value for the particular ISU at the mid-snow season forecast date used. This ISU stratification is achieved by first applying Steps 1-5 to a previous snow season that was as close

167

to average as possible and for which good Landsat pass coverage is available.

After each ISU has been coded according to its stratum, the number of ground sample units (GSU's) consisting of snow courses required to satisfy the user precision criterion is calculated by stratum. The procedure used for this calculation is presented in Appendix I.

Initial implementation of this procedure requires information regarding 1) tabular summaries of individual ISU snow water content index values; 2) the accumulated Landsat snow water content index in each stratum; 3) the ground-based snow water content variability by stratum; 4) the correlation between ISU and GSU data; 5) the total number of ISU's per stratum; and 6) average ISU and GSU costs by stratum.

The ISU and accumulated ISU snow water content index information is obtained from the set of x_i's generated in the stratification process on the earlier snow season Landsat data set.

The total number of ISU's per stratum, N_h, will be known from the statification. An estimated correlation coefficient between ground snow water content estimates and Landsat-based snow water content index values is next calculated by obtaining ground snow course data matched to a small sample of ISU's. The snow course data must have been obtained within two or three weeks of the mid-season snow forecast date used to derive the corresponding Landsat ISU values. Ideally, separate correlation coefficients should be computed for each stratum if a sufficient number (e.g., 10) of snow courses exist for each stratum. Otherwise, a common correlation coefficient (ignoring strata) should be computed by the usual formula (see Appendix I) and applied to all strata.

An estimate of snow water content variability can be obtained by applying the standard formulasfor simple random sampling variance to the snow course/sensor data used to calculate the correlation coefficient. A separate variance should be computed for each stratum. If only a very small number (e.g., $\leq$ 5) snow courses fall in a given stratum, then the variance among all x_i values in the particular stratum can be substituted instead. In this case, the x_i values must be scaled to ground snow water content values by use of a ground-to-Landsat regression equation based on matched GSU and ISU data.

Image preparation and interpretation costs must be documented also for use in calculating sample size. Labor, materials, and overhead costs should be documented on an ISU basis as in the example given in Table I. Cost per GSU (snow course) measurement can be developed from the individual user organization's pre-existing data. All cost data for sample allocation should represent operational costs.

Step 7: For the first year of actual implementation, the calculated number of GSU's per snow water content index stratum should be allocated for given ISU's in those strata. This allocation is based on equal probability selection from the tabular summaries of ISU's generated in Step 6. Consequently, ISU's are numbered from 1 to N_h in a given stratum and a random number table used to select the calculated number of ISU's to which GSU's will be matched.

The snow course or sensor should be located in a snow accumulation and depletion environment representative of the average of such environments covered by the given ISU. If it is not efficient to reallocate an already established network of snow courses and sensors, then the snow water content stratum should be identified for each such ground unit by determining the stratum associated with the ISU covering that ground location. After three to five years of using this remote sensing-aided technique for snow water content estimation, the user may find it desirable from a precision (i.e., variance control) standpoint to reallocate some ground courses to achieve the optimum stratum-by-stratum GSU sample sizes calculated previously. However, before this is done, updated GSU sample sizes should be calculated using stratum-specific ground or image snow water content variance data averaged over successive seasons.

Step 8: Estimates of watershed or sub-watershed snow water content should be calculated, using the equation described in Appendix II. The values thus obtained should be entered into statistical or physical models to predict water yield. For example, the user could employ the remote sensing-aided snow water content estimate as an input variable in a regression equation for predicting water runoff.

Step 9: Finally, the utility of the above-described procedure for using remote sensing as an aid to estimating snow

169

water content should be evaluated in regard to satisfying the water yield forecasting organization's legal or contractual requirements. Utility can be judged by new information gained (e.g., watershed physical relationships), forecasting accuracy or precision improvement, cost savings, or forecast timeliness. Information gained on the precision/cost effectiveness of the procedure and the sensitivity of the water yield forecast models to the resulting snow water content estimates can be used to:

1) refine the model (Step 5) used to calculate the snow water content index;

2) better define snow water content index strata;

3) generate better GSU sample sizes and allocation strategies; and

4) refine the actual snow areal extent interpretation, imagery enhancement, and analysis procedures used in Steps 2, 3, and 4.

Literature Cited

Thomas, R.W. and J.M. Sharp. 1975. "A Comparative Cost Effectiveness Analysis of Existing and Landsat-Aided Systems for Estimating Snow water Content". In *An Integrated Study of Earth Resources in the State of California Using Remote Sensing Techniques*. (NASA Grant NGL 05-003-404). Remote Sensing Research Program and Social Sciences Group, Space Sciences Laboratory, University of California, Berkeley. May.

Sharp, J.M. and R.W. Thomas. 1975. "A Comparison of Operational and Landsat-Aided Snow Water Content Estimation Systems. In *Proceedings of the Workshop on Operational Applications of Satellite Snowcover Observations*, held at South Lake Tahoe, California, August 18-20, 1975. National Aeronautics and Space Administration, Goddard, Maryland. pp. 325-344.

Table I. Example calculation of image sample unit costs for a Landsat-aided manual snow water content inventory[1]

	Total Cost	Cost per ISU[2]
I. Pre-Inventory		
A. Image Acquisition		
3 LANDSAT dates with 3 bands per date @ $3 per band; the costs of 2 of these dates amortized over 5 dates	$12.60	$.006
Resource Photography		
(Medium Scale Aerial Photography for Image Analyst Environmental Type Training)	$14.29	$.006[3]
B. Image Sample Unit		
Grided Landsat Color Composite Print Generation		
Film processing, and Printing		
3 dates @ $11 per date		
The costs of 2 of these dates amortized over 5 dates	$15.40	$.007
Labor 0.5 hours per date @$13.50/hr including overhead, 3 dates, the costs of 2 of which are amortized over 5 dates	$ 9.45	$.004

1. Cost data based on 1975 University of California figures.

2. Cost per image sample unit assuming 2218 (780,000 ha test watershed) image sample units in the watershed(s) of interest.

3. Two $500 flights amortized over 5 years, 7 dates per year, and two watersheds.

171

Table I, Continued

	Total Cost	Cost per ISU
II. Inventory		
A. Interpreter Training		
1 hr per date, @ $13.50/hr 3 dates, the costs of 2 of which are amortized over 5 dates	$18.90	$.009
B. Image Interpretation		
Ave. 6 hrs per date @ $13.50/hr (2218 Image Sample Units)		
3 dates, the costs of 2 of which are amortized over 5 dates	$113.40	$.051
C. Data Keypunching		
6 hrs per date @ $13.50/hr; 3 dates, the costs of 2 of which are amortized over 5 dates	$113.40	$.051
D. Computer Analysis of Image Analyst Results		
0.075/hr @ $40/hr	$ 3.00	$.001
E. Selection of Random Numbers to Define Ground Sample Units		
0.5/hr @ $13.50/hr amortized over 5 dates @ $13.50/hr	$ 1.35	$.001
TOTAL	$301.79	$.136

Appendix I

DETERMINATION OF GROUND SAMPLE SIZE

The ground sample size in each stratum will be defined to be directly proportional to the fraction of total snow water content in that stratum relative to the total snow water volume over the entire watershed. This sample allocation method, known as X-proportional (see Raj 1968:65-68), uses the Landsat snow water content index data as the measure of size. Thus the number of ground snow courses required per stratum is given by

$$n_h = \frac{X_h}{X}, \qquad \text{(equation 1)}$$

where

h = the stratum index,

n = the ground sample size over all strata,

X_h = the sum of Landsat snow water content index values for all image sample units in stratum h and,

X = the sum of Landsat snow water content index values for all image sample units over all strata.

The total ground sample size, n, can be calculated by substituting the expression for n_h given in equation 1 into the standard formula for variance of a stratified sample. Thus

$$\hat{V}(\hat{Y}) = \frac{X}{n} \sum_h \frac{N_h^2}{X_h} \hat{\sigma}_{yh}^2 - \sum_h N_h \hat{\sigma}_{yh}^2, \qquad \text{(equation 2)}$$

where

$\hat{V}(\hat{Y})$ = the estimated variance of the final estimate ($\hat{Y}$) of total snow water content on the watershed,

N_h = the total number of Landsat image sample units in stratum h,

173

n, X, X_h = as defined previously, and

$\hat{\sigma}^2_{yh}$ = the estimated variance for the estimate of snow water content in stratum h. Mathematically,

$$\hat{\sigma}_{yh}^{\ 2} = \frac{n_h - 2}{n_h - 3} \cdot \frac{\hat{S}_{yh}^{\ 2}}{n} \cdot \left(1 - \hat{\rho}_h^2 \left(1 + \frac{1}{n_h - 3}\right)\right), \text{ (equation 3)}$$

where

$\hat{S}_{yh}^{\ 2}$ = the estimated variance among ground snow course measurements of snow water content expressed in inches of water, i.e.,

$$\hat{S}_{yh}^{\ 2} = \sum_i (y_{ih} - \hat{\bar{y}}_h)^2 \div (n_h - 1)$$

where

y_{ih} = average snow water content for snow course i in stratum h, and

$\hat{\bar{y}}_h$ = average estimate of snow water content among snow courses in stratum h,

$\hat{\rho}_h$ = the estimated correlation coefficient between Landsat image sample unit snow water content index values (x_{ih}) and spatially matched ground measurements of snow water content (y_{ih}) in stratum h, i.e.,

$$\hat{\rho}_h = \sum_i (x_{ih} - \hat{\bar{x}}_h)(y_{ih} - \hat{\bar{y}}_h) / \left(\sum_i (x_{ih} - \hat{\bar{x}}_h) \cdot \sum_i (y_{ih} - \hat{\bar{y}}_h)\right)^{\frac{1}{2}}$$

where

$\hat{\bar{x}}_h$ = the estimated average Landsat snow water content index value per image sample unit in stratum h.

After rearranging terms in equation 2, the total ground sample size can be expressed as

$$n = (X \Sigma \frac{N_h^2}{X_h} \hat{\sigma}_{yh}^{\;2} - \Sigma N_h \hat{\sigma}_{yh}^{\;2}) \div \hat{V}(\hat{Y}). \qquad \text{(equation 4)}$$

Equation 4 is used to determine n and subsequently n_h when the final estimate of variance $(\hat{V}(\hat{Y}))$ to be achieved is fixed at some desired level. Therefore, to solve for n, the user must first choose a value of $\hat{V}(\hat{Y})$ in equation 4. The size of V will depend on the amount of sampling error in the final estimate of snow water content that can be tolerated by the user. For comparative purposes, the size of this error can be expressed as the ratio of $\sqrt{V(\hat{Y})}$ to $\hat{Y}$, that is, the standard error of the estimate of watershed snow water content expressed as a fraction of the estimate. The smaller this ratio, the greater the precision of the final snow water content estimate.

It should be noted here that the estimation process itself is assumed to be unbiased, given accurate ground and image sample unit measurements. That is, the expected value of the watershed snow water content estimate (obtained over all possible ground samples) is assumed to equal the actual value. Thus the sample size calculation only considers the error entering through the act of sampling a small fraction of the ground area.

In addition to fixing V, the user must provide estimates for the variance in each stratum, $\sigma_{yh}^{\;2}$. These may be available from earlier studies. If not, they must be estimated by using equation 3. In this case, $\hat{S}_{yh}^{\;2}$ is calculated from ground snow measurements taken in each stratum, $\hat{\rho}_h$ using image data matched spatially with the ground data*, and guesses are made for n and n_h. After solving for n (using equation 4) and then n_h (using equation 1), the revised estimates of n and n_h are substituted back into equation 3 and another solution is obtained for n and n_h. This iterative process should be continued until the resulting estimates of n and n_h stabilize.

If the user chooses not to specify a desired final variance V, but rather would like to minimize V subject to a limiting budget constraint, then the following formula for n should be used:

$$n = \frac{C - c_o}{\Sigma c_h \frac{X_h}{X}} \qquad \text{(equation 5)}$$

*If only a very small number of matched ground and Landsat data pairs are available in each stratum, then these pairs will have to be pooled to calculate a common $\hat{\rho}$ among strata.

175

In equation 5,

C = the total budget available for the snow water content survey,

c_o = the total fixed (non-variable) costs in the inventory including the cost of generating snow water content index estimates for each image sample unit on the Landsat imagery within the watershed(s) of interest,

c_h = the average cost associated with travel to and from, and measurements taken at a ground snow course in stratum h, and

X_h and X = the quantities defined in equation 1.

Once X_h abd X are obtained from the Landsat imagery, equation 5 is used to solve for n and equation 1 is used to solve for the ground sample size, n_h, in each stratum.

Literature Cited

Raj, Des. 1968. *Sampling Theory*. McGraw-Hill Book Company, San Francisco. 302 pp.

Appendix II

FORMULAS FOR ESTIMATING WATERSHED SNOW WATER CONTENT

A linear regression equation is used to combine ground and Landsat image sample unit information to produce a final watershed estimate of total snow water content. This estimation model is expressed as follows for a given stratum:

$$\hat{Y}_h = A_h N_h \hat{\bar{Y}}_h = A_h N_h (\hat{\bar{y}}_h + \hat{b}_h (\hat{\bar{X}}_h - \hat{\bar{x}}_h)) \quad \text{(equation 1)}$$

where:

h = stratum index,

$\hat{Y}_h$ = total estimated snow water content (expressed as a volume of water)for stratum h,

$\hat{\bar{Y}}_h$ = estimated average snow water content (inches* of water) per image sample unit for stratum h,

A_h = area per image sample unit,

N_h = total number of image sample units in stratum h,

$\hat{\bar{y}}_h$ = estimated average snow water content (inches of water) per ground sample unit for stratum h based on a sample of ground sample units,

$\hat{\bar{x}}_h$ = estimated average snow water content index per image sample unit for stratum h based on a sample of image sample units corresponding spatially to the ground units sampled,

$\hat{\bar{X}}_h$ = estimated average snow water content index per image sample unit for stratum h, based on the estimates from all image sample units in stratum h, and

$\hat{\bar{b}}_h$ = estimated regression coefficient between y_h and x_h.

i.e., $\hat{b}_h = (\sum_i^{n_h} (x_{ih} - \hat{\bar{x}}_h)(y_{ih} - \hat{\bar{y}}_h)) \div \sum_i^{n_h} (x_{ih} - \hat{\bar{x}})^2$

where:

x_{ih} = the Landsat image snow water content index for image sample unit i in stratum h,

* or equivalent metric measure of depth.

177

y_{ih} = the ground snow course snow water content (expressed in inches of water) for the snow course located in image sample unit i of stratum h, and

$\hat{\bar{x}}_h$ and $\hat{\bar{y}}_h$ are defined as above.

The stratum-specific estimates may be combined to produce an estimate of total snow water content (expressed as a volume of water) for the entire watershed of interest by the following equation:

$$\hat{Y}_{total} = \sum_{h=1}^{L} \hat{Y}_h \qquad \text{(equation 2)}$$

where L = total number of strata.

Independent Study

A REMOTE SENSING APPROACH TO LAND SURFACE DIFFERENTIATION

Project Scientist: H. Gregory Smith

Remote Sensing Research Program
University of California, Berkeley
May, 1978

A Remote Sensing Approach to Land Surface Differentiation

by

H. Gregory Smith
Remote Sensing Research Program
Berkeley Campus
University of California

Preface

In this study, an attempt was made to distinguish areas of different surface environments from Landsat data, specifically in terms of vegetation, soil and terrain, and to evaluate the utility of Landsat data for such land surface classification. The factors of vegetation, soil and terrain (here meaning the combined effects of slope, aspect, and elevation) are primary in governing the amount of reflected electromagnitic radiation from a given area. Solar radiation incident on an area is differentially reflected due to the nature of the terrain, soil and vegetation; consequently, there tends to be a unique reflected signal that is characteristic of a specific combination of these factors. This study investigates the feasibility of differentiating land surface systems in a specific wildland area of approximately 41,250 acres (64.5 square miles) within the Lassen County portion of the Lassen National Forest near Susanville, California. The information contained in this study is based on the analysis of reflected radiation sensed by the Landsat multispectral (MSS) imaging system.

Classification

When one deals with a task such as land surface investigation, there is added difficulty in classification due to the obscure definition of the individual components. What might be identified as a different land form or surface type may be only a transitional form between larger, more conspicuous or distinct forms. The problem of differentiating individuals can be somewhat reduced by looking at more than a single type of differentiating characteristic. According to R.L. Wright (1972), the principal requirements are that differentiating charactistics should be:

1) Intrinsic properties of the things to be grouped;

2) Observable, measurable, readily accessible, and ideally of a comparatively permanent nature;

3) "Motivating" properties with the maximum number of accessory characteristics;

4) Important for, and capable of application to, the objectives of the classification; and

5) Suitable for the construction of a hierarchy.

180

In addition, the classification scheme itself must be tailored closely to the purpose and objectives for which it was designed. The above basic considerations were instrumental in the design of this investigation.

Approach

In the following study a two-pronged approach was utilized in the analysis of land surface types. The analysis sought to discern areas of physical continuity on the basis of land surface appearance coupled with the aspects of vegetation and land use.

The first part of the investigation dealt with the experimentation and use of various Landsat-1 MSS band combinations and permutations in the form of band ratio color composites as an aid to the manual interpretation of different land systems. The second part utilized a completely objective machine approach to land system differentiation and classification. A minimum of human interaction was used in the machine processing and classification of the study area because it was desirable to determine whether a purely automated approach to land classification produces results comparable to those obtained by the manual approach, or whether the automated approach is even applicable to such a problem.

Discussion and Analysis - Part I

A technique that combines digital computer processing and color compositing has been utilized to enhance the subtle spectral reflectivity differences often characteristic of land surfaces sensed at different wavelengths (*Aviation Week and Space Technology*, October 1977). This procedure is called band ratioing.

In the process of band ratioing, features which have little visible difference compared to their surroundings can be enhanced by emphasizing the relative responses between different spectral bands. Band ratioing eliminates common brightness trends between spectral bands and emphasizes spectral reflectivity differences sensed at different wavelengths. Normally different substrates have different reflectivities in the visible and near-infrared spectral regions. Differences are generally quite subtle and are difficult to discriminate on standard MSS images. In addition, the area being analyzed in this study possesses significant local relief. Band ratioing generally removes first order brightness caused by such topographic, slope and aspect variances (Rowan, *et al.*, 1975).

The actual process of band ratioing requires unique analysis equipment that can be found and utilized in only a very few locations across the United States. Due to the extremely flexible nature of the equipment of the Remote Sensing Research Program (RSRP) on the Berkeley Campus, such a technique was possible within the University of California system.

In the ratioing process, the pixel reflectance sensed in one band is divided by the reflectance measured for that pixel in another band. This is done for each pixel. The resultant ratios, which may be displayed planimetrically in a color code, will show the variations between the slopes of the spectral reflectivity curves of the two wavelength bands. In some instances, differences in albedo are suppressed, and very dissimilar materials easily separable on a standard photographic image may be inseparable on a ratioed image because their spectral reflectivity curves in both wavelength bands are similar. Conversely, a distinct advantage of this method is that one type of material will appear the same or similar in a ratioed image regardless of the local topographic slope angle, since first order brightness trends are usually removed through band ratioing.

Color compositing techniques offer an effective and visually pleasing means of combining ratioed images with standard MSS band images. Up to three bands may be combined utilizing blue, green and red filters. This is a particularly efficient method since two spectrally different areas may be nearly indistinguishable in a black-and-white ratioed image, while proper color combinations of up to three images permits discrimination on the basis of color differences. Manual discriminative ability is greatly increased because information from more than one image can be combined and because the human eye is capable of differentiating many more *hue* values than gray values.

A number of ratios and ratio color composites were tried in dealing with the Lassen study area; they included the following:*

I) MSS 7/MSS 5 --- Red
MSS 7 --- Green
MSS 6 --- Blue

II) MSS 5/MSS 4 --- Red
MSS 6/MSS 5 --- Green
MSS 7/MSS 4 --- Blue

III) MSS 7/MSS 4 --- Red
MSS 6/MSS 5 --- Green
MSS 5/MSS 4 --- Blue

IV) MSS 6/MSS 5 --- Red
MSS 7/MSS 5 --- Green
MSS 7 --- Blue

V) MSS 7/MSS 5 --- Red
MSS 7/MSS 4 --- Green
MSS 6/MSS 5 --- Blue

(Figures X-1 through X-5)

*See pages 4 through 6 for color ratio composite illustrations.

182

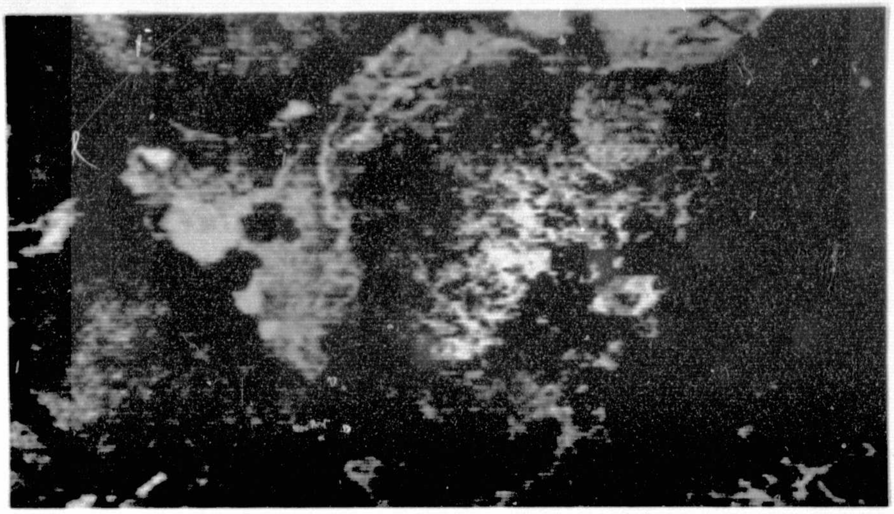

Figure 1. Band-ratio color composite #1

MSS 7/MSS 5 --- Red
MSS 7 --- Green
MSS 6 --- Blue

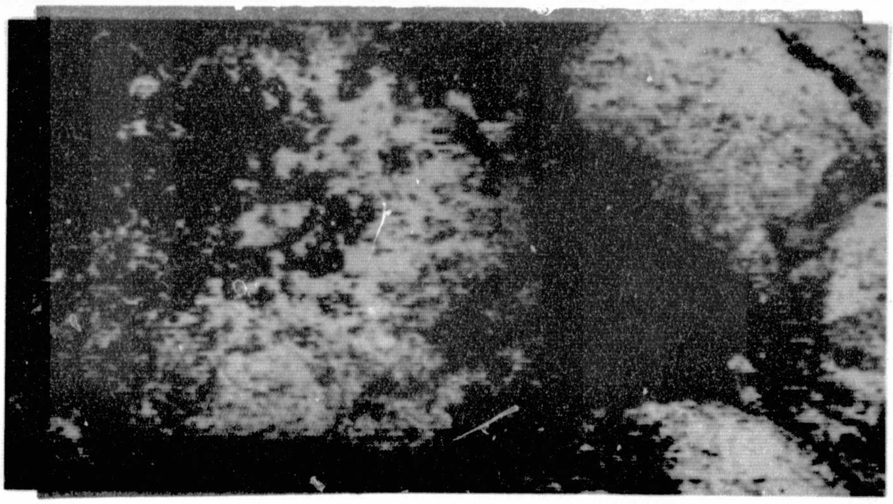

Figure 2. Band-ratio color composite #2.

MSS 5/MSS 4 --- Red
MSS 6/MSS 5 --- Green
MSS 7/MSS 4 --- Blue

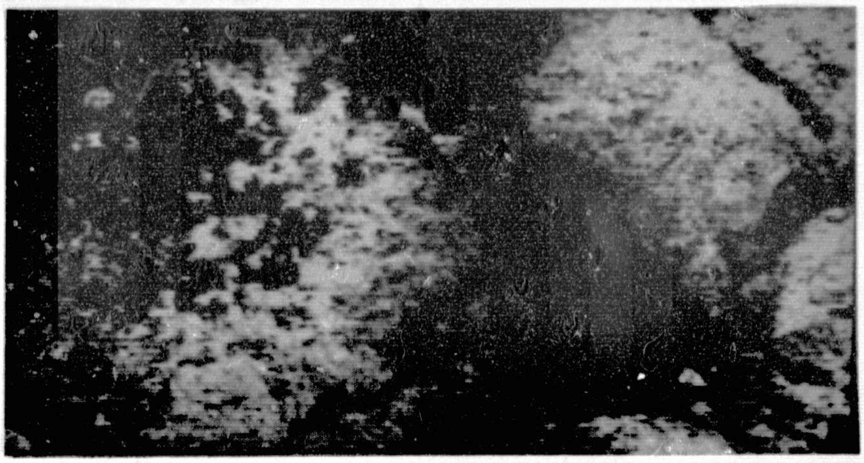

Figure 3. Band-ratio color composite #3.

MSS 7/MSS 4 --- Red
MSS 6/MSS 5 --- Green
MSS 5/MSS 4 --- Blue

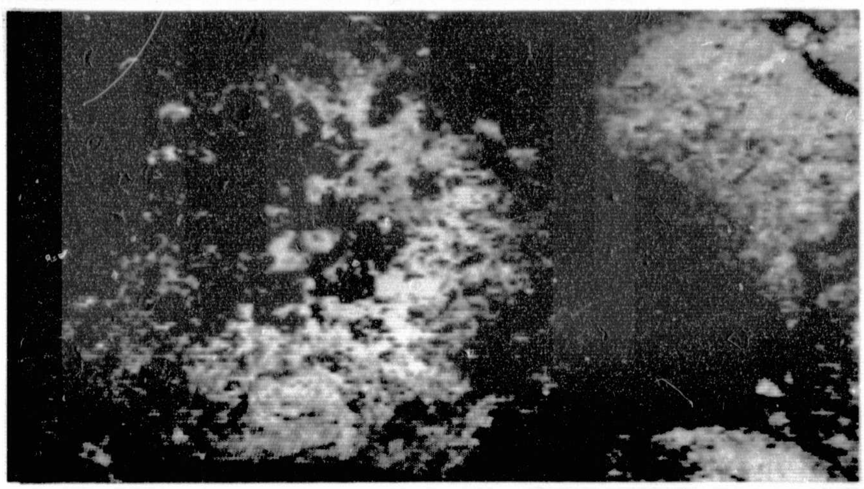

Figure 4. Band-ratio color composite #4.

MSS 6/MSS 5 --- Red
MSS 7/MSS 5 --- Green
MSS 7 --- Blue

184

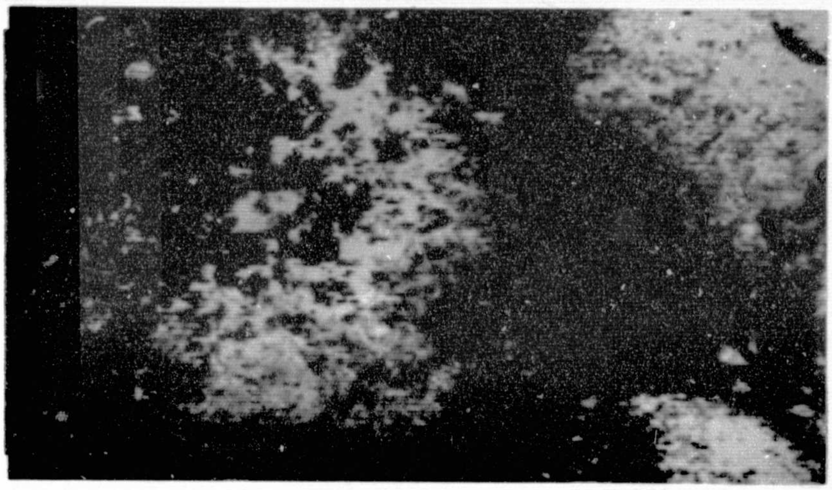

Figure 5. Band-ratio color composite #5.

MSS 7/MSS 5 --- Red
MSS 7/MSS 4 --- Green
MSS 6/MSS 5 --- Blue

Each band ratio color composite was analyzed using available geologic maps, high flight color infrared photography, natural color aerial photography, and on-the-site conventional ground photography.

A discussion of each ratio composite and its individual components follows:

Band ratio color composite #1 - MSS 7/MSS 5 --- Red

MSS 7 --- Green

MSS 6 --- Blue (see page 4)

In general, this particular combination of bands seemed to discriminate the largest number of surface types with the most meaning and accuracy. The MSS 7/MSS 5 component ratio of this composite is of particular interest since it was chosen as being representative of surface flora.

The reasoning behind the use of the MSS 7/MSS 5 ratio is that, as seen from an aerial or space view, vegetation is almost entirely represented by its foliage (i.e., leaves). Other parts of the plant (stem, flowers, fruits, etc.) are usually not visible from above to the degree that the leaf canopy is. Hence, in remote sensing it is the leaf that determines how an individual plant, plant association, or community appears on a photo or image.

Within the range of wavelengths (0.5 - 1.1μ) to which the Landsat MSS is sensitive, foliage typically interacts with solar radiation in the following manner: "Reflection or emission from the leaf's cuticle and epidermis is relatively minor, and ordinarily need not be considered; most of the light from the blue and red ends of the visible spectrum is absorbed by chlorophyll while green light is largely reflected by it, thus accounting for the green appearance of the leaves. Energy from the near infrared part of the spectrum is little affected by the chlorophyll, but is greatly affected by the gross structure of the spongy mesophyll tissues deep within the leaf. Just as snow and foam appear white because, with their spongy structure, they are good reflectors of energy, so the spongy mesophyll is also a good reflector. In fact this tissue appears very white when the overlying portions of the leaf are dissected so as to expose it, but as long as the overlying tissues remain in place, the radiant energy which penetrates the mesophyll (and thereupon is reflected from it) is of far greater intensity in the near infrared than in the visible part of the spectrum." (Colwell, 1968)

From the foregoing statement it is obvious why MSS band 7 (near infrared) was chosen as part of the ratio to represent the vegetation aspect of the environment. Differentiation of forest types is most easily accomplished using MSS band 7 where reflectance separation is great enough so that discrimination is possible. Also, the low values in MSS band 5, coupled with its fluctuation as related

186

to plant vigor, indicate that a combination of MSS bands 7 and 5, that is, one ratioed with the other, will give the image interpreter an idea of both vegetation type and vigor. Other research (Sabins, 1978) has indicated that ratioing two bands not only enhances interpretability in terms of the information represented in the two bands, but also aids in eliminating inconsistencies in the spectral data caused by differing slope, aspect and sun-angle relationships.

The other two components of this first ratio composite are MSS bands 7 and 6. MSS band 7 is included simply as an additional factor in aiding vegetation discrimination. MSS band 6 is used as a spectral indicator of differences in the topographic elements of the landscape (i.e., slope and aspect) including soil. By registering and overlaying these three components, assigning each a primary color (red, green or blue), one can create a color composite that represents a pixel-by-pixel (grid method) classification of the landscape elements. The final product may be both manually (qualitatively) and quantitatively interpreted to determine the accuracy and meaning of such an information display method.

In the present test, through a close visual analysis of this first ratio composite, eight distinct categories of land surface types (or photomorphic units) could be discerned (see Table 1). Each of the eight land surface types defined by its color characteristics on the ratio composite was quantitatively analyzed to determine its spectral characteristics. As seen from the statistical summaries of each of the areas (see Tables 2 through 9), there is a histogram of pixel reflectance values for each band in each of the eight categories. From each of the histograms a mean (representative) reflectance value can be derived that will represent the reflectance value for that land surface type in that particular band or band ratio.

In summary, each of these areas is unique and represents distinct elements of the landscape. Virtually the entire study area may be described through these eight basic land systems. Deviation from any one of the eight basic units seems to occur either in transition zones between units or in areas that are of such great topographic irregularity that reflected radiation does not represent the true surface character (e.g., Fault Zone, Antelope Mountain). Although such a segregation of land units seems to work reasonably well, it must be reiterated that the specificity of the classification is dependent upon the classification's designated purpose. For some purposes an eight-element land classification scheme such as this would be perfectly adequate. For instance, a type of large-scale, regional land surface inventory may be accomplished quite well by using the eight basic land units to build on a higher order classification scheme. Obviously detailed vegetation/habitat discrimination is impractical using such a coarse scheme, but it is conceivable that

ORIGINAL PAGE IS OF POOR QUALITY

Table 1

LAND SURFACE CATEGORIES

Ratio Composite 1

AREA	TONAL DESCRIP.	GEOLOGY	SLOPE/ASPECT	VEGETATION
1	Black	Qru^b-Black vesicular scoriaceous flows of divine basalt, characterized by lack of erosion or weathering, flow surfaces and structures locally well preserved	19.97%/N-NW	Generally non-vegetated
2	Yellow, red brown mixture	Qru^b	10.75%/N-NE	Yellow Pine substrate not obscured
3	Red brown-almost exclusively	Qru^b	9.98%/E-NE	Yellow Pine shrub, underbrush substrate obscured
4	Generally white with red brown, yellow and blue anamolies	Qru^b	15.36%/E	Much less dense Yellow Pine forest with substrate obscured
5	Green brown, yellow, some blue	Qru^b	9.22%/E	Much less dense forest with substrate evident through canopy
6	Intense blue-homogeneous	Qpv^b-Pyroclastic basaltic cinders locally agglutinated, vent tuffs, poorly consolidated rhyolite pumiceous tuff	1.54%/S-SW	Grasses/low sage, some pine, spruce

188

Table 1 (continued)

AREA	TONAL DESCRIP.	GEOLOGY	SLOPE/ASPECT	VEGETATION
7	Light blue-homogeneous	Qal-Recent alluvium alluvial silt, sand, and locally coarse gravel, deltaic slope-wash stream channel, flood-plain deposits, fans partially lacustrine bog and swamp deposits, glacial outwash	0.77%/S	Low sage/grasses
8	Light blue with yellow and red brown interspersed	Qpv[b]	9.22%/NW	Shelterwood cut Yellow Pine - recovery
9	Black (water)	None	None	None

Table 2

RATIO COMPOSITE 1 - FIELD 1

ORIGINAL PAGE IS
OF POOR QUALITY

Summary Statistics

	BAND	MEAN	STDEV	CV	SKEW	KURTOSIS	BAD DATA
Blue	3(7/5)	19.88	1.78	8.97	.73	-.15	0
Green	4(7)	8.60	1.31	15.21	1.97	5.45	0
Red	5(6)	.43	.08	18.09	1.72	4.63	0

BAND 3

```
20 +---------+---------+
   :                   :
   :                   :
   :                   :
   :                   :
15 +---------+---------+
P  :                   :
I  :                   :
X
E  :        x          :
L  :        x          :
10 +--------x+---------+
C  :       xx          :
O  :       xx          :
U
N  :       xxx x       :
T  :       xxx x       :
 5 +-------xxx-x-------+
   :       xxx x       :
   :       xxxxx       :
   :       xxxxxx      :
   :      xxxxxxx x    :
   +---------+---------+
 10.00     20.00     30.00
```

BRIGHTNESS VALUE

HORIZONTAL INCR.=1.

BAND 4

```
20 +---------+---------+
   :       x           :
   :       x           :
   :       x           :
   :       x           :
15 +-------x-+---------+
P  :       x           :
I  :       x           :
X
E  :       xx          :
L  :       xx          :
10 +-------xx+---------+
C  :       xx          :
O  :       xx          :
U
N  :       xx          :
T  :       xx          :
 5 +------xxx+---------+
   :      xxxx         :
   :      xxxx         :
   :      xxxx         :
   :      xxxx x x     :
   +---------+---------+
 00        10.00     20.00
```

BRIGHTNESS VALUE

HORIZONTAL INCR.=1.

BAND 5*

```
20 +---------+---------+
   :                   :
   :                   :
   : x                 :
   : x                 :
15 +-x-------+---------+
P  : x                 :
I  : x                 :
X
E  : x                 :
L  : x                 :
10 +-x-------+---------+
C  : x x               :
O  : x x               :
U
N  : xxx               :
T  : xxx               :
 5 +-xxx-----+---------+
   : xxx               :
   x xxx               :
   x xxxx              :
   xxxxxxx x  x        :
   +---------+---------+
 .31       .70       1.09
```

BRIGHTNESS VALUE

HORIZONTAL INCR.=0.039

190

Table 2 (continued)

*From this type of normal distribution, one would postulate that there is either one type of vegetation or no vegetation in this land unit that dominates the character of the reflected spectral signal. An examination of the band 7 reflectance histogram reinforces this idea. A further examination of high-flight photography and on-the-ground reconnaissance indicates that this area is largely void of any vegetation due to its physical make up and relatively youthful geologic state (basaltic flow).

Table 3

RATIO COMPOSITE 1 - FIELD 2

Summary Statistics

	BAND	MEAN	STDEV	CV	SKEW	KURTOSIS	BAD DATA
Blue	3 (7/5)	34.29	1.62	4.71	.15	-.51	0
Green	4 (7)	21.13	.94	4.43	-.24	-.15	0
Red	5 (6)	1.59	.17	10.73	-.47	-.22	0

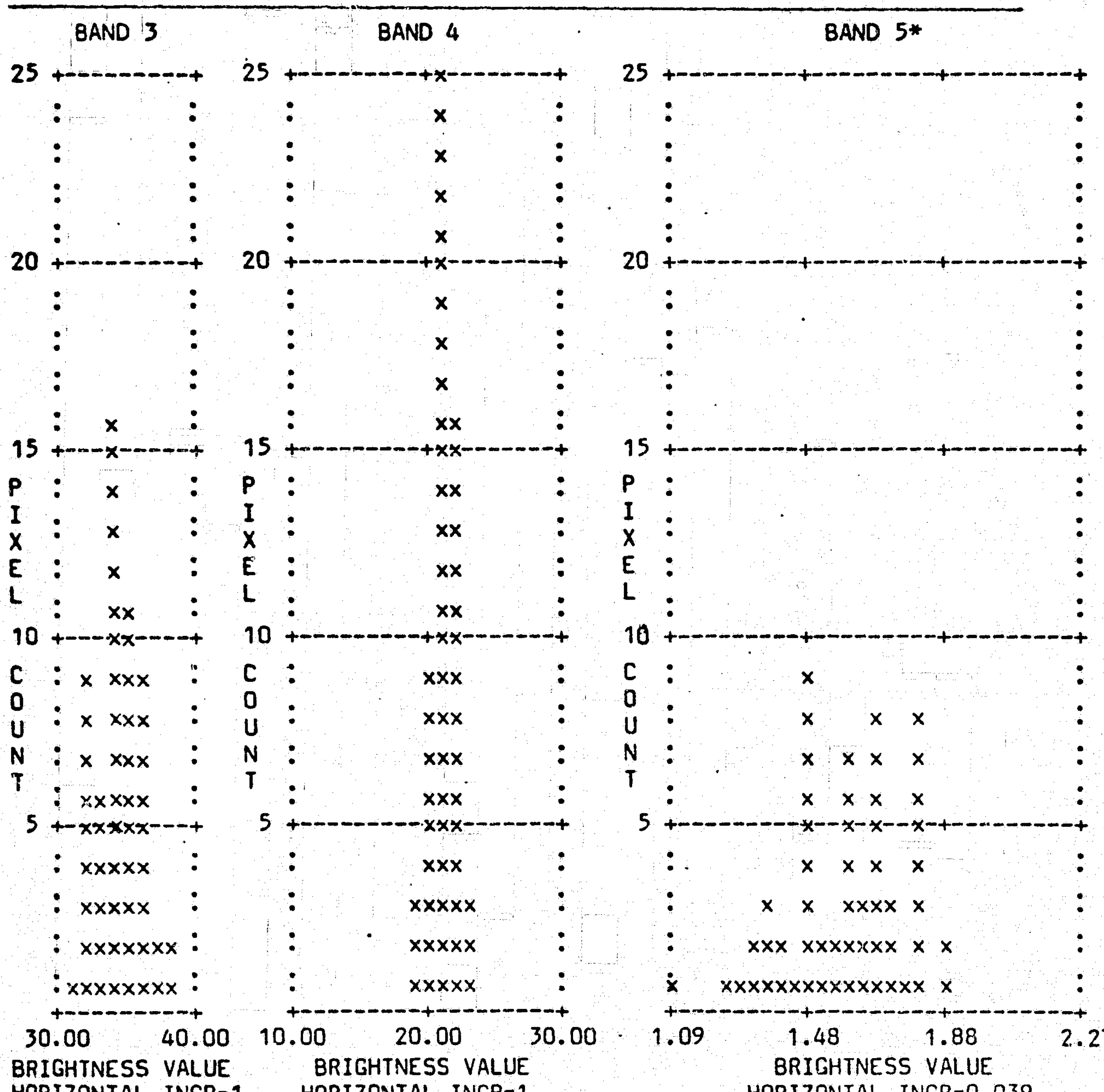

192

Table 3 (continued)

*The broken Gaussian distribution here seems to indicate that the surface is either covered by a number of co-dominant plant species/associations or that the substrate is greatly influencing the spectral signal. Examination of ground truth data substantiates the latter, since this area is dominated largely by one vegetation type that is not dense, and so the underlying substrate plays an important role in the character of the spectral signal reflected from this land unit.

Table 4

RATIO COMPOSITE 1 - FIELD 3

Summary Statistics

	BAND	MEAN	STDEV	CV	SKEW	KURTOSIS	BAD DATA
Blue	3(7/5)	31.45	2.02	6.43	.33	.46	0
Green	4(7)	18.74	1.44	7.71	-.35	.95	0
Red	5(6)	1.29	.21	16.28	-.51	-.29	0

194

ORIGINAL PAGE IS
OF POOR QUALITY

Table 4 (Continued)

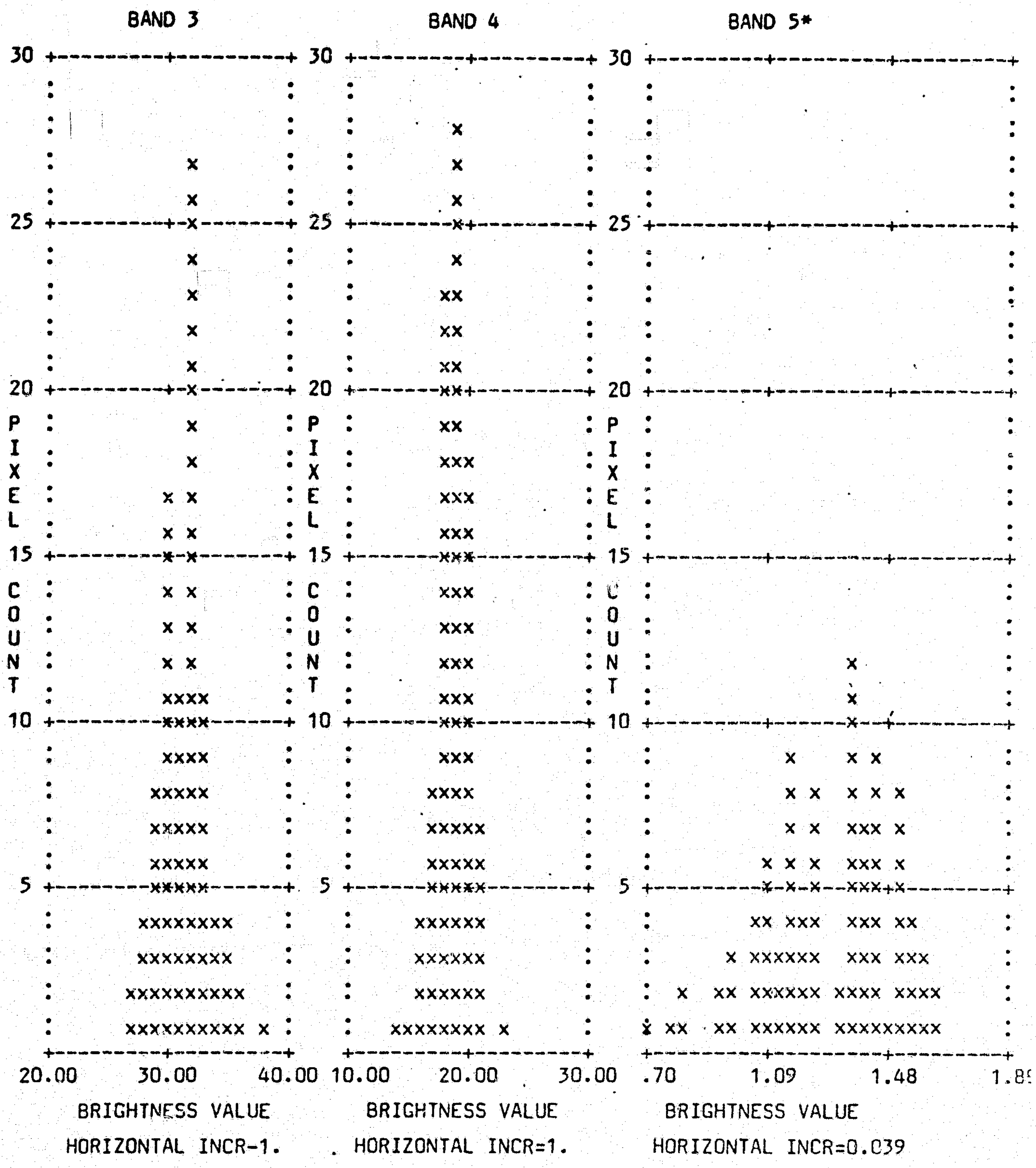

C-3

195

Table 4, Concluded

*The bimodal distribution presented in the band 5 histogram indicates the influence of two dominant factors on the spectral signal. An examination of the site through an on-the-ground visitation showed the two dominant features to be a yellow pine and a big sagebrush community.

196

Table 5

RATIO COMPOSITE 1 - FIELD 4

Summary Statistics

	BAND	MEAN	STDEV	CV	SKEW	KURTOSIS	BAD DATA
Blue	3(7/5)	39.87	2.04	5.11	-.23	.03	0
Green	4(7)	23.75	1.82	7.68			0
Blue	5(6)	1.52	.29	19.15			0

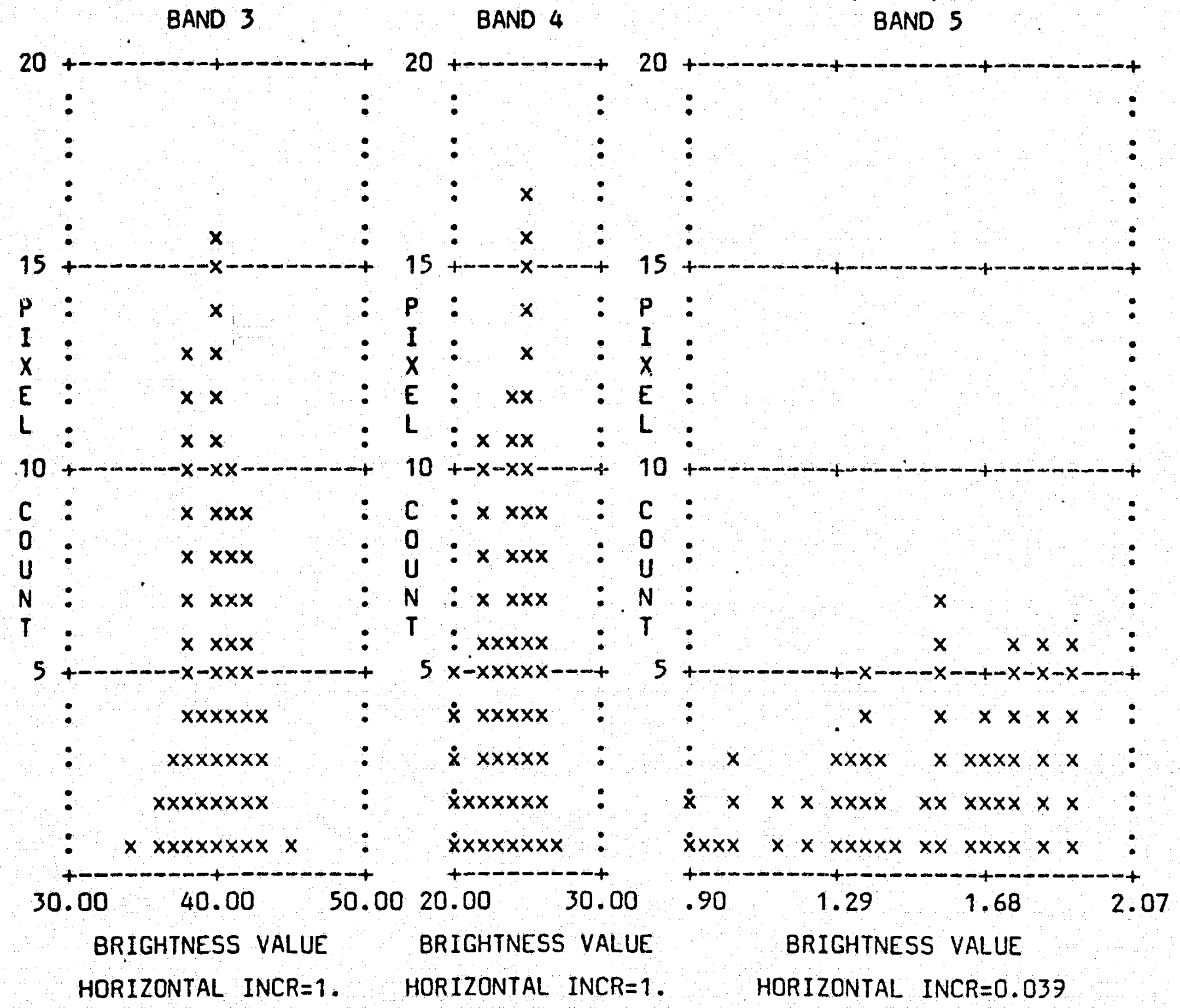

Table 6

RATIO COMPOSITE 1 - FIELD 5

Summary Statistics

	BAND	MEAN	STDEV	CV	SKEW	KURTOSIS	BAD DATA
Blue	3(7/5)	34.87	2.12	6.09	.05	.46	0
Green	4(7)	20.23	1.12	5.54	.52	.16	0
Red	5(6)	1.08	.15	13.86	-2.08	17.63	0

198

Table 6, (Continued)

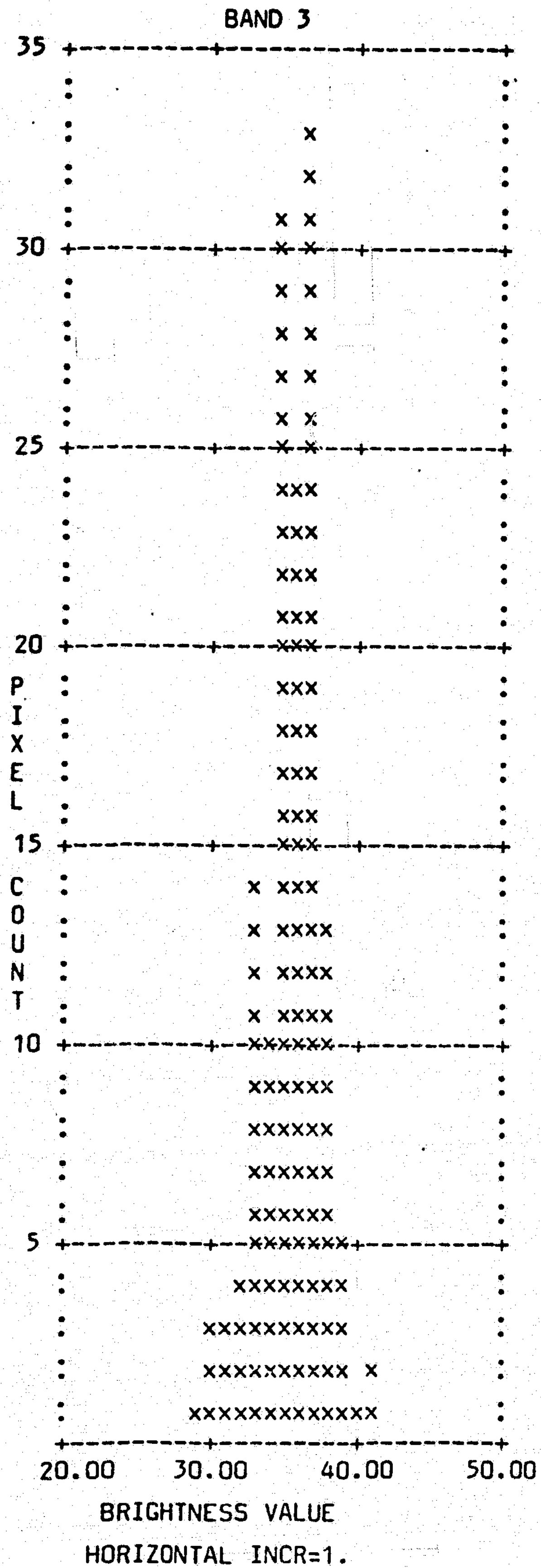

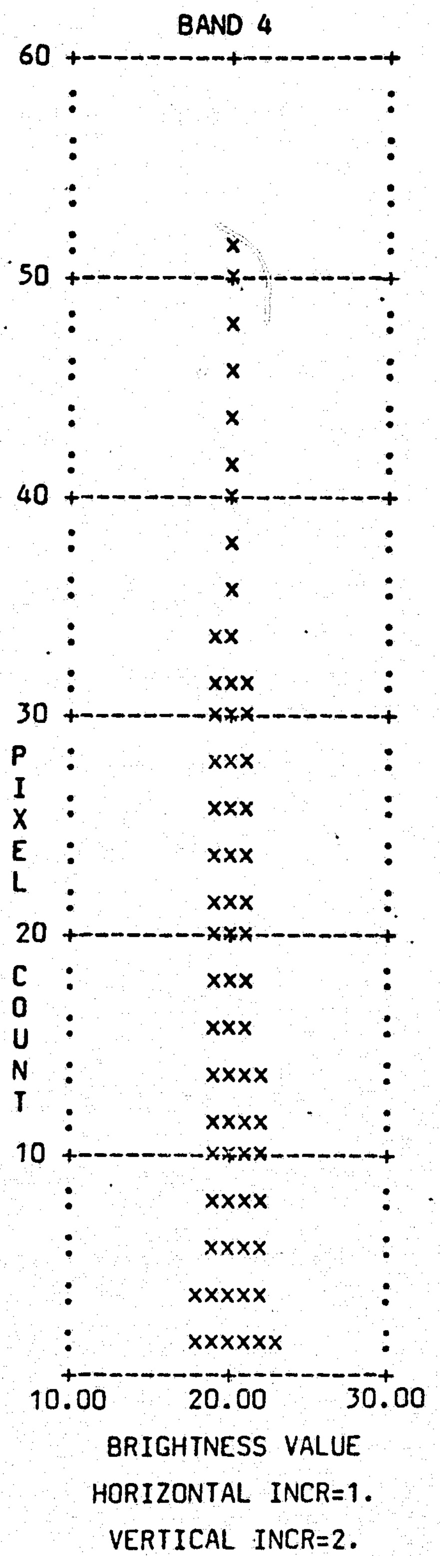

Table 6, (Continued)

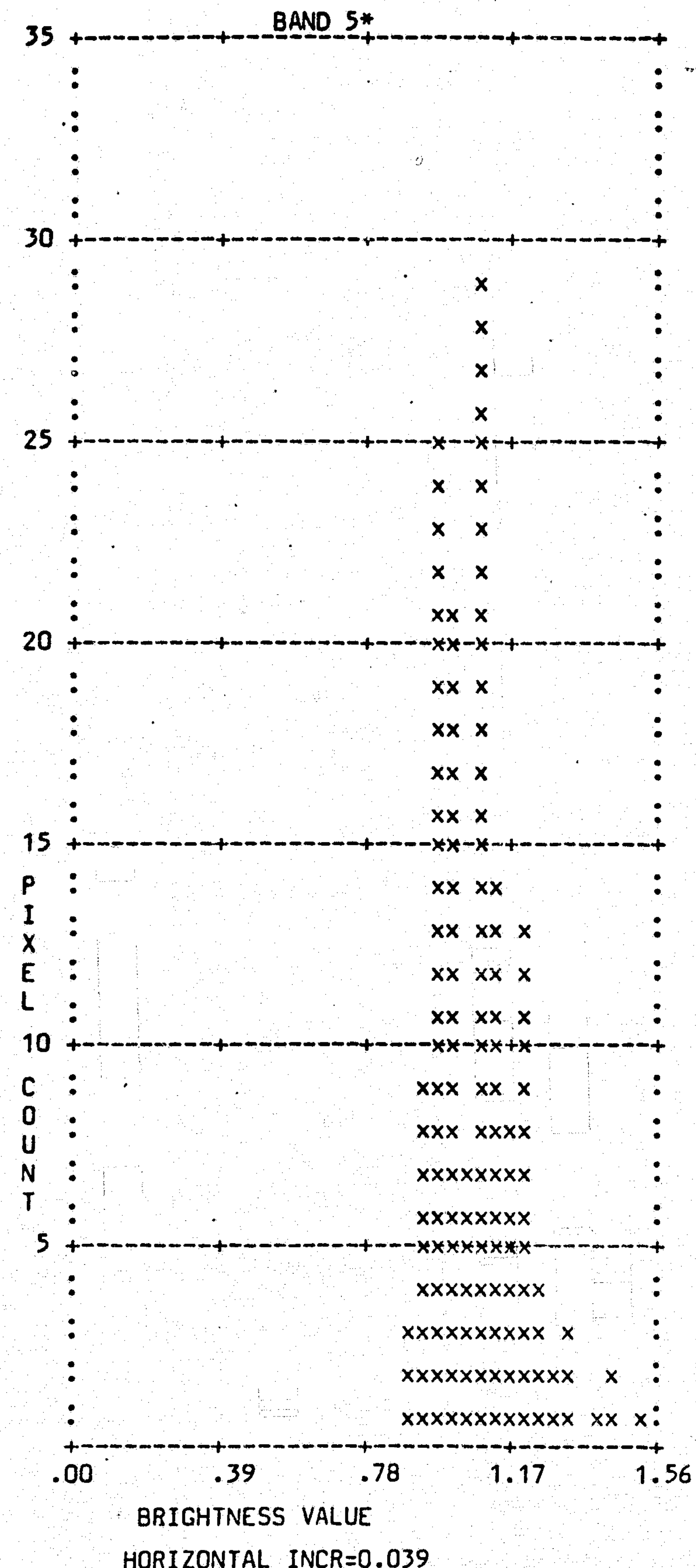

ORIGINAL PAGE IS
OF POOR QUALITY

201

Table 6, Concluded

*The represented land unit system illustrates a high dominance by one factor of the environment. Field investigation shows this area possesses a sparse Yellow Pine forest cover with little or no underbrush, and a high percentage of the substrate exposed; hence the nearly Gaussian distribution.

Table 7

RATIO COMPOSITE 1 - FIELD 6

ORIGINAL PAGE IS
OF POOR QUALITY

Summary Statistics

	BAND	MEAN	STDEV	CV	SKEW	KURTOSIS	BAD DATA
Blue	3(7/5)	39.74	1.99	5.00	.01	-.14	0
Green	4(7)	19.09	.76	3.99	.02	.82	0
Red	5(6)	.53	.05	9.32	1.33	2.04	0

207

Table 7, (Continued)

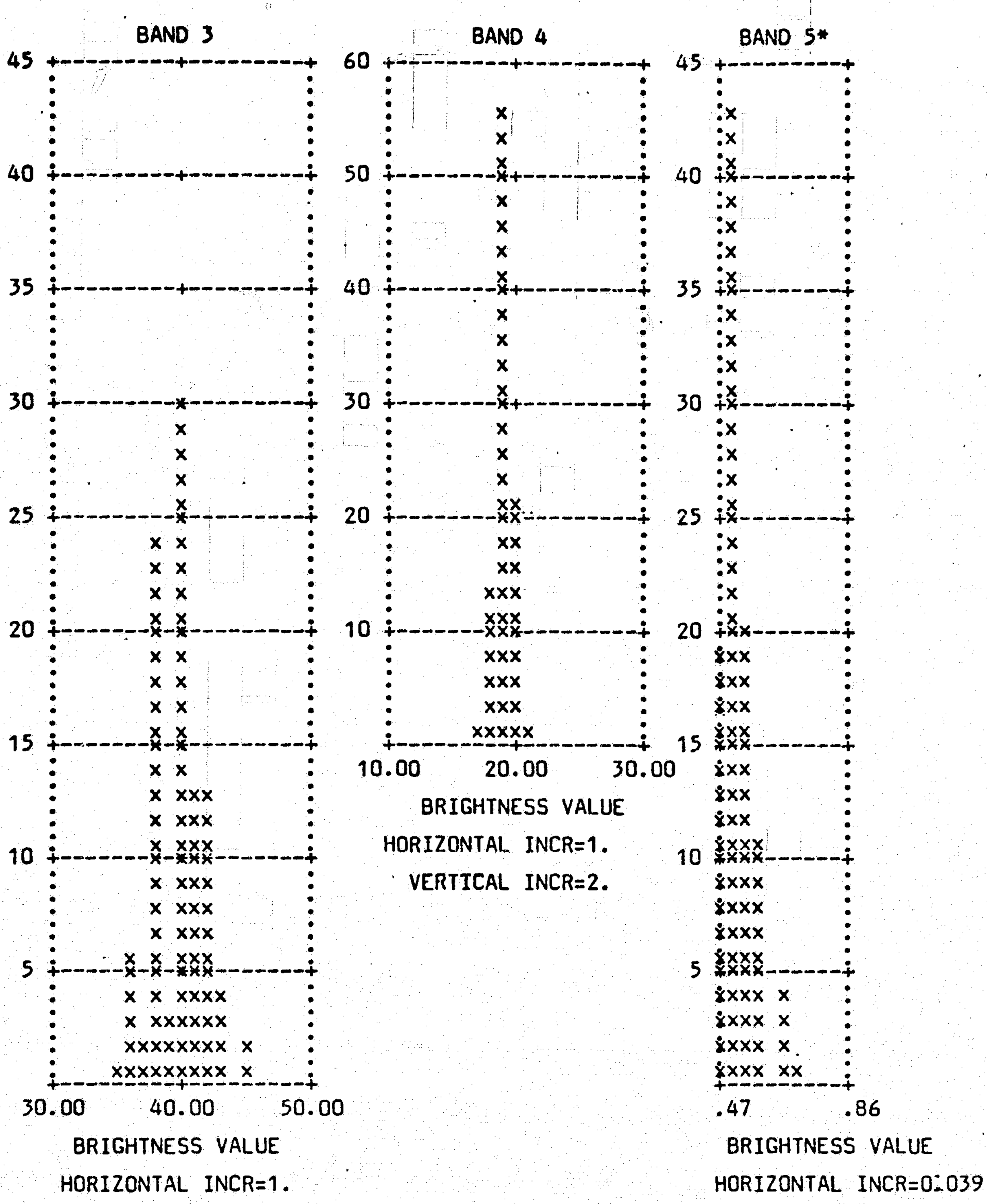

Table 7, Concluded

*This particular distribution showing very little covariance, illustrates how dominant one particular ground cover is in this land unit. Ground visitation showed an alluvial flat nearly void of larger vegetation types (mainly a sage/grass association); hence the highly non-variant signature.

204

Table 8

RATIO COMPOSITE 1 - FIELD 7

Summary Statistics

	BAND	MEAN	STDEV	CV	SKEW	KURTOSIS	BAD DATA
Blue	3(7/5)	47.12	2.26	4.80	-.34	-.45	0
Green	4(7)	27.04	1.73	6.38	.08	-1.22	0
Red	5(6)	.74	.15	19.62	.32	-1.39	0

BAND 3

```
20 +------x--+---------+
   :      x            :
   :      x            :
   :      x            :
   :      x            :
15 +------x--+---------+
P  :      x            :
I  :      x            :
X  :      x            :
E  :      x            :
L  :      x            :
10 +------x--+---------+
C  :      x            :
O  :      x            :
U  :      x            :
N  :      x            :
T  :      x  x         :
 5 +--x-x-xxxx---------+
   :  x x xxxx         :
   :  x x xxxxx        :
   :  x x xxxxx        :
   : xxxxxxxxxx        :
   +---------+---------+
 40.00     50.00     60.00
     BRIGHTNESS VALUE
  HORIZONTAL  INCR=1.
```

BAND 4

```
20 +---------+---------+
   :                   :
   :                   :
   :                   :
   :                   :
15 +---------+---------+
P  :                   :
I  :                   :
X  :                   :
E  :                   :
L  :    x              :
10 +----x----+---------+
C  :    xx xx          :
O  :    xxxxx          :
U  :    xxxxx          :
N  :    xxxxx          :
T  :    xxxxx          :
 5 +----xxxxx+---------+
   :    xxxxxx         :
   :    xxxxxx         :
   :   xxxxxxx         :
   :   xxxxxxx         :
   +---------+---------+
 20.00     30.00     40.00
     BRIGHTNESS VALUE
  HORIZONTAL  INCR=1.
```

BAND 5*

```
20 +---------+---------+
   :                   :
   :                   :
   :                   :
   :                   :
15 +---------+---------+
P  :                   :
I  : x                 :
X  : x                 :
E  : x                 :
L  : x                 :
10 +-x-------+---------+
C  : x                 :
O  :xx      x          :
U  :xx      x          :
N  :xx    x x          :
T  :xx    x x          :
 5 +xx----x-x+---------+
   :xx    x x          :
   :xxx   xxxx         :
   xxxx   xxxx         :
   xxxxxxxxxxxxxx      :
   +---------+---------+
  .55       .94       1.33
     BRIGHTNESS VALUE
  HORIZONTAL  INCR=0.039
```


ORIGINAL PAGE IS
OF POOR QUALITY

Table 8, Concluded

*This type of bimodal distribution would seem to indicate a dominance by two vegetation complexes or individuals within this land unit. Field reconnaissance has shown this to be the situation. The land unit is a mosaic of areas of exclusive grass dominance and areas of sagebrush/grass association dominance.

206

Table 9

RATIO COMPOSITE 1 - FIELD 8

Summary Statistics

	BAND	MEAN	STDEV	CV	SKEW	KURTOSIS	BAD DATA
Blue	3(7/5)	36.89	1.54	4.18	-.24	-.23	0
Green	4(7)	21.30	.93	4.37		-.43	0
Red	5(6)	.92	.09	9.48	.43	2.32	0

207

ORIGINAL PAGE IS
OF POOR QUALITY

Table 9, (Continued)

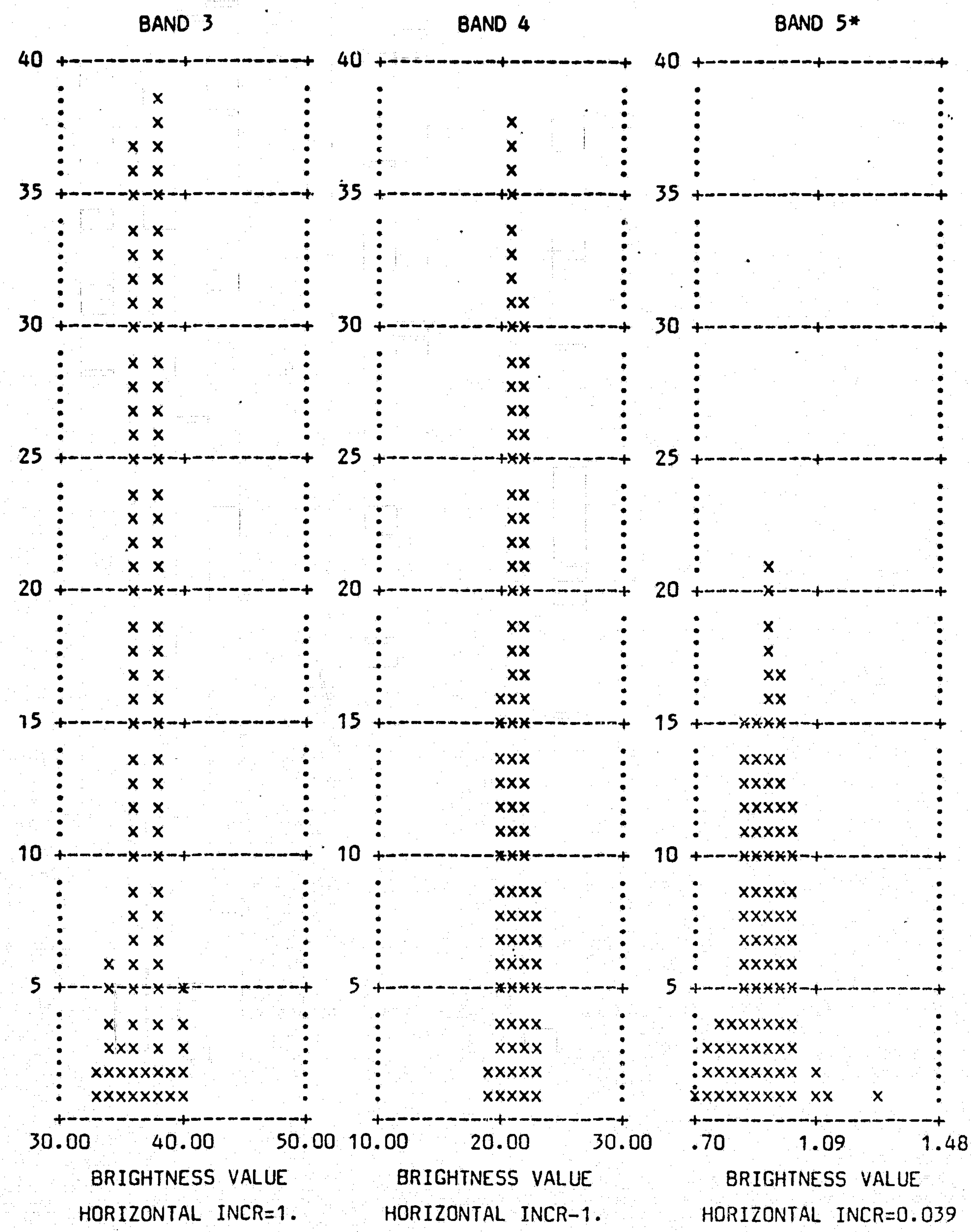

208

Table 9, Concluded

*The nature of this thinned (shelterwood cut) area is one of a conglomeration of ground covering elements. Yellow Pine covers this land unit in a sparse distribution, while an understory of sagebrush with grasses covers part of the space in between, with yet a large percentage of the area being non-vegetated. This probably accounts for the normal yet slightly dispersed distribution of reflection values.

a method of band ratio compositing could be developed for such a purpose. Again, this elementary land system breakdown was done only for the area designated in this study, and therefore, this is the only area for which it can be used with confidence. By gambling to a limited degree, this eight-unit designation scheme may be extrapolated to an expansive area adjacent to the test site that is of the same general climatic/topographic make-up.

Band ratio color composite #2 - MSS 5/MSS 4 --- Red
MSS 6/MSS 5 --- Green
MSS 7/MSS 4 --- Blue (see page 4)

This particular composite represents a conglomeration of ratios that involve combinations that have been used in earlier geologic investigations (MSS 5/MSS 4, MSS 6/MSS 5) (Short and Marrs, 1975), as well as a ratio (MSS 7/MSS 4) that was developed in this study. The band 7 to band 4 ratio was designed to illustrate a maximum amount of contrast between vegetated and unvegetated surfaces, while the other two components are essentially representative of varying substrate composition. Within the band 7 to band 4 ratio, band 7, as noted previously, is a good representative of living vegetation because of the high infrared reflectance of live vegetation. Band 4 represents a secondary peak in vegetation radiation reflection. Hence, in the presence of vegetation, both the band 7 and band 4 peaks will be present and result in a relatively high 7/4 ratio. Conversely, a lack of vegetation will result in a much lower band reflectance, and a lower band 4 reflectance (but not to the same degree as band 7) resulting in a lower 7/4 ratio.

As shown on page 4, the riparian vegetation that dominates the stream channel directly south of Crater Mountain is displayed with a high 7/4 ratio (coded blue in this illustration). Relatively sparse vegetation on the flanks of Crater Mountain itself shows a light blue to green cast signifying the presence of the vegetation canopy along with a substantial part of the substrate coming through to influence the signature. Probably the most striking aspect of this composite is the way in which the band 5 to band 4 ratio picks up exposed geology. Along the upper flanks of Crater Mountain the exposed basaltic flows are given a reddish cast, while the lower elevation alluvial flats, made up of alluvium and exposed volcanic rock, show up as an intense red. The incompletely regenerated timber cut (on Antelope Mountain) registers a reddish cast showing the substantial influence of the substrate on the spectral signature. The overall whitish cast given to a majority of the vegetated areas (especially on the flanks of the surrounding mountains) indicates an approximate equal contribution of color by each of the band ratios in the composite. This would seem to indicate that these areas are

210

vegetated, but the substrate is playing at least an equal role in affecting the reflected spectral signature.

Band ratio color composite #3 - MSS 7/MSS 4 --- Red
MSS 6/MSS 5 --- Green
MSS 5/MSS 4 --- Blue (see page 5)

This composite differs from the previous one only in that each of the band ratios was assigned a different color. As can be seen, the results are the same (i.e., areas of corresponding color on ratio composite #2 also correspond in color on ratio #3, but are portrayed in colors different from those in ratio composite #2). The intention here was to show that although both composites present the same data, different modes of presentation may permit easier qualitative interpretation. For example, in ratio composite #2, the riparian vegetation is slightly easier to distinguish from the surrounding alluvial flat merely because of the adjacent tonal contrast. This suggests that there is some utility in experimentation with color schemes attached to each band ratio composite. To make as many distinctions as possible, all possible color combinations should be viewed at least once.

Band ratio color composite #4 - MSS 6/MSS 5 --- Red
MSS 7/MSS 5 --- Green
MSS 7 --- Blue (see page 5)

In this particular display MSS band 7 and the 7/5 ratio again reinforced each other in representing the ground vegetation cover. All greens, yellows, whites, and light blues represent some type of vegetation cover. Darker blue correlates well with exposed substrate and volcanic rock and illustrates how MSS band 7 represents more than just vegetation, and should not be used solely as an indicator of vegetation.

Band ratio color composite #5 - MSS 7/MSS 5 --- Red
MSS 7/MSS 4 --- Green
MSS 6/MSS 5 --- Blue (see page 6)

As indicated by the band 7 to band 5 ratio, vegetation on the slopes of Crater Mountain is of a sparse nature, with its spectral signature heavily influenced by the substrate (as indicated by the 6/5 ratio). Vegetation is shown with a blue to blue-violet color while other areas are white showing the mixed influence of vegetation, substrate and topography. Exposed geology again seems to be highly correlated to the 6/5 ratio, exhibiting a green color on this composite.

In concluding this section, we should restate that the purpose in experimenting with different band ratio combinations was to determine if individual land units or systems could be distinguished, and to look more closely at the problem areas that needed to be field checked.

Within each particular land unit, basaltic rocks were easily distinguished, exhibiting a dark tonal signature on all of the composites investigated. Alluvial areas were easily discriminated, as were all areas of exposed substrate. Vegetated areas were rather easily noted, but confusion with the substrate was encountered when the surface was not entirely covered by a vegetation canopy. Referring to ratio composite #1, spectral histograms and plots provided an added dimension in aiding the manual interpretation of the different ratio composites. Often, the 7/5 band ratio could be compared with band 7 to verify the presence, extent and diversity of vegetation. MSS band 6 was somewhat useful in illustrating substrate consistency. In the other sets of composites, ratios such as 6/5 and 5/4 aided in surface geology interpretation, and 7/5 and 7/4 ratios were of considerable import in interpreting vegetation.

Although the land units identified in this part of the study may have been on a somewhat small scale, they have clearly served to indicate the potential value and importance of more detailed cost intensive investigations along this same line. The amount of data displayed within a color ratio composite may never be fully recognized, and for this reason, additional experiments should be undertaken to exploit these information sources to the limit that existing technology permits.

Another major channel of application involves the use of computerized classification routines that classify raw Landsat data with a minimum of human effort and interaction. The second part of this study will institute this method and compare the results with those obtained through the band ratio method.

Discussion and Analysis - Part II

The following analysis involves the use of two classification procedures in ordering into discrete spectral classes the spectral reflectance values of each of the four MSS bands for each pixel in the study area. The computer classification includes an unsupervised clustering algorithm (ISOCLAS) and a supervised classification procedure using a maximum likelihood decision rule (CALSCAN).

ISOCLAS (Iterative Self-Organizing Clustering Algorithm) is a

212

large computer program developed at the Johnson Space Center (as ISOCLS) and later adapted to the CDC 7600 system at the Lawrence Berkeley Laboratory by the personell of the Remote Sensing Research Program. Several controlling inputs allow the user to control the size and number of clusters developed by the program. (A cluster in this case represents a number of pixels grouped together into a spectrally homogeneous group.)

Aside from this minimal number of human inputs, the program acts on its own to classify the digital spectral information provided to it. Because the program produces a classification-type cluster map on which each cluster requires post-processing identification and interpretation, it is frequently referred to as an unsupervised classification scheme.

In the case of wildland areas, such as the study area involved here, ISOCLAS is commonly run on a smaller area (sub-area) within the larger one. The sub-area, in the mind of the interpreter, must possess a good cross section of spectral classes represented within the entire larger study area. The final outcome is that the small sub-area has been classified into a number of clusters, each representing a set of unique reflectance characteristics. This information is then used to "seed" or supervise the supervised classification algorithm, CALSCAN.

CALSCAN, referred to as the maximum likelihood classification algorithm, requires some type of initial input data on which to base its final classification. This can be either in the form of a training set (i.e., spatial sample(s) of digital data of a known ground feature selected by the user from which the spectral characteristics are calculated and used as supervisory data on which the classification is based) or previously calculated spectral statistics, such as output from ISOCLAS. The input data is then used as a basis in the calculation of the maximum likelihood ratio within the algorithm. Briefly, the maximum likelihood ratio is a probability decision rule used to classify an area of interest (target) from multispectral data. In its simplest form, the likelihood ratio is Pt/P_b, or the probability P of an unknown spectral measurement being classified as the target t, to the probability of an unknown spectral measurement being classified as background b. When $Pt/P_b \geq 1$, the decision is t; when $Pt/P_b \leq 1$, the decision is b. Probability density functions are calculated from the spectral samples provided as input (training sets or statistics). As the number of training sets increases, the mathematical computation of the maximum likelihood ratio increases in complexity. As a result, computer analysis is necessary. The entire process, from the generation of training sets or statistics through the maximum likelihood classification, is known as automatic data processing (ADP) or automatic spectral pattern recognition of multispectral remotely sensed data.

Within this study, the order of events was much the same as the procedure just described. Initially, Crater Mountain was chosen as the test area (sub-area) that would be processed through the unsupervised classification algorithm (ISOCLAS). The Crater Mountain area (200 pixels by 150 pixels) was chosen primarily because of its substantial local relief (as great as any feature within the entire study area), variety of slope and aspect,classes, and diversity of vegetation and surface types which seemed to cover the entire spectrum of land classes possible for the greater study area. The output, in the form of a class map, depicts eleven different spectral groupings. Gross patterns and trends were recognized and differentiated, but no substantial effort was undertaken to interpret the exact significance of each spectral class at this point in the analysis. The statistical information that resulted from this classification was used as input into the supervised classifier in the form of means, standard deviation and covariance, and correlation matrices. The supervised classification routine (CALSCAN) was then run using these training statistics. Final output from the algorithm was in the form of a class map designating which class each pixel had been assigned to and a probability map siting the probability of misclassification for each pixel. The latter output product is currently unavailable, but is particularly useful for detailed inventory analyses in which it is important to know the probability associated with each class when estimating the areal extent or physical volume of particular features. The output class map is shown on the following page (Figure 6 and a description and analysis of the results follows.

A multistage analysis procedure was utilized to determine the significance of each of the eleven spectral classes produced by the maximum likelihood classifier (CALSCAN). "Multistage" in this case refers to the use of different scales of imagery and high flight photography to sample and verify areas of interest. In this part of the investigation, a standard Landsat color composite (scale 1:100,000) was utilized along with a 1:435,750 scale enlargement of a Landsat color composite, high flight RB-57 1:130,000 scale natural color and color infrared photography, and ground reconnaissance photos. As a supplement to the different types of imagery used, ancillary information in the form of geologic and topographic maps was also referred to in evaluating the eleven spectral classes. Table 10 shows the results obtained.

As with the color ratio composite method of land surface identification, the validity of computer classification has been shown. The land surface types identified in Table 10 correspond closely to those land surfaces described in Table 1. Hence, for the type of small scale land surface phenomena investigated in this study, both methods appear to be comparable. Ideally, a combination of both

214

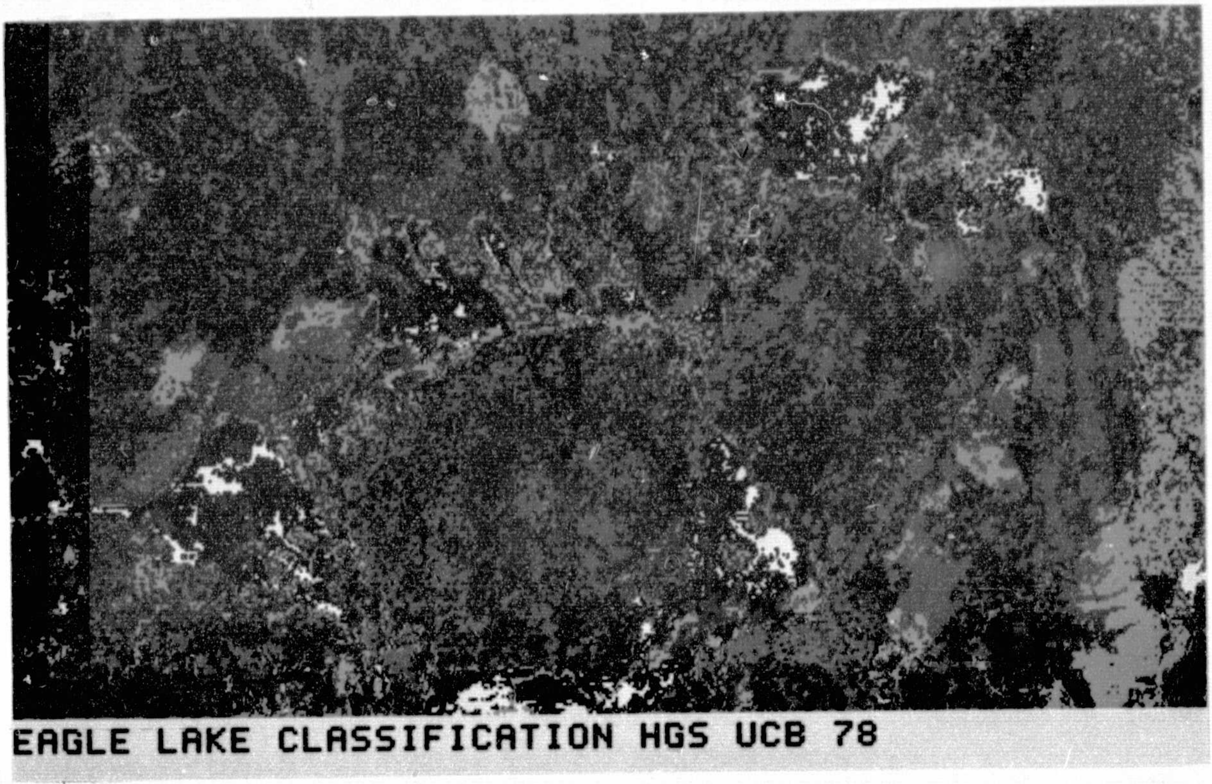

Figure 6. CALSCAN classification summary. (Refer to detailed caption on following page.)

ORIGINAL PAGE IS
OF POOR QUALITY

CALSCAN Classification Summary

	Total	Class 1	2	3	4	5	6	7	8	9	10	11
Pixel Count	150,000	3218	36603	15872	10696	24832	23326	8755	19042	5813	884	959
Percent of Total	100	2.15	24.40	10.58	7.13	16.55	15.55	5.84	12.69	3.88	.59	.64
Acres (Pixel Count x 1.1)	165,000	3540	40263	17459	11766	27315	25659	9631	20946	6394	972	1055

Figure 6. Caption, continued

216

Table 10

LAND SURFACE CLASSES - AUTOMATIC CLASSIFICATION

Class No.	Description/Location	Identification
1	Intermittent patches distributed throughout the extent of the alluvial flats	Very rocky, largely barren basaltic area
2	Generally confined to northern slopes, and slightly higher altitudes (related to aspect and altitude)	Densley forested, Pine, underbrush present
3	Located along stream channels within the alluvial flats	Wet meadow and riparian vegetation
4	Generally located in the transition zones between higher areas and the alluvial flats	Vegetational transition zone (big sage/ bunchgrass) to forest
5	Generally found at the interface of two areas dominated by a single class (i.e. 2, 6; 2; 4; 2, 7; etc.)	Transitional zone exhibiting the effects of a location adjacent to two highly dominant cover classes
6	Found in higher areas, largely in conjunction with class 2	Sparse/low density forest; underbrush largely lacking
7	Distributed throughout the alluvial flat areas, and exclusively confined to them	Alluvial areas covered with bunchgrass and low sage
8	Located almost exclusively on SE facing slopes	Confusion class, illustrating the affects of a relatively low sun angle or a high relief area
9	Found on the upper reaches of Crater Mtn., in exposed rift areas	Unvegetated basalt flows
10	Found in proximity with class 9	Exposed basalt vegetated (underbrush only)
11	Crater Lake (on Cr. Mtn.) Poison Lake (W. of Cr. Mtn.)	Water

methods (ISOCLAS/CALSCAN classification of the band ratio data) and a qualitative as well as quantitative analysis of both products would serve as the best method in a more detailed land surface type investigation.

Conclusion

1. Comparability and Use

The degree of validity and usefulness of the color ratio composite method of land surface identification/classification and the automatic data processing approach appear to be comparable. Each can be used independently of the other if the facilities are not available to generate both products, but as a method of checking and verification the greatest accuracy can be expected from using the two products in conjunction with each other.

2. Applicability of the Techniques

The type of information generated here through the classification of spectral data may be used as input into data base systems and as inputs into regional planning decisions or resource inventories. Models of the physical environment that require information on surface types (e.g., climatic process models, geologic/geomorphic process models, or water resource models used in predicting runoff) could use this type of data.

3. Further Investigation

There is much opportunity for new and more in depth investigation concerning band ratio analysis and computer processing of spectral data. With adequate funding, a combination of the two methods involving experimentation with new band ratios and later ISOCLAS/CALSCAN computer processing of the results could provide new insight into land surface differentiation. More detailed (larger scale) differentiation of land surface types could open new areas of possible application of the technique. Included among these could be soil group/association identification, geologic small scale mapping, detailed vegetative mapping, terrain analysis, water quality analysis, and the monitoring of disturbance activities (e.g., mining and logging).

218

Selected References

Avery, T. Eugene, *Interpretation of Aerial Photographs*, Burgess Publishing Company, 1960.

CALSCAN Users' Manual, Remote Sensing Research Program, U.C. Berkeley.

Colwell, R.N., "Remote Sensing of Natural Resources", 218:54, *Scientific American*, 1968.

Daus, Stephen J. and M.J. Cosentino, "The Use of Analysis of Variance Procedures for Defining Ground Conditions of Categories Generated in an Automatic Analysis of Landsat MSS Digital Data", pp. 298-306, *1977 Machine Processing of Remotely Sensed Data Symposium.*

"Earth Resources Benefits to Expand", *Aviation Week and Space Technology*, pp. 45-63, October 17, 1977.

Hoffer, Roger M., "Techniques and Applications for Computer Aided Analysis of Multispectral Scanner Data, *Laboratory for Application of Remote Sensing, Information Note 062276, 1976.*

Hunt, Graham R. and J.W. Salsbury, "Visible and Near Infrared Spectra of Minerals and Rocks I", Silicate Minerals, Lunar and Planetary Branch, Air Force Cambridge Research Laboratories, Hansom Field, Bedford, MS, pp. 283-300, Volume 1, *Modern Geology*, 1970.

ISOCLAS Users' Manual, Remote Sensing Research Program, U.C. Berkeley.

Manual of Photographic Interpretation, George Banta Company, Inc., Menashoa, WI, 1960.

Manual of Remote Sensing, Volumes I and II, American Society of Photogrammetry, 1975.

Proceedings of the NASA Earth Resources Survey Symposium, Volume I-B, Geology-Information Systems and Services, Houston, TX, June 1975.

Rowan, Lawrence C., *et al.*, *Discrimination of Rock Types and Detection of Hydrothermally Altered Areas in South Central Nevada By Use of Computer-Enhanced ERTS Images*, USGS Professional Paper, 1975.

Swain, Philip H., "Pattern Recognition: A Basis for Remote Sensing Data Analysis", *Laboratory for Applications of Remote Sensing Information Note 111572*, 1972.

Waz, Douglas M., *Terrain Analysis: A Guide to Site Selection Using Aerial Photographic Interpretation,*

Wright, R.L., "Principles in a Geomorphological Approach to Land Classification", *Zeitschift fur Geomorphologie,* pp. 351-371, N.F. Bd 16, Heft 4, December 1972.